



Chair of Ceramics

Doctoral Thesis



Application of Some Digital Techniques to
Optimize the Thermomechanical Behavior
of Refractory Linings

Aidong Hou

October 2019

AFFIDAVIT

I declare on oath that I wrote this thesis independently, did not use other than the specified sources and aids, and did not otherwise use any unauthorized aids.

I declare that I have read, understood, and complied with the guidelines of the senate of the Montanuniversität Leoben for "Good Scientific Practice".

Furthermore, I declare that the electronic and printed version of the submitted thesis are identical, both, formally and with regard to content.

Date 24.10.2019

Signature Author
Aidong, Hou

ACKNOWLEDGEMENTS

It is my pleasure to express my sincere gratitude to the people who contribute to my PhD work and life.

First of all, I would like to thank my supervisors. I would like to thank **Prof. Harald Harmuth** to support me to come to Austria and his continuous support for my PhD work. His immense knowledge and expertise, rigorous academic attitude, and working style for perfect deeply affect me. It's a great honor to work with him and a great luck to have such a good example for academic career. My sincere thanks also go to **Dr. Shengli Jin** for his support in my academic and daily life. His patient guidance helped me in all the time of research and writing of papers and thesis. I enjoyed all the discussions with him and his passion in the science encourages and inspires me a lot. His enthusiastic organization of activities, e.g. BBQ and hiking, made my PhD life more enjoyable. I would also like to express my sincere appreciation to **Dr. Dietmar Gruber** for his patient supervision throughout the PhD. His scientific visions helped me to change my way of thinking from eastern to western. I was always benefited from his useful comments and suggestions for research and publications. I am indebted to **Prof. Helmut Schweiger** for his excellent lecture in computational mechanics and kind support to edit my thesis.

Furthermore, I would like to thank all my colleagues at the Chair of Ceramics for their kindness and patience to explain culture difference and I enjoyed the atmosphere of diverse cultures a lot. Especially, I would like to thank **Anastasia Kucheryavaya**, **Soheil Samadi**, **Thanh Hung Nguyen**, and **Behnam Akbari** for all the Mensa, tea, cake and laughing time.

Sincere appreciation is also given to great friends in Leoben. It is a great luck to meet **Dr. Shuqin Zhang** at the very beginning of my PhD and to be close friends with her. I would like to thanks for all of her share and support in life and study, especially for teaching me cooking and tutoring me mathematics. I would also like to thank for her colleagues at the Chair of Mathematics and Statistics, **Prof. Jörg Thuswaldner**, **Prof. Arnold R. Kräuter**, **Manuela Resch**, **Dr. Mario Weitzer**, **Dr. Myriam Amri**, **Dr. Jonas Jankauskas**, for all the activities

(festivals, BBQ, hiking) to have me. I am also very grateful for all the care from **Prof. Qingtao Meng's family, Prof. Bo Liu's family, and Dr. Weiping Yao's family.**

My sincere thanks also go to study partners and friends I met at TU Graz. I'm grateful to **Carla Bach Fabris** for her kind cooperation and help during the "Computational Geotechnics" lecture. Her serious study attitude encouraged me to overcome difficulties in study. I would also like to thank **Enkhe Darmaev** for the friendship outside of lecture and his share of Russian culture. My sincere appreciation also goes to **Alexander Ferk** for his friendly "Hello" in the "Neural Network" lecture, explaining me Austrian culture, correcting my German, and guiding and exploring Graz with me.

A special gratitude is given to my family: my grandparents (unfortunately both passed away during my PhD, grandmother in 2016 and grandfather in 2018), my parents, bother, uncles, aunts, cousins, and little and lovely nephews. Great thanks for all the support throughout of my life. Today is 24th October 2019, this thesis is also special used to commemorate the first anniversary of my grandfather's death, hope he and my grandmother can receive my message in the higher place. I will remember all the love they gave to me.

Financial support by the China Scholarship Council and the Austrian Competence Centre for Excellent Technologies research programme in "Advanced Metallurgical and Environmental Process Development" (K1-MET) is gratefully acknowledged.

ABSTRACT

Refractory linings are vital components of high temperature vessels. Successful lining concept design can avoid the premature wear of refractory linings, allow for more economically efficient configuration of refractories, and improve the efficiency of high-temperature processes and save energy [1]. The thermal and thermomechanical behavior of refractory linings has a significant influence on the lifetime of vessels and is affected by many factors, for instance, the geometry of vessels, the properties of refractory lining, and the process conditions. The direct measurement of stresses at high temperature conditions is nearly impossible. This hinders the proper applications of refractory linings for the specific conditions. The present thesis aims to optimize the lining concept of a steel ladle considering the influence of multiple factors and to predict the thermal and thermomechanical performance of the lining concept.

A set of tools in the Taguchi method were used for the lining concept optimization. These tools are orthogonal arrays (OAs), analysis of variance (ANOVA), and signal-to-noise (S/N) ratio. Lining configurations were designed by OAs and finite element simulations were performed with the commercial software ABAQUS to survey the thermal and thermomechanical behavior of the designed lining concepts. The significance of factors was quantitatively ranked by ANOVA and the optimal levels of each factor were evaluated by S/N ratios. Backpropagation artificial neural network (BP-ANN) was applied to predict lining concept performance.

The results show that the proposed two lining concepts optimized by the Taguchi method showed a substantial decrease in heat loss through the steel shell and thermomechanical load at the hot face of the working lining [1]. The performance of 128 lining concepts was predicted by BP-ANN models. High prediction accuracy can be achieved by applying suitable BP-ANN models. The coefficients of determination are 0.9970, 0.9950, 0.9364 for maximum compressive stress at the hot face of the working lining, end temperature and the maximum tensile stress at the cold end of the steel shell, respectively. In addition, the guidelines to define minimum training dataset size, node number in the hidden layer, and training algorithms were proposed to optimize BP-ANN architectures for a steel ladle system.

TABLE OF CONTENTS

1. PROBLEM DEFINITION AND METHODOLOGY APPLIED	1
2. STATE OF THE ART.....	2
2.1. Refractory linings of industrial vessels	2
2.1.1. Metallurgical vessels for iron and steel industry	2
2.1.2. Rotary kilns for cement industry	5
2.1.3. Channel induction furnace for foundry industry	6
2.2. Methods applied for optimization and prediction	7
2.2.1. The Taguchi method.....	7
2.2.1.1. Introduction.....	7
2.2.1.2. Orthogonal arrays (OAs).....	8
2.2.1.3. Analysis of variance (ANOVA).....	9
2.2.1.4. Signal-to-noise (S/N) ratio	9
2.2.2. Back-propagation artificial neural network (BP-ANN)	10
2.2.2.1. Introduction.....	10
2.2.2.2. Establishment of ANN models	12
2.2.2.2.1. The dataset properties.....	12
2.2.2.2.2. Training algorithms	13
2.2.2.2.3. Node number in the hidden layer	16
3. INVESTIGATIONS AND RESULTS	18
3.1. Optimization of steel ladle lining via the Taguchi method	19
3.1.1. Factor significance ranking	20
3.1.2. Optimal levels.....	21
3.1.3. Proposal and validation of optimal lining concepts.....	21
3.2. Prediction of thermal and thermomechanical responses with BP-ANN models	22
3.2.1. Architectural parameters study of BP-ANN model.....	23
3.2.1.1. Dataset properties.....	23
3.2.1.2. Node number in the hidden layer.....	26
3.2.1.3. Training algorithms.....	28

3.2.2. Thermal and thermomechanical responses prediction by BP-ANN models	30
4. CONCLUSION	33
5. OUTLOOK.....	34
6. REFERENCES	35
7. LIST OF APPENDED PUBLICATIONS	52
8. COLLECTION OF PUBLICATIONS.....	54

1. Problem definition and methodology applied

Steel ladles act as transportation vessels and refining units, and subjected to a severe operating environment during service. The lifetime of steel ladles depends significantly on the thermal and thermomechanical behavior of refractory linings. The performance of refractory linings is affected by many factors, for instance, the geometry and the material properties of linings; and it is tough to directly measure the temperatures and stresses in the linings during service. Therefore, it's necessary to evaluate the thermal and thermomechanical performance of various lining concepts numerically.

As the performance of refractory linings is affected by many factors, application of advanced measures to efficiently facilitate the decision-making is of importance. The application of the finite element method combined with the Taguchi method is promising. To this end, suitable orthogonal array shall be defined to design the lining concepts. With the modelling results, significance of factors and their optimal levels shall be obtained with proposed optimal lining concepts.

The instantaneous prediction of thermal and thermomechanical performance of optimized lining concepts is also desirable for efficient lining concepts design. Artificial neural network (ANN) is a powerful and commonly used predictive technique. The training dataset contains 160 lining configurations obtained by applying five orthogonal arrays. The thermal and thermomechanical responses were obtained from finite element simulations. The prediction accuracy of ANN is mainly affected by the complexity of the problem, the quality of the dataset and architectural parameters. Therefore, guidelines shall be investigated to define dataset size, node number in the hidden layer based on the variation/response complexity, minimum number of input variables, and training algorithms for the steel ladle system.

2. State of the art

Refractory linings play a significant role in high temperature industrial vessels, such as, metallurgical vessels for iron and steel industry, rotary kilns for cement industry, and channel induction furnace for foundry industry. These vessels are subjected to a severe operating environment during service and their performances influence the operation processes. The campaign lives of refractory linings depend on their thermal and thermomechanical behavior.

It is a tough task to directly measure stresses and temperatures especially at the working lining of vessels in service. With mathematical and numerical modellings, the qualitative and quantitative predictions of these quantities and analysis of refractory material damage and failure mechanics [2-8] are possible. To facilitate the optimization of refractory linings, many numerical simulations have been performed to reveal the thermal and thermomechanical performance of refractory linings in a variety of vessels considering the influence of refractory materials and their properties, lining thicknesses, lining structures, and process conditions.

2.1. Refractory linings of industrial vessels

2.1.1. Metallurgical vessels for iron and steel industry

Blast furnace is a complex industrial reactor used to produce hot metal from iron ore [9]. The lifetime of a blast furnace significantly depends on the lining erosion. The dissection of blast furnace shows that lining erosion mainly centers on two parts: one is the hearth side wall and bottom, and another is the bosh, belly and lower shaft [10]. S. Kumar [11] found that the hot metal, cooling conditions and coke-bed states influence the temperature profile and the refractory wear in the blast furnace hearth. H. W. Gudenau [12] found that bricks having a high thermal conductivity show high resistance to crack and spall formation; wear in the heart zone can be reduced much more efficiently by adding aluminum oxide to the carbon bricks than by increased cooling measures. D. Gruber et al. [13] investigated the role of the ramming mix to avoid harmful thermomechanical stresses. The results showed that the thickness and the compressibility of the ramming mix are the major parameters to avoid too high compressive stresses within the ceramic cup. Compared with cast iron and aluminum, copper is found to be a better alternative for blast furnace cooling staves [14].

RH degassers are important secondary steelmaking equipment and are widely used in the production of high grade steels [15]. Processes of decarburization, denitrogenation, and dehydrogenation are carried out in RH degassers. The RH degasser is comprised of an upper vessel, a lower vessel, and two snorkels [3]. These components act as an integrated vacuum chamber after submergence of the snorkels into the liquid steel [3]. Snorkels undergo severe thermomechanical loads due to the normal cyclic operations including preheating, submerging, and idle time. S. Jin et al. [3] investigated the thermomechanical failure mechanism of the magnesia chromite bricks in the wear lining. The results showed that at the beginning of the submerging process, tensile failure occurs closest to the hot face of the lowest course of bricks prior to shear failure or creep. Furthermore, shear failure and creep contribute to the joint opening at the hot face. The concept of using less brittle material for the wear lining and a relative stiff monolith for the outer lining of the snorkel indicated that the tensile failure occurring from the hot thermal shock can be mitigated. F. Damhof et al [16] found that a reduction in the idle time of the degassing installation reduces the damage and consequently increases the lifetime of the refractory concrete lining. The presence of joints in the RH snorkel can reduce the stresses in the lining by up to 50% [17].

Converters are vessels used to convert carbon-rich liquid hot metal from blast furnace to low-carbon steel [18]. The converter vessel consists of a spherical bottom, a cylindrical shell, and an upper cone [18]. The lining of oxygen converters consists of working lining and permanent lining. During the blowing of gas, the refractory lining of an oxygen converter is under arduous conditions of aggressive slag, oxidizing atmosphere and high temperature. The lining wear is most serious in the zone in contact with the slag. Expansion allowance and joint conditions affect the damage of refractory structures [17, 19-22]. A high conductivity and low thermal expansion of the working lining can reduce the thermal stress of a converter [19]. D. Gruber et al. [22] identified that bending stresses generated by the thermal expansion of the lining is a principal failure reason in the bottom/wall transition zone of an investigated case. K. Andreev et al. [17, 20] found that the stress needed to close the joint is proportional to the material stiffness; temperature influences the joint closure by changing the stiffness of material and by reducing the initial joint gap due to thermal expansion.

Torpedo cars are essential components of the supply system during transportation of hot metal from the blast furnace to the secondary refining area. There are several factors that concurrently influence the performance of torpedo car lining. For instance, mechanical stress caused by the weight of the hot metal, the erosive effect caused by the liquid metal when filling up, transporting, and emptying the torpedo car, the chemical stress caused by reactive interaction of the solid and liquid phase, and the thermal stress caused by the temperature drop [23]. These factors lead to the intense slag corrosion and structural spalling of the working linings. Jin et al. [24] modeled the thermomechanical behavior of refractory linings in a torpedo car considering the working lining spalling. The results revealed that the application of a proper insulating material can decrease the heat loss, thermal shock intensity, and joint opening at the hot face although the joint opening during refining stages worsens when severe spalling occurs in certain cycles. The application of compliant insulating materials gives rise to mild thermomechanical loads in the steel shell [24]. Liu et al. [25] established a mathematical model to evaluate the heat preservation performance of the torpedo ladle with and without an insulating lining. The results showed that the torpedo ladle with a nanoporous insulating layer can effectively increase the thermal resistance and improve thermal storage capacity. A two-dimensional finite element model was developed by L. F. V. Gonzalez et al. [2] to compute the temperature distribution in a torpedo car holding pig iron.

Steel ladles, composed of refractories and steel construction components, act as transportation vessels and refining units for the steel melt. Refractory linings insulate the steel shell from the steel melt, and thus reduce the heat loss from the steel shell. A well-lined steel ladle offers efficient temperature control of the steel melt and is beneficial to the steel quality and productivity [26-29]. The performance of a steel ladle is influenced by many factors; for instance, material properties, lining design and thicknesses, and process conditions. The refractory failure analysis [30-32] and the thermomechanical behavior [33-35] of steel ladle linings have been extensively studied with numerical modelling. The ladles with the working lining material of low thermal conductivity, thermal expansion, and Young's modulus showed a better performance in saving energy and reducing average shell temperatures and equivalent stress [36, 37]. Compared with high alumina bricks and alumina magnesia carbon bricks, magnesia carbon bricks perform better on the heating capacity and the lining temperature uniformity [38]. The thickness of the working lining has an impact on the temperature distribution, and the steel shell temperature

increases as the thickness decreases [37, 39-41]. The application of an insulating layer reduces heat loss and the shell temperature [36, 39, 42-45]. Thermal stresses caused by thermal expansion can be released by an expansion joint [46, 47]. Preheating reduces the compressive stress at the hot face of the working lining [34, 42, 48]. The preferable preheating time is 15-20h [49]. An increased preheating temperature can reduce the temperature drop of the steel melt and the temperature gradient of ladle linings [50].

2.1.2. Rotary kilns for cement industry

Rotary kilns are widely used in the cement, metallurgical, chemical industries, etc [51]. Cement kilns are used for the pyro-processing stage of manufacturing of ordinary Portland cement clinker and clinkers of other types of hydraulic cements, in which calcium oxide reacts with silica, alumina and iron oxide-bearing minerals to form a mixture of calcium silicates, aluminates and a calcium aluminate ferrite [52]. As the kiln is heated and rotates during production, it is subjected to a complex stress/strain condition. The state of the refractory lining impacts critically on the availability of the kiln. If the lining is significantly deteriorated and can no longer protect the steel shell from the heat, the production will be shut down and lead to high maintenance costs and production delays [5].

Production capacity and lifetime can be improved with increasing knowledge of lining failure mechanisms. D. Ramanenka et al. [5] studied the influence of ovality, brick's Young's modulus and friction coefficient on stress and brick displacement at two rotational speeds in cold state. It was found that the induced loads in the lining are harmless regardless of the tested conditions – challenging the traditional beliefs [5]. Brick displacements were significantly affected by rotational speed and ovality. The influence of heating and cooling rates on the stress state of the brick lining in a rotary kiln was studied with finite element simulations [53]. The conducted simulations showed that considerable tensile stress may appear in a large area of the brick during the initial heating stage. The positive effect of lower heating rate on the tensile stress was considerable. Five hypothetical cooling rates were investigated: 2, 4, 8, 16 and 32h from steady state temperature (1250 °C) to the ambient temperature for the hot face of the brick lining. The hypothetical cooling rates showed that very high tensile stresses may occur on the surface of the bricks, potentially leading to surface spalling if too fast cooling rates were applied [53]. Axial compaction is highly important on the stress development in the lining [53]. It is recommended

to always to achieve a tight compaction of the brick lining and to take measures to lower the heating and cooling rates. Three commercial alumina silicate bricks were evaluated in compression until failure for a temperature range of 25-1300 °C and the data were used for modelling stress levels of a hot rotary behavior at steady state after the expansion of the system [4]. It was found that for all three brick types the compressive strength increased with rising temperature with a peak in the vicinity of 1000 °C. The maximum increase was between 50 and 150% for the different brick types. After passing 1100 °C the compressive strength rapidly and considerably decreased. The numerical results indicated that severe boundary conditions (expansion of the lining is highly restricted) can potentially lead to a compressive stress up to 34 MPa in the brick lining at steady state [4]. The created model has high potential for being used as a tool in investigations of the lining in hot state. A numerical model was developed by S. EI. Fakkoussi et al. [54] to evaluate the mechanical strength of steel shims and vital components in the drive system of a cement kiln. The results provide a guide to the accurate prediction of the optimal preventative maintenance interval for the rotary cement kilns drive element [54].

2.1.3. Channel induction furnace for foundry industry

Induction furnaces are used extensively for melting, holding and casting metals or alloys in the foundry industry [55]. There are two basic designs of induction furnaces, the core type or channel furnace and the coreless one. The channel induction furnace is preferred for continuous production, owing to its off-shift melting capacity, excellent metal homogeneity and high efficiency [56]. A channel induction furnace consists of a refractory-lined vessel and one or several inductors. An electromagnetic field is created when alternating current from an inductor passes through the inductor coil. Eddy current induced by the electromagnetic induction flows in the charge materials and generates the heat for melting and holding [57]. The efficiency of the furnace is the ratio of the energy used for melting the charge materials to the energy input to the system. The frequency has a critical influence on the energy loss and is one of the main issues when constructing an efficient channel furnace [58]. Thermal stresses in the refractory lining caused by high temperatures during the loading cycle can cause erosion of the lining and premature inductor failure [59, 60].

N. T. T. Hang et al. [58] investigated the influence of three coil shapes (rectangular, extruded and 180 °extruded inductor) on the efficiency of a channel induction furnace through simulation

in two-dimensional space using ANSYS. The highest efficiency of 98.01% is achieved at the remarkable low frequency of 9 Hz because the energy loss at 9 Hz is the minimum in the frequency range of 0 Hz to 60 Hz. The 180° extruded inductor has a higher efficiency than the rectangular and extruded inductor at frequencies higher than 9 Hz. A three-dimensional mathematical model was developed to analyze the magnetic and temperature fields in a lined inductor of melting-holding furnace for copper melting [61]. Two stabilization pauses are necessary to maintain an even temperature of the inductor lining and reduce temperature gradients. Furthermore, the control of the temperature distribution and the gradient could serve as parameters for the diagnosis of the furnace condition. A tool based on a thermal model and unidirectional axial channel flow estimation was developed to monitor the thermal regime of the inductor [59, 60]. The information provided by the tool can be used for the different operating conditions to monitor possible failure resulting from temperature related erosion of the refractory. For the possible energy savings and extension of the volume capacity, 16 lining concepts of a channel induction furnace were designed by an orthogonal array with considering different lining materials and thicknesses [57]. Finite element simulations were carried out to determine the temperatures and stresses during the preheating and holding. A thickness-thickness-temperature isothermal map was provided to show the acceptable thickness range of working and insulating linings. Thermal and thermomechanical evaluations were performed for two channel induction furnaces with different insulating materials [56]. Compared with the channel induction furnace with an insulation currently used in the factory, the other one with a lighter insulation reduces the heat loss from the steel shell and material consumption. Moreover, the thermomechanical loads in the refractory linings and steel shell remain within a reasonable range [56].

2.2. Methods applied for optimization and prediction

2.2.1. The Taguchi method

2.2.1.1. Introduction

The Taguchi method was developed by G. Taguchi in the late 1940s as a process optimization technique [62] and is generally implemented in both the design and manufacturing phase of a product. It is used to assess how product quality is affected by controllable and uncontrollable factors in order to determine optimal levels for control factors in relation to product specification

and usage requirements [63]. Successful applications of the Taguchi method have taken place in many areas, for example, manufacturing processes [64-68], material design and development [69-73], and geometry design [74, 75].

The main techniques for design stage in the Taguchi method are orthogonal arrays (OAs), analysis of variance (ANOVA), and signal-to-noise (S/N) ratio. In general, the applications of the Taguchi method includes the following steps [76-80]: (1) definition of the investigated problem and the goals; (2) determination of factors that have influences on the responses and the levels of these factors; (3) experimental design using orthogonal arrays; (4) performance of experiments; (5) evaluation of the factor significance via ANOVA and determination of the optimal levels of the factors by S/N ratios; (6) validation of optimal cases.

2.2.1.2. Orthogonal arrays (OAs)

The experimental design of the Taguchi method is carried out by orthogonal arrays, which are highly fractional factorial designs, capable to consider the effects of multiple factors on the responses, and yield a minimum number of experiments [76]. An orthogonal array can be denoted by $OA(N, k, s, t)$, where N is the number of rows, k is the number of columns, s is the number of symbols, and t is the strength. In orthogonal arrays the number of rows is equivalent to the number of experiments and each row presents a combination of factor-levels in a certain experiment; the number of columns equals to the number of factors and each column indicates one factor; the number of symbols equals to the number of levels [76]. In an orthogonal array with a strength of t , the occurrence of any level of every factor is equal in each column, and all combinations of levels in t factors occur with equal frequency. These properties are called the balancing and orthogonality properties of orthogonal arrays [81]. For example, $OA(4, 3, 2, 2)$ is an array with the strength of two and can be represented by the following matrix:

$$\begin{bmatrix} 0 & 0 & 0 \\ 0 & 1 & 1 \\ 1 & 0 & 1 \\ 1 & 1 & 0 \end{bmatrix}$$

There are two levels in the first column, 0 and 1, both occur twice in this column. This is the balancing of orthogonal arrays. As the strength of the orthogonal array is two, so the second and the last columns are taken to explain the orthogonality. There are four level combinations of

these two columns: [0,0], [1,1], [0,1], [1,0]. The total number of rows is four, hence each combination occurs once. In addition, according to the number of factors and their levels, different orthogonal arrays can be used in the Taguchi method. There are two types of orthogonal arrays: pure orthogonal arrays and mixed-level ones. In a pure orthogonal array, the number of levels is the same for all factors. If this is not the case, a mixed-level orthogonal array can be applied.

2.2.1.3. Analysis of variance (ANOVA)

ANOVA can be used to estimate the significance of each factor. It's a multivariate statistical technique for inferring whether there are really differences between the averages of variables in a population, based on the experimental results [82]. In order to determine whether the differences are significant, the differences between the experiments, variance, are calculated with ANOVA. The sum of squares, the degree of freedom, and the percentage of contribution are included in an ANOVA table. There are three types of the sum of squares, namely, the total sum of the squares, the factor sum of the squares, and the error sum of squares (also called experimental error) that is calculated by subtracting the sum of all factor sums of squares from the total sum of squares. The factor with the highest percentage of the contribution is ranked the highest in terms of the relative significance among all the factors, because it has a major contribution in the overall variance. There are several advantages of ANOVA [83]: (1) sum of squares of each factor is accounted; (2) high error contribution indicates that some necessary factors have not been included in the study; (3) the confidence interval for optimal conditions can be constructed; (4) the results can be statistically validated.

2.2.1.4. Signal-to-noise (S/N) ratio

The signal-to-noise (S/N) ratio is extensively used as a quality index, rather than being merely associated with the signal and noise [1]. S/N ratio follows a transformation of the trial results into a logarithmic scale, which changes the results of unknown nonlinear behavior into a linear relationship with the influencing factors [62]. Based on the quality characteristics to be optimized, different S/N ratios can be chosen [1,62]: smaller-the-better, nominal-the-best, and larger-the-better. The S/N ratios can be calculated by equations (1) - (3). The experimental conditions with the highest S/N ratios are selected as optimal conditions.

$$\text{Smaller-the-better: } S/N = -10\log\left(\frac{1}{n_i}\sum_{j=1}^{n_i} y_{ij}^2\right) \quad (1)$$

$$\text{Nominal-the-best: } S/N = -10\log\left(\frac{1}{n_i}\sum_{j=1}^{n_i} (y_{ij} - \bar{y}_i)^2\right) \quad (2)$$

$$\text{Larger-the-better: } S/N = -10\log\left(\frac{1}{n_i}\sum_{j=1}^{n_i} \frac{1}{y_{ij}^2}\right) \quad (3)$$

Where n_i is the number of experiments at the i^{th} level, y_{ij} is the value of the j^{th} observation at the i^{th} level, and \bar{y}_i is the mean value of the observations at the i^{th} level of a factor.

2.2.2. Back-propagation artificial neural network (BP-ANN)

2.2.2.1. Introduction

Artificial neural network (ANN) is a popular machine learning technique started in 1940s [84] and also an abstract computational model based on the organizational structure of the human brain [85]. ANN is capable to represent any nonlinear mapping to the required accuracy [86] and has many advantageous characteristics, which include generalization, adaptation, universal function approximation, parallel data processing, robustness, etc. [84]. Therefore, it has been widely applied in various areas such as function approximation, process control, clustering, pattern recognition, and prediction [87]. Among these applications, predictive models based on ANN technique were extensively employed to solve real world nonlinear problems in civil engineering [88-94], material design and development [95-106], structure damage detection [107-109], geotechnical engineering [110-113], and steelmaking industry [114-121].

An ANN is composed of a set of interconnected processing units, called nodes or neurons [84,122]. The nodes are arranged in layers: one input layer, one output layer, and one or more hidden layer(s) between the input and the output layers [87]. Each node in the input layer is connected to every node in the hidden layer, which is connected to the nodes in the output layer. The connection between two nodes is called synapse, and each synapse has an associated strength or weight, which affects the output of the node. Figure 1 is a schematic of a three-layer ANN model [122]. Input variables (x) are introduced to the network as a vector corresponding to the nodes in the input layer. These input variables are multiplied by their respective weights (w) and a bias (b) is added, yielding a summation (S) for each node of the hidden layer, as shown in

equation (4) [122]. An activation function is used to limit the amplitude of the summation of each hidden layer node, which is the input for the next layer nodes, as depicted by equation (5) [122].

$$S_k = \sum_{j=1}^{N_v} w_{jk} x_j + b \quad (4)$$

$$O_k = f(S_k) \quad (5)$$

Where N_v is the number of input variables, k is the node index in the hidden layer, S_k is the sum at the k^{th} node in the hidden layer, f is the activation (e.g. logistic function, hyperbolic tangent function, Gaussian function), w_{jk} is the weight of the j^{th} input at the k^{th} node, x_j is the j^{th} input, b is the bias and O_k is the output of the k^{th} node in the hidden layer. The information transfer between the hidden layer and output layer follows the same mathematical process. The obtained values from output layer (y) are a function of input values (x) and the weights (\vec{w}) in the network.

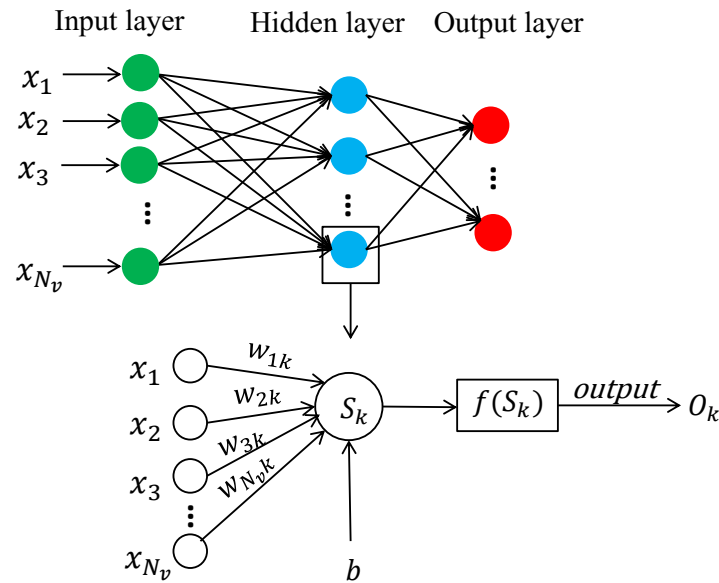


Figure 1. A schematic of a three-layer ANN model [122].

The main architecture of ANN can be divided into single-layer networks, multilayer perception networks, recurrent networks, and mesh networks according to the interconnection of nodes and the composition of layers [84]. The multilayer perception (MLP) network trained with error backpropagation (BP) algorithms is usually preferable to solve prediction problems [102]. Backpropagation algorithm is a supervised learning method and requires a dataset of input-

output vector pairs [88]. It contains two main phases, referred to as the forward and backward phases, respectively [124]. In the forward phase, the inputs are processed layer-by-layer until the production of the corresponding outputs. The predicted values at the output layer are compared with the target values and errors are calculated. The performance of the network is represented by a so called error function $E(\bar{w})$ (eq.6) which is defined as the half sum of squared differences between the outputs from the network y and the target values d , considering all training samples [84]. In the backward phase, weights among layers are adjusted to minimize the error $E(\bar{w})$ [84]. There is a loop between the two phases to obtain an optimal \bar{w}^* so that the error $E(\bar{w}^*)$ of the whole sample set is as low as possible.

$$E(\bar{w}) = \frac{1}{2} \sum_{i=1}^{N_t} (d_i - y_i(\bar{w}))^2 \quad (6)$$

Where N_t is the total number of training samples, d_i is the target value of the i^{th} training sample, and $y_i(\bar{w})$ is the output value of the i^{th} training sample from the network.

2.2.2.2. Establishment of ANN models

The predictive quality of a BP-ANN model is influenced by the properties of the dataset [125-128], training algorithms [129-132], and the architectural parameters [106], especially the number of hidden layers and node number of each layer.

2.2.2.2.1. The dataset properties

Three items need to be taken into account considerably for a representative dataset design. First is the input variable selection. The selected variables should be informative enough to survey the input-output relations [126]. Second is the quality of the dataset. The data should be collected in a way that ensures they are distributed evenly in the entire variable space [106]. The last one is the dataset size. The minimum training dataset size largely depends on the nature or the complexity of the problem and applied ANN architecture [106]. According to an empirical rule, the minimum dataset size is approximately 10 times the number of weights and biases in the network [133].

2.2.2.2.2. Training algorithms

Training algorithms perform the minimization of the error $E(\vec{w})$ (eq. 6) by adjusting the weight vector \vec{w} [134]. Many training algorithms have been developed to minimize the error function with different strategies [135-138]. The commonly-used training algorithms are based on gradient descent, conjugate gradient, quasi-Newton, one-step-secant, and Bayesian regularization method.

Gradient descent method

The gradient descent with momentum and adaptive learning rate (GDX) algorithm is an advanced gradient descent approach adding a momentum item and adaptive learning rate in the weight adjustment formula. The GDX algorithm [135] adjusts the weights along the steepest gradient of the error function (eq.6) with considering both the current gradient descent and the recent changes of the weights. The amount of weight update of iteration r is determined by the so called delta rule and calculated according to equation (7):

$$\Delta \vec{w}_r = -\eta \frac{\partial E(\vec{w}_r)}{\partial \vec{w}_r} + \alpha \Delta \vec{w}_{r-1} \quad (7)$$

where w is the weights, $E(\vec{w})$ is the error function, η is called learning rate, and α is called momentum and may defined by the user in the range (0,1). The value of momentum determines the size of the contribution of the most recent weights update on the current weights adjustment [137]. A higher momentum value leads to a larger training step and hence a faster training [137]. Conversely, lower momentum value slows down the training speed [139]. Similarly, the larger the learning rate, the faster the training. But, if the learning rate is too large, the network reacts quickly to the input changes and may become unstable [139] whilst the training may be inefficient with a small learning rate.

Conjugate gradient method [135-137]

A series of line searches along conjugate directions were employed in conjugate gradient method to determine the optimal step size of the weight update. The conjugate gradient training includes three steps [135]. The first step [135] is the initialization of weights and the search direction indicated with d_0 (eq.8). The second step [135] is to search a local minimum in error along a

certain search direction; the weights will be adjusted to the local minimum point (eq.9). The third step [135] is to calculate the conjugate of the pervious search direction as the new search direction (eq.10); the global minimum error is obtained through iterations.

$$\vec{d}_0 = -\frac{\partial E(\vec{w}_0)}{\partial \vec{w}_0} = \vec{g}_0 \quad (8)$$

$$\vec{w}_{r+1} = \vec{w}_r + \eta_r \vec{d}_r \quad (9)$$

$$\vec{d}_{r+1} = \vec{g}_{r+1} + \beta_r \vec{d}_r \quad (10)$$

Where \vec{g}_r is the negative gradient vectors ($-\nabla E(w_r)$) in iteration r ; parameter β_r can be calculated by using either the Fletcher-Reeves algorithm (eq. 11) or the Polak-Ribiere algorithm (eq. 12) [137]. The widely used algorithms based on conjugate gradient method are Fletcher-Reeves (CGF), Polak-Ribiere (CGP), Powell-Beale (CGB), and scaled conjugate gradient (SCG).

$$\beta_r = \frac{(\vec{g}_{r+1})^T \vec{g}_{r+1}}{(\vec{g}_r)^T \vec{g}_r} \quad (11)$$

$$\beta_r = \frac{(\vec{g}_{r+1})^T [\vec{g}_{r+1} - \vec{g}_r]}{(\vec{g}_r)^T \vec{g}_r} \quad (12)$$

In CGF and CGP, the parameter β_r is calculated by equation (8) and (9), respectively. The CGB uses the same learning model to compute the conjugate direction with CGF, but resets the search direction to the negative of the gradient using a method described by Powell when the error function is non-quadratic [140]. Therefore, CGB requires a slightly larger memory space than other conjugate gradient algorithms due to the computation of the restarting procedure. The SCG is a variation of the conjugate gradient method and uses second order information obtained from Levenberg-Marquardt algorithm [140]. The weights are still adjusted along the conjugate directions [140]. However, a parameter is used to adjust Hessian matrix and assures that it is positive-definite at each iteration, avoiding the need to perform a line search. The SCG may require more iterations to converge than other conjugate gradient algorithms, but it usually involves less computation complexity and requires less computer memory for each iteration since no line search is needed [140].

Quasi-Newton method [135, 137, 138]

A local quadratic approximation of the error function (eq.6) is used for weight update in the Newton's method. The weight update of the iteration r of the Newton's method [84] is based on the Hessian matrix (H_r , the matrix of second order derivatives) of error function $E(\vec{w})$, as show in equation (13). The quasi-Newton method updates an approximate Hessian matrix (B) by a function of the gradient. The computational complexity is substantially reduced compared with the Newton's method. Broyden–Fletcher–Goldfarb–Shanno (BFGS) update is considered to be one of the most successful procedures to iteratively approximate Hessian matrix. The equations (14) - (16) are applied in the BFGS for Hessian matrix approximation (B_{r+1}) and weights for iteration $r+1$ [138]. When compared with conjugate gradient algorithms, the BFGS generally converges in fewer iterations and is more suitable for small networks with limited number of weights, but requires more complex computations and larger memory usage for each iteration.

$$\vec{w}_{r+1} = \vec{w}_r - H_r^{-1} \vec{g}_r \quad (13)$$

$$\vec{G}_r = \vec{g}_{r+1} - \vec{g}_r \quad (14)$$

$$\vec{W}_r = \vec{w}_{r+1} - \vec{w}_r \quad (15)$$

$$B_{r+1} = B_r + \frac{\vec{G}_r \vec{G}_r^T}{\vec{G}_r^T \vec{W}_r} - \frac{B_r \vec{W}_r \vec{W}_r^T B_r}{\vec{W}_r^T B_r \vec{W}_r} \approx (H_{r+1})^{-1} \quad (16)$$

One-step-secant (OSS) method [139]

The OSS represents an attempt to bridge the gap between the conjugate gradient and the quasi-Newton algorithms to fulfill the need for a secant approximation with smaller storage and computation requirements. The OSS does not store the complete Hessian matrix and assumes that the previous Hessian was the identity matrix [140]. The additional advantage of the OSS is that the new search direction can be calculated without computing a matrix inverse. Therefore, the OSS requires less storage and computation per iteration than the BFGS, but slightly more than the conjugate gradient algorithms.

Bayesian regularization method [141-145]

The Bayesian regularization (BR) algorithm aims to minimize a linear combination of mean sum of squared network errors $E(\vec{w})$ (eq.6) and the sum of squared network weights $S(\vec{w})$ [141]. The

added item $S(\vec{w})$ can improve the generalization capability (the ability to handle new data with the acquired knowledge through the learning process). The regularization can be expressed as follows [141]:

$$F(\vec{w}) = \beta E(\vec{w}) + \alpha S(\vec{w}) \quad (17)$$

$$S(\vec{w}) = \frac{1}{2} \sum_{i=1}^m w_i^2 \quad (18)$$

where $F(\vec{w})$ is the objective function, $E(\vec{w})$ is the sum of squared errors, m is the total number of network weights, $S(\vec{w})$ is a weight decay regularizer, and α and β are the parameters determine how much the weight decay regularizer is involved in the error function $F(\vec{w})$. The parameters α and β now become additional objectives of the network optimization process and need to be determined.

In a Bayesian network, the network weights are assumed to be random variables. The density function [142-144] of the weights and parameter α and β are then determined using Bayesian's theorem, which is described by the following equation:

$$P(x|D, \alpha, \beta, M) = \frac{P(D|x, \beta, M)P(x|\alpha, M)}{P(D|\alpha, \beta, M)} \quad (19)$$

where x is the vector containing the weight and bias in the network; D represents the data vector; and M is the neural network model being used. Forsee and Hagan [145] assumed that the noise in the data was a Gaussian distribution. The optimization of the regularization parameters α and β requires computing the Hessian matrix of $F(\vec{w})$ at the minimum point w^{MP} [142]. Forsee and Hagan [145] proposed a Gauss-Newton approximation to the Hessian matrix, which is possible if the Levenburg-Marquardt training algorithm is used to locate the minimum. This technique reduces the potential for arriving at local minima, and thus increases the generalizability of the network.

2.2.2.2.3. Node number in the hidden layer

The definition of proper architectural parameters, especially the hidden layers number and the node number in each layer, is challenging for ANN model establishment. Generally, an ANN model with one single hidden layer is sufficient to survey the input-output relations [133].

Therefore, the determination of the suitable node number in the hidden layer is the key issue. The proper node number in the hidden layer depends on the problem nature or complexity and the node numbers in the input and output layers [146]. In general, an ANN model with a larger number of nodes in the hidden layer can achieve more accurate training results and is capable to model more complicated relations, but increases the risk of over-fitting. Contrarily, an ANN model with a smaller number of nodes in the hidden layer may be insufficient to depict the underlying relations [134]. To seek an optimal node number, many researchers employed the trial and error method with a diverse range of node numbers [147-151]. Some researchers merely followed the rules of thumb and the application of rules can significantly reduce the number of trials. The common used empirical rules [84, 152-159] are summarized as follows:

$$N_h = (N_i + N_o)^{1/2} + a \quad a \in [0,10] \quad (20)$$

$$N_h = (N_i + N_o)^{1/2} + a \quad a \in [1,10] \quad (21)$$

$$N_h = (N_i \times N_o)^{1/2} \quad (22)$$

$$N_h = N_{train}/(N_i + 1) \quad (23)$$

$$N_h = \frac{1}{2} (N_i + N_o) + N_{train}^{1/2} \quad (24)$$

$$N_h = \frac{2}{3} N_i + N_o \quad (25)$$

$$N_h \leq 2N_i \quad (26)$$

$$2\sqrt{N_{train}} + N_o \leq N_h \leq 2N_{train} + 1 \quad (27)$$

where N_i , N_h , and N_o are the node numbers in the input, hidden, and output layers; N_{train} is number of training samples; and a is an empirical integer not larger than 10.

3. Investigations and results

A steel ladle of Voestalpine was the object used for lining concept optimization. Figure 2 (a) depicts the simplified two-dimensional model representing a horizontal cut through the slag-line position in the upper part of the steel ladle [1]. The outer diameter of the steel ladle is 1.828m. The model is composed of a two-half brick working lining, a monolithic permanent lining, a fiber board, and a steel shell. Another model including an additional insulating lining was established for lining concept optimization, as shown in Figure 2 (b) [1]. The permanent lining was made of bricks in this model. The radial expansion allowance between two bricks in both two models was 0.4 mm. Factors were lining and steel shell thicknesses, thermal conductivity, and Young's modulus of lining materials and listed in Table 1 [1]. The interested thermal and thermomechanical responses were the end temperature and the maximum tensile stress at the cold end of the steel shell, and the maximum compressive stress at the hot face of the working lining.

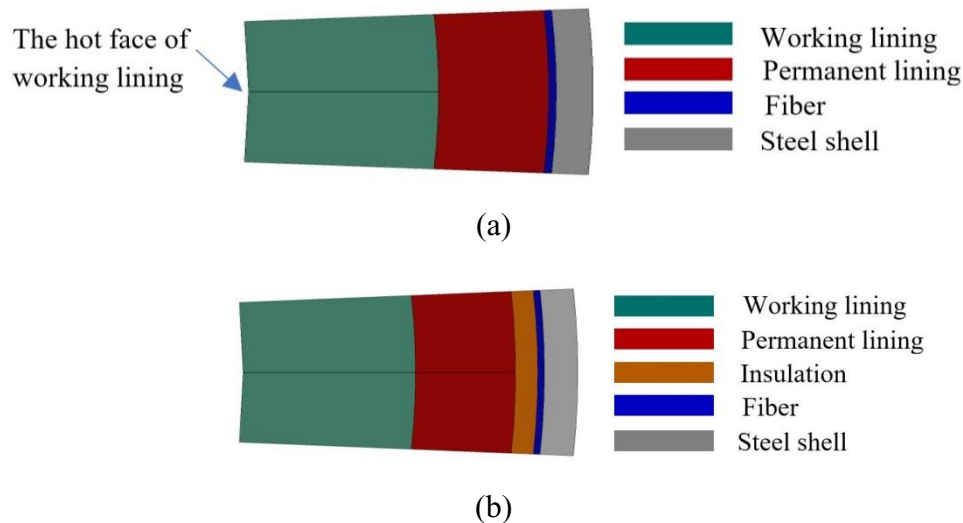


Figure 2. Two-dimensional model of (a) the reference steel ladle case; (b) the steel ladle for the lining concept optimization study [1].

Table 1. Geometrical and material property variations of the steel ladle [1].

Impact factors		Label of factors
Thickness	Working lining	A
	Permanent lining	B
	Insulation lining	C
	Steel shell	J
Thermal conductivity	Working lining	D
	Permanent lining	E
	Insulation lining	F
Young's modulus	Working lining	G
	Permanent lining	H
	Insulation lining	I

FE-modeling of the steel ladle, taking into account elastic material behavior, was performed using the commercial software, ABAQUS. The simulation [1] included the preheating of the hot face of the working lining to 1100 °C over 20h, and a subsequent thermal shock caused by tapping the steel melt of 1600 °C into the ladle. After a refining period of 95 min, a 50 min idle period proceeded. Displacement of linings was allowed in the radial direction and constrained in the circumferential direction with a symmetry condition [1]. The heat transfer between the liquid melt and the hot face of the working lining, the cold end of the steel shell, and the atmosphere was defined as being temperature-dependent using a surface film condition function [1]. The interfaces between linings were crossed by heat flux, and a heat transfer coefficient allowing for radiation and convection was applied [1].

3.1. Optimization of steel ladle lining via the Taguchi method

Thirty-two lining configurations defined in terms of a mixed-level orthogonal array $L_{32} (4^9 \times 2^1)$ were used to optimize steel ladle lining with respect to their thermal and thermomechanical behavior. Ten factors were of interest, nine of which had four levels and the thickness of the steel shell had two levels. The results [1] of ANOVA and S/N ratios are summarized in Figures 3 and 4.

3.1.1. Factor significance ranking

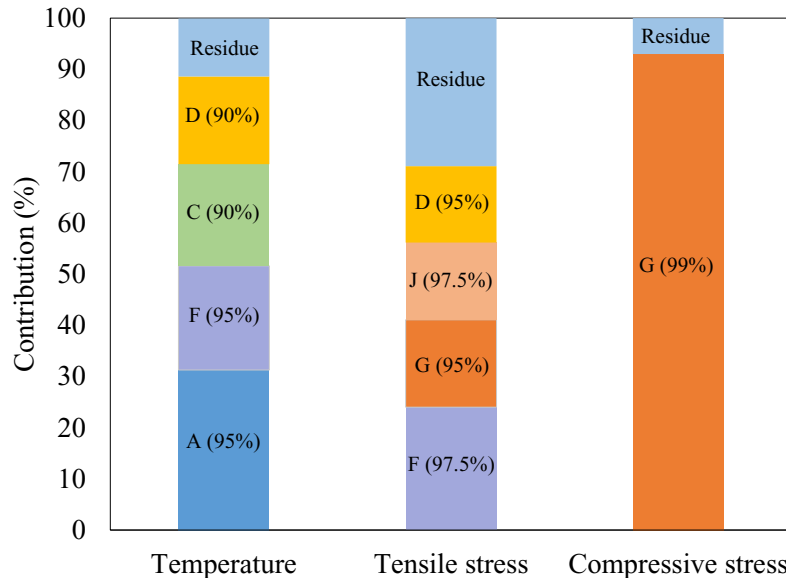


Figure 3. Contribution and confidence levels (in parentheses) of factors for thermal and thermomechanical responses [1].

Figure 3 shows the significance of factors to thermal and thermomechanical responses according to ANOVA. The top four significant impact factors to the temperature at the cold end of the steel shell were the thickness of the working lining (A), the thermal conductivity of the insulation material (F), the thickness of insulation material (C), and the thermal conductivity of the working lining material (D), in descending order [1]. Their individual confidence levels were all higher than 90% and they together contributed 89% to the variance of the temperature at the cold end of the steel shell. The thermal conductivity of the insulation material (F), the Young's modulus of the working lining material (G), the thickness of the steel shell (J), and the thermal conductivity of the working lining material (D) were the first top four impact factors to the maximum tensile stress at the cold end of the steel shell. Each of them had confidence levels higher than 95% and contributed 71% to the variance of the tensile stress [1]. The Young's modulus of the working lining material (G) had an overwhelming influence on the maximum compressive stress at the hot face of the working lining, with a 93% contribution [1].

3.1.2. Optimal levels

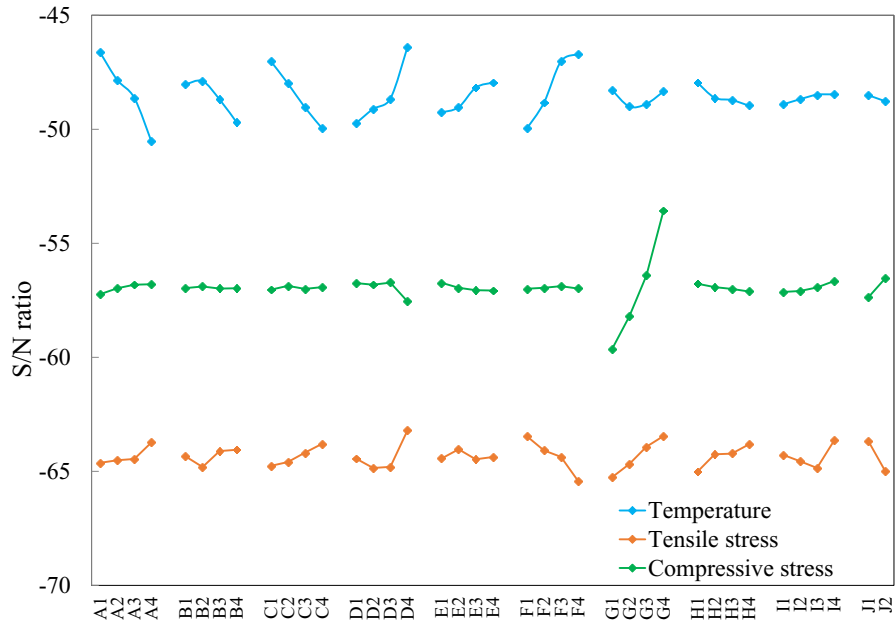


Figure 4. S/N ratios for the thermal and thermomechanical responses [1].

Figure 4 shows the optimal S/N ratios of the individual factors for the temperature at the cold end of the steel shell, the maximum tensile stress at the cold end of the steel shell, the maximum compressive stress at the hot face of the working lining were A1B2C1D4E4F4G1H1I3J1, A4B4C4D4E2F1G4H4I4J1, and A4B2C2D3E1F3G4H1I4J2, respectively [1].

3.1.3. Proposal and validation of optimal lining concepts

With taking into account the results of ANOVA, S/N ratios, and the practical materials, two optimal lining concepts were proposed. The details of lining structure and material properties are shown in Table 2 [1]. The comparison of the dimensionless responses between the reference case and the two optimal lining concepts is given in Table 3 [1]. The temperature at the cold end of the steel shell and the maximum compressive stress at the hot face of the working lining were decreased by 19% and 26% for case 1, and 25% and 25% for case 2, with a slight increase of the maximum tensile stress at the steel shell [1].

Table 2. Two proposed optimized lining concepts with different insulation materials [1].

	Thickness (mm)	Thermal conductivity (W m ⁻¹ K ⁻¹)	Young's modulus (GPa)	Thermal expansion coefficient (10 ⁻⁶ K ⁻¹)
Working lining	155.0	9.0	40	12.0
Permanent lining	52.5	2.2	45	5.0
Insulation (Case1)	37.5	0.5	3	6.0
Insulation (Case2)	37.5	0.4	4	5.6
Steel shell	30.0	50.0	210	12.0

Table 3. Comparison of results for the reference case and optimal cases without changing the volumetric capacity of the steel ladle [1].

	Dimensionless temperature at the cold end of the steel shell	Dimensionless maximum tensile stress at the steel shell	Dimensionless maximum compressive stress at the hot face of the working lining
Reference case	1	1	1
Optimal case 1	0.81	1.16	0.74
Optimal case 2	0.75	1.19	0.75

3.2. Prediction of thermal and thermomechanical responses with BP-ANN models

The training dataset contained 160 samples constituted by ten factors and three responses obtained from FE simulations. Three-layer BP-ANN models developed using MATLAB were employed to predict the thermal and thermomechanical responses. The responses were predicted by the leave-one-out (LOO) cross validation method. The quantities used to quantitatively assess the performance of the BP-ANN models were maximum relative error of all testing results (RE_MAX), mean relative error (MRE), relative root mean squared error (RRMSE), and coefficient of determination (B), as shown in equations (28) - (31) [122]:

$$RE_MAX = Max\left(\frac{|d_i - y_i|}{d_i}\right) \quad (28)$$

$$MRE = \frac{1}{n} \sum_{i=1}^n \frac{|d_i - y_i|}{d_i} \quad (29)$$

$$RRMSE = \frac{\sqrt{\frac{1}{n} \sum_{i=1}^n (d_i - y_i)^2}}{\bar{d}} \quad (30)$$

$$B = 1 - \frac{\sum_{i=1}^n (d_i - y_i)^2}{\sum_{i=1}^n (d_i - \bar{d})^2} \quad (31)$$

where n is the number of the testing samples, y_i is the predicted value of the i^{th} testing sample by the BP-ANN models, d_i is the response value of the i^{th} sample from FE modeling, and \bar{d} is the mean response value of all testing samples received from the FE modeling. The influence of the dataset properties (variable completeness and dataset size), the node number in the hidden layer, and training algorithms on the BP-ANN prediction performance were investigated.

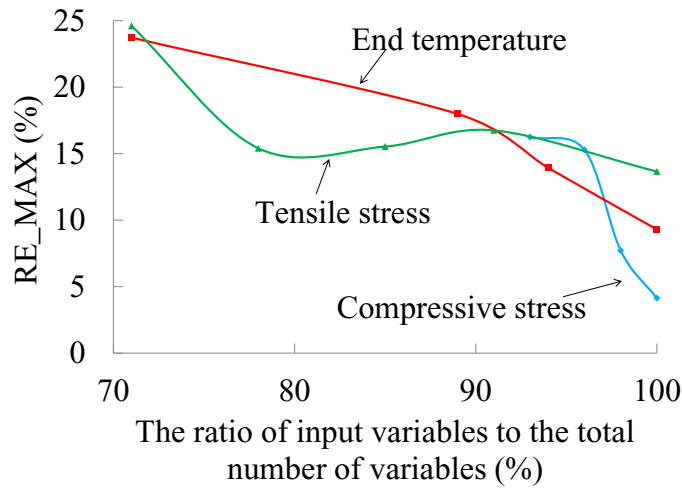
3.2.1. Architectural parameters study of BP-ANN model

3.2.1.1. Dataset properties

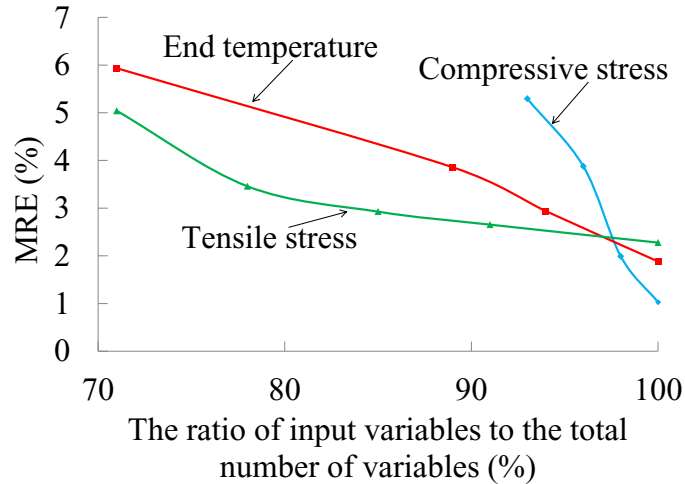
The influence of variable completeness (the ratio of input variables to the total number of variables) on the BP-ANN prediction performance is shown in Figure 5 [146]. The definition of the symbols is show in Table 1 and combinations of input variables together with their contribution to the response are listed in Table 4 [146]. In general, for all three responses, lower RE_MAX, MRE and larger B can be achieved with increasing variable completeness [146]. The minimum numbers of variables for temperature, tensile stress, and compressive stress were 5, 6, and 3 to reach arbitrarily defined error tolerances, i.e. 15% for RE_MAX, 3% for MRE, and 0.90 for B [146].

Table 4. Variable combinations and their contribution to the response for BP-ANN models [146].

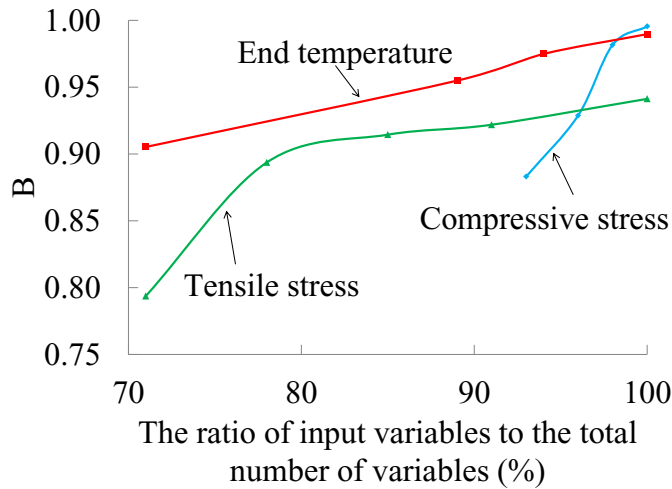
Response	Number of input variables	Variable labels	Contribution to response (%)
Compressive stress	1	G	93
	2	G, J	96
	3	G, J, D	98
	10	A - J	100
End temperature	3	A, D, F	71
	4	A, D, F, C	89
	5	A, D, F, C, E	94
	10	A - J	100
Tensile stress	4	F, G, D, J	71
	5	F, G, D, J, C	78
	6	F, G, D, J, C, H	85
	7	F, G, D, J, C, H, I	91
	10	A - J	100



(a)



(b)



(c)

Figure 5. Performance assessment (a) RE_MAX, (b) MRE, and (c) B of BP-ANN models with different variable completeness [146].

Seven cases were applied to test the appropriate dataset size for reliable BP-ANN models with the end temperature as response. The dataset contains 160 cases and was designed by five orthogonal arrays, each with 32 runs. The lining configurations from the orthogonal array containing the maximum and minimum level values constituted the boundary space, termed space A, and were used only for BP-ANN model training. The lining configurations from the other four orthogonal arrays were named as spaces B, C, D, and E [122]. The maximum level values of all ten variables in space B, C, D, and E were defined in a descending order, and their minimum level values were in an ascending order accordingly [122]. Spaces B-E were used for

BP-ANN model training and testing. The dataset size of ABC, ABD, and ABE is 96; that of ABCD, ABCE, and ABDE is 128, and that of ABCDE is 160 [122]. Dimensionless performance was calculated for each quantity relative to its largest value, shown in Figure 6 [122]. Generally, better performance is achieved by increasing the dataset size. A conservative minimum sample size for the present study was 160, which is 16 times the number of input variables [122].

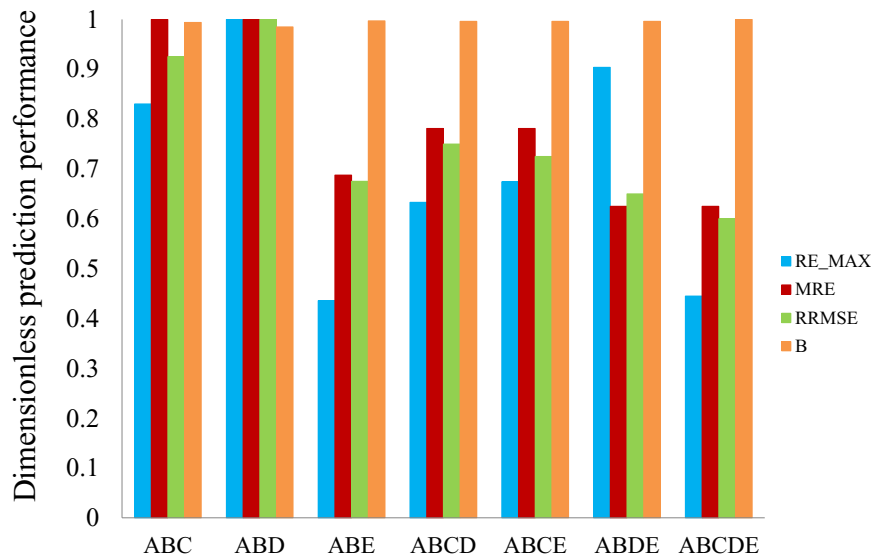
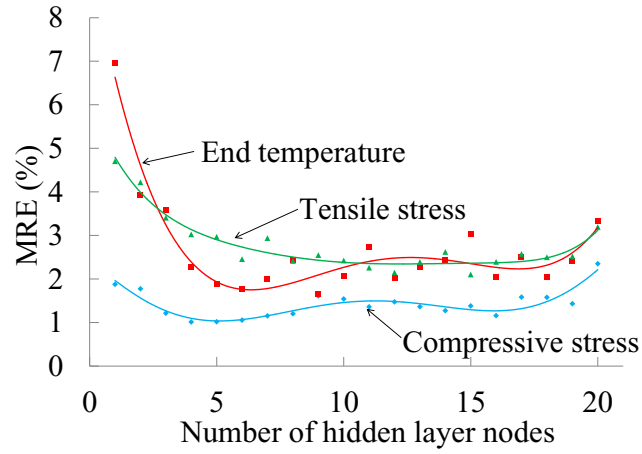


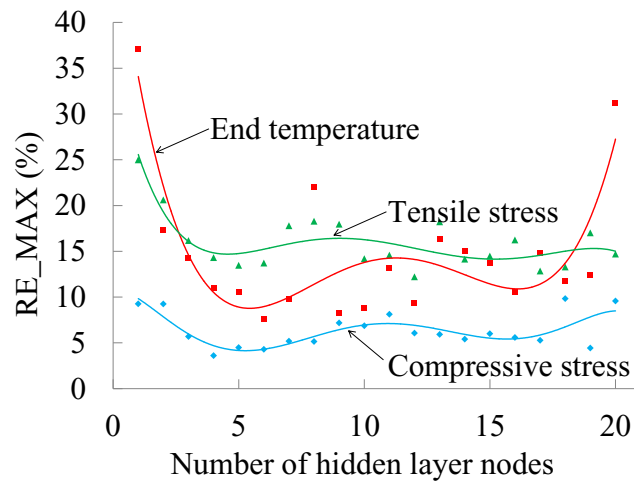
Figure 6. Performance assessment of the BP-ANN for temperature prediction with different dataset sizes [122].

3.2.1.2. Node number in the hidden layer

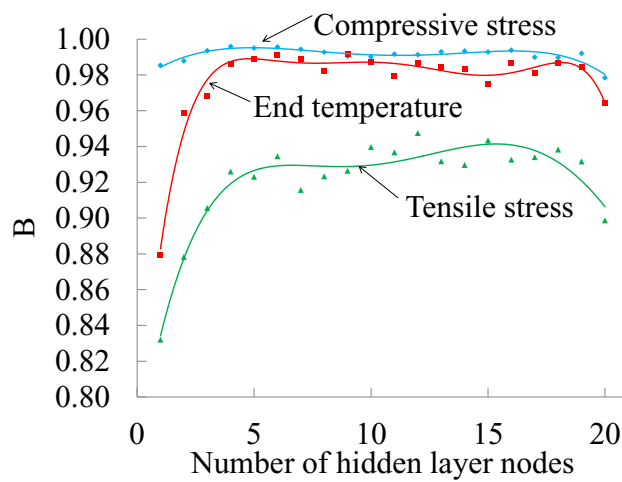
The node number in the hidden layer was varied from 1 to 20 for each response. The assessment of the prediction performance (Figure 7) shows that the performance was significantly improved by increasing the node number in the hidden layer to 7. However, the performance was oscillatory with further increasing node number; the larger number of nodes may lead to overfitting and affect the generalization capability [146]. It also shows that each response had different optimal ranges. The range was 4 to 6 for the maximum compressive stress at the hot face of the working lining, 5 to 7 for the end temperature of the steel shell, and 10 to 12 for the maximum tensile stress at the cold end of the steel shell [146].



(a)



(b)



(c)

Figure 7. Performance assessment (a) RE_MAX, (b) MRE, (c) B of the BP-ANN models with different node numbers in the hidden layer [146].

Guidelines were also proposed to define node number in the hidden layer for a steel ladle system as a function of the node number in the input layer weighted with a function A of the percent value of the significant variable contributing above 90% to the response (PF), as well as the node number in the output layer [146]. The guidelines are shown in equations 21–23 [146] and in Figure 8 [146].

$$\text{Lower boundary: } N_h = AN_i + N_o \quad (21)$$

$$\text{Upper boundary: } N_h = (A + 0.2) N_i + N_o \quad (22)$$

$$A = f(PF) = 0.2982 - 0.001242 (1 - e^{0.08836*PF}) \quad (23)$$

where A is a function of PF, N_i , N_h , and N_o are the node numbers in the input, hidden, and output layers, respectively.

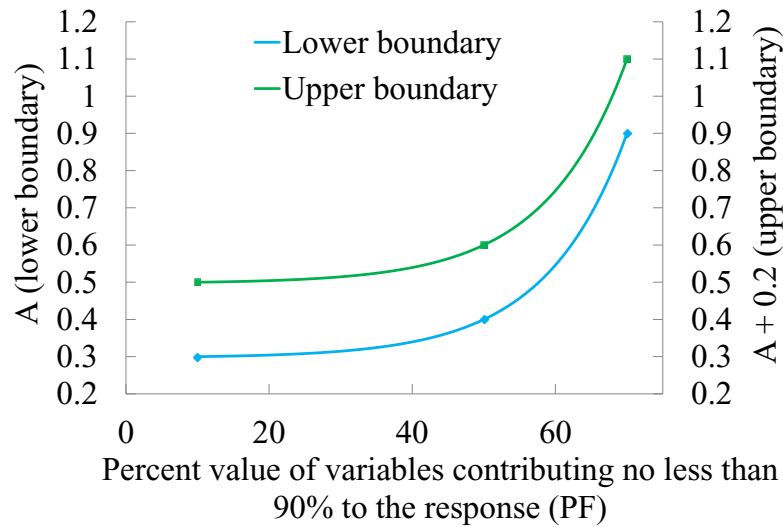


Figure 8. The relation between PF and A [146].

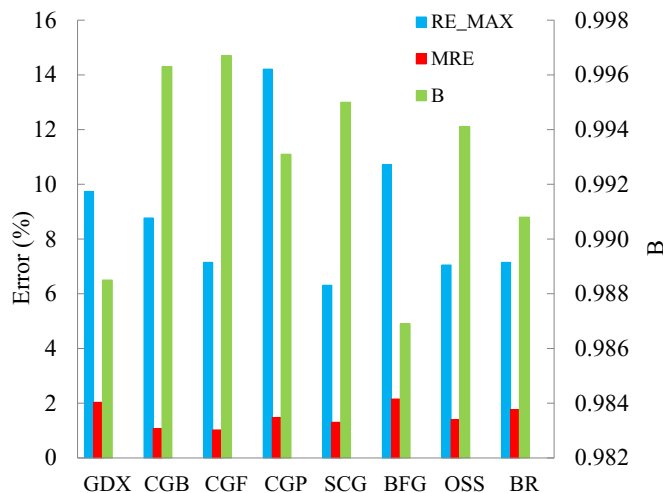
3.2.1.3. Training algorithms

Eight training algorithms (listed in Table 5) were employed individually to predict end temperature at the cold end of the steel shell. The performance results are presented in Figure 9. As shown in Figure 9 (a) [122], the RE_MAX and MRE from the cases with CGF, SCG, OSS, and BR were less than those from GDX, CGB, CGP, and BFG. However, calculations with algorithms SCG and OSS were time consuming, as shown in Figure 9 (b) [122]. Therefore, the

algorithms CGF and BR were proposed to predict the thermomechanical responses. It is demonstrated that the BP-ANN model using BR performed better than the model with CGF for thermomechanical responses. Therefore, BP-ANN models with BR were proposed for the further steel ladle study.

Table 5. Training algorithms employed in this study [122].

Training algorithm	Brief description
GDX	Gradient descent with momentum and adaptive learning rate back-propagation
CGB	Conjugate gradient back-propagation with Powell-Beale restarts
CGF	Conjugate gradient back-propagation with Fletcher-Reeves updates
CGP	Conjugate gradient back-propagation with Polak-Ribière updates
SCG	Scaled conjugate gradient back-propagation
BFG	BFGS quasi-Newton back-propagation
OSS	One-step secant back-propagation
BR	Bayesian regularization back-propagation



(a)

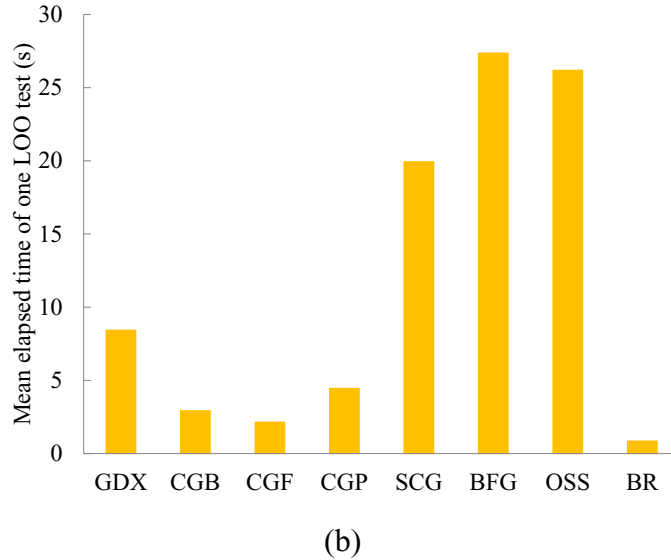
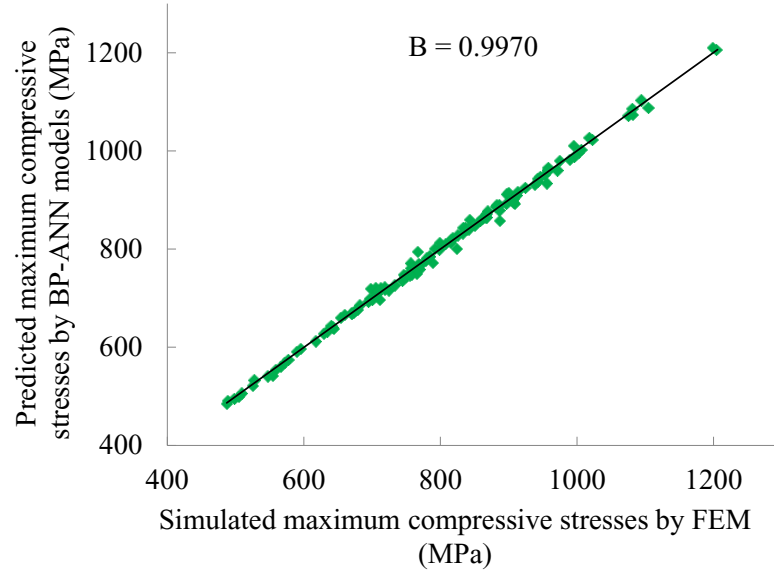


Figure 9. Performance assessment of the BP-ANN model for (a) temperature prediction based errors, and (b) computation time with different training algorithms [122].

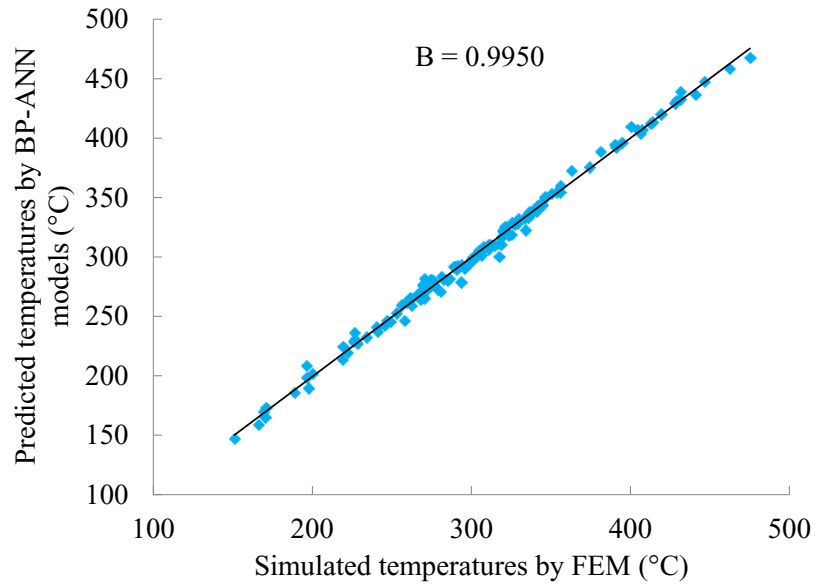
3.2.2. Thermal and thermomechanical responses prediction by BP-ANN models

The dataset contained 160 lining configurations, 32 of which acted as boundaries and only used for training, the remaining 128 lining configurations were tested by leave-one-out cross validation. Three BP-ANN models with different node numbers in the hidden layer (4 to 6 for compressive stress, 5 to 7 for temperature, and 10 to 12 for tensile stress) were employed to predict the individual response. The BP-ANN models were trained with BR algorithm. The comparison of predicted values (mean values from three models with different node numbers of intermediate layer) from BP-ANN models and the simulated values with FEM is shown in Figure 10. The coefficients of determination are 0.9970, 0.9950, 0.9364 for maximum compressive stress, end temperature, and the maximum tensile stress, respectively. The prediction accuracy for maximum tensile stress is lower than that for maximum compressive stress and end temperature. It's because the prediction accuracy is influenced by the complexity of variation/response space defined by the percent value of the significant variable contributing above 90% to the response (PF). In general, the more complex the problem is, the more complex BP-ANN model is needed. The PFs are 10%, 50% and 70% for maximum compressive stress, end temperature and maximum tensile stress, respectively. Therefore, the prediction accuracy for

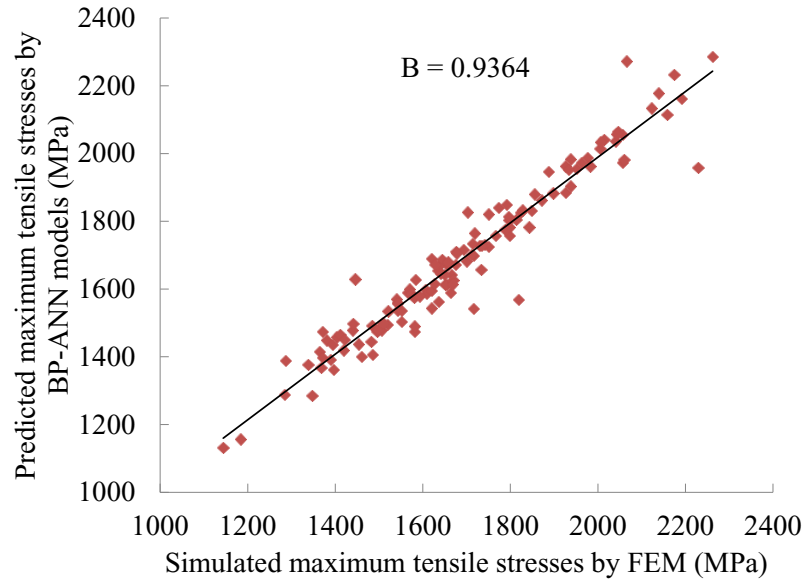
maximum tensile stress is lower than that for other two responses and it's possible to be improved by applying BP-ANN models with more complex structures, e.g. more than one hidden layers.



(a)



(b)



(c)

Figure 10. Comparison results (a) compressive stress, (b) temperature, and (c) tensile stress between predicted values with BP-ANN models and the simulated values with FEM.

4. Conclusion

The lining concept parameter study of a steel ladle using the FE method revealed the complicated effects of the lining structure and material properties on the thermal and thermomechanical responses [1]. The significant factors and optimal levels can be efficiently identified by using the Taguchi approach [1]. The statistical study using the Taguchi method facilitates lining concept design and decision making. The thicknesses of the working lining and insulation, the Young's modulus of the working lining, and the thermal conductivity of the insulation should be taken into account for lining concept design of a steel ladle. Thicker working lining and insulation are beneficial to reduce heat loss. The working lining material with lower Young's modulus can reduce the maximum compressive stress at the hot face of the working lining and the maximum tensile stress at the cold end of the steel shell. The application of the insulation with lower thermal conductivity tends to reduce the end temperature at the cold end of the steel shell, but increases tensile stress at the cold end of the steel shell. The dependency of lining behavior on the parameters mentioned above helps to find a common optimal of technical and economic performance.

BP-ANN model was successfully applied to predict the thermal and thermomechanical responses in a steel ladle system with the acceptable prediction accuracy. The prediction performance of a BP-ANN model is influenced by the properties of the dataset and the architectural parameters. A representative dataset can be obtained by applying multiple orthogonal arrays. The dataset size shall be larger than 16 times the number of the variables [122]. The minimum numbers of input variables of significance determined by the Taguchi method for the BP-ANN model were three, five, and six for the maximum compressive, the end temperature, and the maximum tensile stress [146]. The guidelines to define node numbers in the hidden layer were proposed according to the variation/response complexity and node numbers in the input and output layers [146]. The preferable node number ranges for maximum compressive stress, the end temperature, and the maximum tensile stress were four to six, five to seven, and ten to twelve, respectively [146]. The Bayesian regularization (BR) training algorithm was proposed to predict the responses in the steel ladle system [122].

5. Outlook

The methodology presented here combines finite element simulations and the Taguchi method to facilitate decision-making in refractory lining optimization. The application of this methodology, while taking into account irreversible refractory material behavior, e.g., tensile failure, shear failure and creep, is of interest for future research [1].

The application of multiple orthogonal arrays is an advanced tool to achieve a representative variation/response space. The BP-ANN method allows an efficient search for optimized lining concepts for vessels from both energy savings and better thermomechanical performance points of view [122]. The proposed multiple orthogonal arrays and BP-ANN methods are also promising for the optimization of ironmaking and steelmaking processes and material recipe development [122].

The study of the influence of variation/response space complexity and variable completeness on BP-ANN model establishment evidently and exemplarily shows that the variation/response complexity plays a determinant role in the architecture establishment of a BP-ANN model, which is often neglected in the application of ANN models [146]. The comparison study also demonstrates that the proposed guidelines to optimize BP-ANN architectural parameters for a steel ladle system are efficient and can be extended into other fields in defining an optimal node number of the hidden layer in a three-layer BP-ANN model [146].

6. References

- [1] A. Hou, S. Jin, H. Harmuth, D. Gruber, A method for steel ladle lining optimization applying thermomechanical modeling and Taguchi approaches, *JOM*, vol. 70, no.11, pp. 2449 – 2456, 2018.
- [2] L. F. Verdeja-González, M. F. Barbés-Fernández, R. González-Ojeda, G. A. Castillo, R. Colás, Thermal modelling of a torpedo-car, *Revista de Metalurgia*, vol. 41, pp. 449-455, 2005.
- [3] S. Jin, D. Gruber, H. Harmuth, R. Rössler, Thermomechanical failure modeling and investigation into lining optimization for a Ruhrstahl Heraeus snorkel, *Engineering Failure Analysis*, vol. 62, pp. 254-262, 2016.
- [4] D. Ramanenka, M-L. Antti, G. Gustafsson, P. Jonsén, Characterization of high-alumina refractory bricks and modelling of hot rotary kiln behaviour, *Engineering Failure Analysis*, vol. 79, pp. 852-864, 2017.
- [5] D. Ramanenka, J. Stjernberg, P. Jonsén, FEM investigation of global mechanisms affecting brick lining stability in a rotary kiln in cold state, *Engineering Failure Analysis*, vol. 59, pp. 554-569, 2016.
- [6] P. Boisse, A. Gasser, J. Poirier, J. Rousseau, Simulations of thermomechanical behavior of composite refractory linings, *Composites Part B: Engineering*, vol. 32, no. 5, pp. 461-474, 2001.
- [7] A. Gasser, P. Boisse, Y. Dutheillet, J. Poirier, Experimental and numerical analyses of thermomechanical refractory lining behaviour, *Proceedings of the Institution of Mechanical Engineers, Part L: Journal of Materials: Design and Applications*, vol. 215, no. 1, pp. 41–54, 2001.
- [8] P. Boisse, A. Gasser, J. Rousseau, Computations of refractory lining structures under thermal loadings, *Advances in Engineering Software*, vol. 33, pp. 487-496, 2002.
- [9] X. Xu, C. Hua, Y. Tang, X. Guan, Modeling of the hot metal silicon content in blast furnace

- using support vector machine optimized by an improved particle swarm optimizer, *Neural Computing and Application*, vol. 27, no. 6, pp. 1451-1461, 2016.
- [10] K. Zheng, Z. Wen, X. Liu, Y. Ren, W. Wu, H. Qiu, Research status and development trend of numerical simulation on blast furnace lining erosion, *ISIJ International*, vol. 49, no. 9, pp. 1277-1282, 2009.
- [11] S. Kumar, Heat transfer analysis and estimation of refractory wear in an iron blast furnace hearth using finite element method, *ISIJ International*, vol. 45, no. 8, pp. 1122-1128, 2005.
- [12] H. W. Gudenau, M. Scheiwe, R. Sieger, Simulation of thermochemical and thermomechanical load in blast furnace hearth, *Steel research: Process metallurgy*, vol. 64, no. 11, pp. 535 -541, 1993.
- [13] D. Gruber, K. Andreev, H. Harmuth, FEM simulation of the thermomechanical behaviour of the refractory lining of a blast furnace, *Journal of Materials Processing Technology*, Vols. 155-156, pp. 1539-1543, 2004.
- [14] T. R. Mohanty, S. K. Sahoo, M. K. Moharana, Study on blast furnace cooling stove for various refractory linings based on numerical modeling, *IOP Conference Series: Materials Science and Engineering*, vol. 115, 2016.
- [15] D. Niu, Q. Liu, Z. Wang, S. Ren, Y. Lan, M. Xu, Study on the removal of gases in RH refining progress through experiments using vacuum induction furnace, in *6th International Symposium on High-Temperature Metallurgical Processing*, pp. 551-558, 2015.
- [16] F. Damhof, W. A. M. Brekelmans, M. G. D. Geers, Predictive FEM simulation of thermal shock damage in the refractory lining of steelmaking installations, *Journal of Materials Processing Technology*, vol. 211, no. 12, pp. 2091-2105, 2011.
- [17] K. Andreev, S. Sinnema, A. Rekik, E. Blond, A. Gasser, Effects of dry joints on compressive behaviour of refractory linings, *International Forum on Science and Education of Refractories*, 2011.
- [18] H. Jalkanen, L. E. Holappa, Converter steelmaking, in *Treatise on Process Metallurgy (first*

- edition*), vol. 3, pp. 223-270, Elsevier, 2013.
- [19] X. Chen, Q. Chang, C. Chen, Y. Zhang, Simulation of the thermo-mechanical behavior and failure of refractory of converter, *Advanced Materials Research*, Vols. 255-260, pp. 4139-4142, 2011.
- [20] K. Andreev, S. Sinnema, A. Rekik, S. Allaoui, E. Blond, A. Gasser, Compressive behaviour of dry joints in refractory ceramic masonry, *Construction and Building Materials*, vol. 34, pp. 402-408, 2012.
- [21] Y. Hino, Y. Kiyota, Y. Hattori, Thermal stress analysis of BOF accounting for friction force experimentally measured, *ISIJ International*, vol. 50, no. 8, pp. 1125-1133, 2010.
- [22] D. Gruber, K. Andreev, H. Harmuth, Optimisation of the lining design of a BOF converter by finite element simulations, *Steel Research International*, vol. 75, pp. 455-461, 2004.
- [23] V. Petrov, R. Hirjak, D. Chudikova, V. Misaneckova, M. Kotora, S. Cempa, M. Baba, R. Simko, A. Maslejoval, M. Cernik, Optimization and design of a new torpedo lining, *Interceram – International Ceramic Review*, vol. 67, no. 6, pp. 14-21, 2018.
- [24] S. Jin, H. Harmuth, D. Gruber, A. Buhr, S. Sinnema, L. Rebouillat, Thermomechanical modelling of a torpedo car by considering working lining spalling, *Ironmaking & Steelmaking*, 2018, DOI: 10.1080/03019233.2018.1495797.
- [25] S. Liu, J. Yu, L. Han, Z. Li, Z. Yan, Thermal insulation performance analysis of nanoporous thermal insulating materials applied in torpedo ladle, *Materials Research Innovations*, vol. 18, pp. 250-254, 2014.
- [26] A. Ghosh, *Secondary Steelmaking: Principles and Applications*, Florida: CRC Press, 2000.
- [27] A. Zimmer, Á. N. C. Lima, R. M. Trommer, S. R. Bragança, C. P. Bergmann, Heat transfer in steelmaking ladle, *Journal of Iron and Steel Research International*, vol. 15, no. 3, pp. 11-60, 2008.
- [28] O. Volkova, D. Janke, Modelling of temperature distribution in refractory ladle lining for steelmaking, *ISIJ International*, vol. 43, no. 8, pp. 1185-1190, 2003.

- [29] C. E. Baukal Jr, *Industrial Combustion Pollution and Control*, New York: CRC Press, 2003.
- [30] N. Schmitt, Y. Berthaud, J.F. Hernandez, P. Meunier, J. Poirier, Damage of monolithic refractory linings in steel ladles during drying, *British Ceramic Transactions*, vol. 103, no. 3, pp. 121-133, 2004.
- [31] K. Andreev, H. Harmuth, FEM simulation of the thermo-mechanical behaviour and failure of refractories—a case study, *Journal of Materials Processing Technology*, vol. 143–144, pp. 72-77, 2003.
- [32] S. Yilmaz, Thermomechanical modelling for refractory lining of a steel ladle lifted by crane, *Steel Research International*, vol. 74, pp. 485-490, 2003.
- [33] A.V. Zabolotskii, Model of heating of the lining of a steel-teeming ladle, *Refractories and Industrial Ceramics*, vol. 51, no. 4, pp. 263-266, 2010.
- [34] D. Gruber, H. Harmuth, Durability of brick lined steel ladles from a mechanical point of view, *Steel Research International*, vol. 79, pp. 913-917, 2008.
- [35] N. Schmitt, F. Hild, E. Blond, Thermal stresses in the working lining of a ladle during the steel refining process, in *the Fourth International Symposium Advances in Refractories for the Metallurgical Industries IV*, Ontario, Canada, 2004.
- [36] M. F. Santos, M. H. Moreira, M. G. G. Campos, P. I. B. G. B. Pelissari, R. A. Angélico, E. Y. Sako, S. Sinnema, V. C. Pandolfelli, Enhanced numerical tool to evaluate steel ladle thermal losses, *Ceramics International*, vol. 44, no. 11, pp. 12831-12840, 2018.
- [37] G. Li, P. Qu, J. Kong, G. Jiang, L. Xie, Z. Wu, P. Gao, Y. He, Influence of working Lining parameters on temperature and stress field of ladle, *Applied Mathematics & Information Sciences*, vol. 7, no. 2, pp. 439-448, 2013.
- [38] H. Li, L. Zheng, X. Luo, F. Liu, W. Liu, Numerical simulation for temperature field of ladle linings of different materials during baking, *Refractories*, vol. 06, 2014.
- [39] B. Glaser, M. Görnerup, D. Sichen, Fluid flow and heat transfer in the ladle during teeming, *Steel Research International*, vol. 82, pp. 827-835, 2011.

-
- [40] B. Glaser, M. Görnerup, D. Sichen, Thermal modelling of the ladle preheating process, *Steel Research International*, vol. 82, pp. 1425-1434, 2011.
- [41] E. D. G. Krishna, S. Shamshoddin, R. Ande, Numerical simulation of fluid flow and heat transfer in a ductile iron ladle during holding and teeming, *Journal of Thermal Sciences and Engineering Applications*, vol. 11, no. 1, 2019.
- [42] D. Gruber, H. Harmuth, Thermomechanical behavior of steel ladle linings and the influence of insulations, *Steel Research International*, vol. 85, pp. 512-518, 2014.
- [43] W. Cheng, Y. Sun, G. Li, J. Kong, G. Jiang, Z. Li, W. Chang, H. Liu, Simulation analysis of stress distribution and its influence factors of the new structure ladle, *Applied Mathematics & Information Sciences*, vol. 11, no. 2, pp. 611-619, 2017.
- [44] G. Li, J. Liu, G. Jiang, H. Liu, Numerical simulation of temperature field and thermal stress field in the new type of ladle with the nanometer adiabatic material, *Advances in Mechanical Engineering*, vol. 7, no. 4, pp. 1-13, 2015.
- [45] C. Rahm, M. Kirschen, A. Kronthaler, Energy savings through appropriate ladle lining concepts, *RHI Bulletin*, no. 1, pp. 38-43, 2008.
- [46] W. Chang, G. Li, J. Kong, Y. Sun, G. Jiang, H. Liu, Thermal mechanical stress analysis of ladle lining with integral brick joint, *Archives of Metallurgy and Materials*, vol. 63, no. 2, pp. 659-666, 2018.
- [47] A. Gasser, P. Boisse, J. Rousseau, Y. Dutheillet, Thermomechanical behaviour analysis and simulation of steel/refractory composite linings, *Composites Science and Technology*, vol. 61, no. 14, pp. 2095-2100, 2001.
- [48] D. Gruber, T. Auer, H. Harmuth, J. Rotsch, Thermo-mechanical FE-Simulation of a teeming ladle slag line, in *2nd International Conference on Simulation & Modeling of Metal - Processes in Steelmaking*, Graz, Austria, 2007.
- [49] S. Jin, T. Auer, D. Gruber, H. Harmuth, M. H. Frechette, Y. Li, Thermo-mechanical modelling of steel ladle process cycles, *Interceram / Refractories manual*, pp. 37-41, 2012.

- [50] B. Cheng, P. Li, S. Tan, Q. Zhao, Effect of preheating temperature on stress and temperature of ladle lining during the molten steel holding process, *Journal of Iron and Steel Research*, vol. 27, no. 9, pp. 39-43, 2015.
- [51] W. Curran, Solid waste treatment and disposal, in *Industrial Waste Treatment Handbook (Second Edition)*, pp. 363-408, Butterworth-Heinemann, 2006.
- [52] R. Saidur, M. S. Hossain, M. R. Islam, H. Fayaz, H. A. Mohammed, A review on kiln system modeling, *Renewable and Sustainable Energy Reviews*, vol. 16, pp. 2487-2500, 2011.
- [53] D. Ramanenka, G. Gustafsson, P. Jonsén, Influence of heating and cooling rate on the stress state of the brick lining in a rotary kiln using finite element simulations, *Engineering Failure Analysis*, vol. 105, pp. 98-109, 2019.
- [54] S. El. Fakkoussi, H. Moustabchir, A. Elkhalfi, C. I. Pruncu, Analytical and numerical analysis of the tire tightening system of a cement kiln, *International Journal on Interactive Design and Manufacturing (IJIDeM)*, 2019, <https://doi.org/10.1007/s12008-019-00592-5>.
- [55] V. R. Gandhewar, S. V. Bansod, A. B. Borade, Induction furnace – a review, *International Journal of Engineering and Technology*, vol. 3, no. 4, pp. 277-284, 2011.
- [56] S. Jin, H. Harmuth, D. Gruber, Thermal and thermomechanical evaluations of channel induction furnace applying strong insulation containing lightweight aggregates, *Ironmaking & Steelmaking*, vol. 45, no. 6, pp. 514-518, 2018.
- [57] S. Jin, D. Gruber, H. Harmuth, J. Soudier, P. Meunier, H. Lemaistre, Optimisation of monolithic lining concepts of channel induction furnace, *International Journal of Cast Metals Research*, vol. 27, no. 6, pp. 336-340, 2014.
- [58] N. T. T. Hang, U. Ludtke, Numerical simulation of channel induction furnace to investigate frequency-dependent efficiency, in *2016 IEEE International Conference on Sustainable Energy Technologies (ICSET)*, pp. 90-95, 2016.
- [59] J. I. Ghojel, R. N. Ibrahim, Computer simulation of the thermal regime of double-loop channel induction furnaces, *Journal of Materials Processing Technology*, vols. 153-154, pp.

- 386-391, 2004.
- [60] J. I. Ghojel, Thermal analysis of twin-channel induction furnaces, *Metallurgical and Materials Transactions B*, vol. 34, no. 5, pp. 679-684, 2003.
- [61] M. A. Shcherba, Three-dimensional modeling of electromagnetic and temperature fields in the inductor of channel-type furnace for copper heating, in *2017 IEEE First Ukraine Conference on Electrical and Computer Engineering (UKRCON)*, pp. 427-431, 2017.
- [62] R. K. Roy, *A Primer on the Taguchi Method (Second Edition)*, US, Society of Manufacturing Engineers, 2010.
- [63] W. P. Gardiner, G. Gettinby, Taguchi methods, in *Experimental Design Techniques in Statistical Practice*, Woodhead Publishing, pp. 289-321, 1998.
- [64] R. Padmanabhan, M. C. Oliveira, J. L. Alves, L. F. Menezes, Influence of process parameters on the deep drawing of stainless steel, *Finite Elements in Analysis and Design*, vol. 43, no. 14, pp. 1062-1067, 2007.
- [65] S. K. Karna, R. V. Singh, R. Sahai, Application of Taguchi method in process optimization, in *Proceedings of the National Conference on Trends and Advances in Mechanical Engineering*, Faridabad, Haryana, 2012.
- [66] G. Dong, G. Wijaya, Y. Tang, Y. F. Zhao, Optimizing process parameters of fused deposition modeling by Taguchi method for the fabrication of lattice structures, *Additive Manufacturing*, vol. 19, pp. 62-72, 2018.
- [67] H. Jiang, Z. Li, T. Feng, P. Wu, Q. Chen, Y. Feng, S. Li, H. Gao, X. He, Factor analysis of selective laser melting process parameters with normalised quantities and Taguchi method, *Optics & Laser Technology*, vol. 119, pp. 105592, 2019.
- [68] R. Pundir, G. H. V. C. Chary, M. G. Dastidar, Application of Taguchi method for optimizing the process parameters for the removal of copper and nickel by growing *Aspergillus* sp., *Water Resources and Industry*, vol. 20, pp. 83-92, 2018.
- [69] A. Joshaghani, A. A. Ramezani-pour, O. Ataei, A. Golroo, Optimizing pervious concrete

- pavement mixture design by using the Taguchi method, *Construction and Building Materials*, vol. 101, pp. 317-325, 2015.
- [70] Y. Liu, C. Liu, W. Liu, Y. Ma, S. Tang, C. Liang, Q. Cai, C. Zhang, Optimization of parameters in laser powder deposition AlSi10Mg alloy using Taguchi method, *Optics & Laser Technology*, vol. 111, pp. 470-480, 2019.
- [71] M. Ebrahimi, I. Mobasherpour, H. B. Bafrooei, F. S. Bidabadi, M. Mansoorianfar, Y. Orooji, A. Khataee, C. Mei, E. Salahi, T. Ebadzadeh, Taguchi design for optimization of structural and mechanical properties of hydroxyapatite-alumina-titanium nanocomposite, *Ceramics International*, vol. 45, no. 8, pp. 10097-10105, 2019.
- [72] P. Madhukar, N. Selvaraj, C. S. P. Rao, G. B. V. Kumar, Tribological behavior of ultrasonic assisted double stir casted novel nano-composite material (AA7150-hBN) using Taguchi technique, *Composites Part B: Engineering*, vol. 175, pp. 107136, 2019.
- [73] E. Teimortashlu, M. Dehestani, M. Jalal, Application of Taguchi method for compressive strength optimization of tertiary blended self-compacting mortar, *Construction and Building Materials*, vol. 190, pp. 1182-1191, 2018.
- [74] N. M. Ghazaly, M. M. Makrahy, K. R. Mahmoud, K. A. Abd-El-Gwwad, A. M. Abd-El-Tawwab, Optimization of geometric parameters of a new wedge brake using Taguchi approach, *International Journal of Mechanical Engineering*, vol. 3, no. 11, pp. 1-13, 2013.
- [75] M. Firouzi, A. Niknejad, S. Ziaee, M. R. Hematiyan, Optimization of H-shaped thin-walled energy absorber by Taguchi method and a new theoretical estimation for its energy absorption, *Thin-Walled Structures*, vol. 131, pp. 33-44, 2018.
- [76] W. P. Gardiner, G. Gettinby, Taguchi methods, in *Experimental Design Techniques in Statistical Practice*, Woodhead Publishing, pp. 289-321, 1998.
- [77] J. Berk, S. Berk, ANOVA, Taguchi, and other design of experiments techniques, in *Quality Management for the Technology Sector*, Butterworth-Heinemann, pp. 106-123, 2000.
- [78] G. Wilson, Taguchi's techniques, in *Six Sigma and the Product Development cycle*,

- Butterworth-Heinemann, pp. 107-178, 2005.
- [79] H. J. C. Souza, M. B. Silva, C. B. Moyses, F. L. Alberto, F. J. Pontes, U. R. Ferreira, R. N. Duarte, C. E. S. Silva, Robust design and Taguchi method application, in *Design of Experiments - Applications*, IntechOpen, pp. 1-19, 2013.
- [80] K. Krishnaiah, P. Shahabudeen, Taguchi methods, in *Applied Design of Experiments and Taguchi Methods*, New Delhi, PHI Learning Pvt. Ltd., pp. 198-201, 2012.
- [81] T. P. Bagchi, Use of orthogonal arrays, in *Taguchi Methods Explained: Practical Steps to Robust Design*, New Delhi , Prentice-Hall of India, pp. 90-104, 1993 .
- [82] G. Lei, J. Zhu, Y. Guo, Design optimization methods for electrical machines, in *Multidisciplinary Design Optimization Methods for Electrical Machines and Drive Systems*, Springer-Verlag Berlin Heidelberg, pp. 107-157, 2016.
- [83] K. Krishnaiah, P. Shahabudeen, Data analysis from Taguchi experiments, in *Applied Design of Experiments and Taguchi Methods*, New Delhi, PHI Learning Pvt. Ltd., pp. 211-231, 2012.
- [84] I. N. Silva, D. H. Spatti, R. A. Flauzino, L. H. B. Liboni, S. F. R. Alves, *Artificial Neural Networks*, Switzerland, Springer International Publishing, 2017.
- [85] W. S. McCulloch, W. Pitts, A logical calculus of the ideas immanent in nervous activity, *The Bulletin of Mathematical Biophysics*, vol. 5, no. 4, pp. 115-133, 1943.
- [86] W. Pedrycz, A. V. Vasilakos, Computational intelligence: A development environment for telecommunications networks, in *Computational Intelligence in Telecommunications Networks*, US, CRC Press, pp. 1-28, 2000.
- [87] S. Chakraverty, S. Mall, Preliminaries of artificial neural network, in *Artificial Neural Networks for Engineers and Scientists: Solving Ordinary Differential Equations*, US, CRC Press, pp. 1-9, 2017.
- [88] R. Kumar, R. K. Aggarwal, J. D. Sharma, Energy analysis of a building using artificial neural network: A review, *Energy and Buildings*, vol. 65, pp. 352-358, 2013.
- [89] B. T. Pham, M. D. Nguyen, K. T. T. Bui, I. Prakash, K. Chapi, D. T. Bui, A novel artificial

- intelligence approach based on multi-layer perceptron neural network and biogeography-based optimization for predicting coefficient of consolidation of soil, *CATENA*, vol. 173, pp. 302-311, 2019.
- [90] T. F. Awolusi, O. L. Oke, O. O. Akinkulore, A. O. Sojobi, O. G. Aluko, Performance comparison of neural network training algorithms in the modeling properties of steel fiber reinforced concrete, *Heliyon*, vol. 5, no. 1, pp. e01115, 2019.
- [91] D. T. Bui, V. H. Nhu, N. D. Hoang, Prediction of soil compression coefficient for urban housing project using novel integration machine learning approach of swarm intelligence and multi-layer perceptron neural network, *Advanced Engineering Informatics*, vol. 38, pp. 593-604, 2018.
- [92] I. Flood, Towards the next generation of artificial neural networks for civil engineering, *Advanced Engineering Informatics*, vol. 22, no. 1, pp. 4-14, 2008.
- [93] S. R. Mohandes, X. Zhang, A. Mahdiyar, A comprehensive review on the application of artificial neural networks in building energy analysis, *Neurocomputing*, vol. 340, pp. 55-75, 2019.
- [94] E. Rodrigues, Á. Gomes, A. R. Gaspar, C. H. Antunes, Estimation of renewable energy and built environment-related variables using neural networks – A review, *Renewable and Sustainable Energy Reviews*, vol. 94, pp. 959-988, 2018.
- [95] R. Rajeshwari, S. Mandal, Prediction of compressive strength of high-volume fly ash concrete using artificial neural network, in *Sustainable Construction and Building Materials*, vol. 25, Singapore, Springer, pp. 471-483, 2019.
- [96] M. A. S. Matos, S. T. Pinho, V. L. Tagarielli, Predictions of the electrical conductivity of composites of polymers and carbon nanotubes by an artificial neural network, *Scripta Materialia*, vol. 166, pp. 117-121, 2019.
- [97] S. Koley, T. Ray, I. Mohanty, S. Chatterjee, M. Shome, Prediction of electrical resistivity of steel using artificial neural network, *Ironmaking & Steelmaking*, vol. 46, no. 4, pp. 383-391, 2019.

- [98] P. V. Yekta, F. J. Honar, M. N. Fesharaki, Modelling of hysteresis loop and magnetic behaviour of Fe-48Ni alloys using artificial neural network coupled with genetic algorithm, *Computational Materials Science*, vol. 159, pp. 349-356, 2019.
- [99] A. Belayadi, B. Bourahla, Neural network model for 7000 (Al-Z) alloys: Classification and prediction of mechanical properties, *Physica B: Condensed Matter*, vol. 554, pp. 114-120, 2019.
- [100] T. Akter, S. Desai, Developing a predictive model for nanoimprint lithography using artificial neural networks, *Materials & Design*, vol. 160, pp. 836-848, 2018.
- [101] M. Muruganath, Artificial neural networks in materials modelling, in *Soft Computing in Textile Engineering*, Woodhead Publishing, pp. 25-44, 2011.
- [102] J. R. Mohanty, B. B. Verma, D. R. K. Parhi, P. K. Ray, Application of artificial neural network for predicting fatigue crack propagation life of aluminum alloys, *Archives of Computational Materials Science and Surface Engineering*, vol. 1, no. 3, pp. 133-138, 2009.
- [103] S. H. Sadati, J. A. Kaklar, R. Ghajar, Application of artificial neural networks in the estimation of mechanical properties of materials, in *Artificial Neural Networks - Industrial and Control Engineering Applications*, In Tech, pp. 117-130, 2011.
- [104] J. Ghaisari, H. Jannesari, M. Vatani, Artificial neural network predictors for mechanical properties of cold rolling products, *Advances in Engineering Software*, vol. 45, no. 1, pp. 91-99, 2012.
- [105] C. Bilim, C. D. Atiş, H. Tanyildizi, O. Karahan, Predicting the compressive strength of ground granulated blast furnace slag concrete using artificial neural network, *Advances in Engineering Software*, vol. 40, no. 5, pp. 334-340, 2009.
- [106] L. A. Dobrzański, J. Trzaska, A.D. Dobrzańska-Danikiewicz, Use of neural network and artificial intelligence tools for modeling, characterization, and forecasting in material engineering, in *Comprehensive Materials Processing*, vol. 2, Elsevier, pp. 161-198, 2014.
- [107] R. Ghiasi, M. R. Ghasemi, M. Noori, Comparative studies of metamodeling and AI-Based techniques in damage detection of structures, *Advances in Engineering Software*, vol. 125,

pp. 101-112, 2018.

- [108] C. S. N. Pathirage, J. Li, L. Li, H. Hao, W. Liu, P. Ni, Structural damage identification based on autoencoder neural networks and deep learning, *Engineering Structures*, vol. 172, pp. 13-28, 2018.
- [109] G. F. Gomes, Y. A. D. Mendéz, P. S. L. Alexandrino, S. S. Cunha, A. C. Ancelotti, The use of intelligent computational tools for damage detection and identification with an emphasis on composites – A review, *Composite Structures*, vol. 196, pp. 44-54, 2018.
- [110] H. Moayedi, M. Mosallanezhad, A. S. A. Rashid, W. A. W. Jusoh, M. A. Muazu, A systematic review and meta-analysis of artificial neural network application in geotechnical engineering: theory and applications, *Neural Computing and Applications*, 2019, <https://doi.org/10.1007/s00521-019-04109-9>.
- [111] I. T. Bahmed, K. Harichane, M. Ghrici, B. Boukhatem, R. Rebouh, H. Gadouri, Prediction of geotechnical properties of clayey soils stabilised with lime using artificial neural networks (ANNs), *International Journal of Geotechnical Engineering*, vol. 13, no. 2, pp. 191-203, 2019.
- [112] M. Koopialipoor, A. Fahimifar, E. N. Ghaleini, M. Momenzadeh, D. J. Armaghani, Development of a new hybrid ANN for solving a geotechnical problem related to tunnel boring machine performance, *Engineering with Computers*, 2019, <https://doi.org/10.1007/s00366-019-00701-8>.
- [113] A. A. Shahri, An optimized artificial neural network structure to predict clay sensitivity in a high landslide prone area using piezocone penetration test (CPTu) data: A case study in southwest of Sweden, *Geotechnical and Geological Engineering*, vol. 34, no. 2, pp. 745-758, 2016.
- [114] M. R. Jamli, N. M. Farid, The sustainability of neural network applications within finite element analysis in sheet metal forming: A review, *Measurement*, vol. 138, pp. 446-460, 2019.
- [115] S. S. Miriyala, V. R. Subramanian, K. Mitra, Transform-ANN for online optimization of

- complex industrial processes: casting process as case study, *European Journal of Operational Research*, vol. 264, no. 1, pp. 294-309, 2018.
- [116] F. He, D. He, A. Xu, H. Wang, N. Tian, Hybrid model of molten steel temperature prediction based on ladle heat status and artificial neural network, *Journal of Iron and Steel Research International*, vol. 21, no. 2, pp. 181-190, 2014.
- [117] T. C. Park, B. S. Kim, T. Y. Kim, I. B. Jin, Y. K. Yeo, Comparative study of estimation methods of the endpoint temperature in basic oxygen furnace steelmaking process with selection of input parameters, *Korean Journal of Metals and Materials*, vol. 56, no. 11, pp. 813-821, 2018.
- [118] I. J. Cox, R. W. Lewis, R. S. Ransing, H. Laszczewski, G. Berni, Application of neural computing in basic oxygen steelmaking, *Journal of Materials Processing Technology*, vol. 120, no. 1-3, pp. 310-315, 2002.
- [119] F. He, L. Zhang, Prediction model of end-point phosphorus content in BOF steelmaking process based on PCA and BP neural network, *Journal of Process Control*, vol. 66, pp. 51-58, 2018.
- [120] Y. Tunçkaya, E. Koklukaya, Comparative performance evaluation of blast furnace flame temperature prediction using artificial intelligence and statistical methods, *Turkish Journal of Electrical Engineering & Computer Sciences*, vol. 24, pp. 1163-1175, 2016.
- [121] R. Strąkowski, K. Pacholski, B. Więcek, R. Olbrycht, W. Wittchen, M. Borecki, Estimation of FeO content in the steel slag using infrared imaging and artificial neural network, *Measurement*, vol. 117, pp. 380-389, 2018.
- [122] A. Hou, S. Jin, H. Harmuth, D. Gruber, Thermal and thermomechanical responses prediction of a steel ladle using a back-propagation artificial neural network combining multiple orthogonal arrays, *Steel Research International*, vol. 90, pp. 1900116, 2019.
- [123] A. Alibakshi, Strategies to develop robust neural network models: Prediction of flash point as a case study, *Analytica Chimica Acta*, vol. 1026, pp. 69-76, 2018.

- [124] C. C. Aggarwal, *Neural networks and deep learning*, Springer International Publishing, pp. 23-58, 2018.
- [125] S. Liu, A. Zolfaghari, S. Sattarin, A. K. Dahaghi, S. Negahban, Application of neural networks in multiphase flow through porous media: predicting capillary pressure and relative permeability curves, *Journal of Petroleum Science and Engineering*, vol. 180, pp. 445-455, 2019.
- [126] G. H. Kim, S. H. Kim, Variable selection for artificial neural networks with applications for stock price prediction, *Applied Artificial Intelligence*, vol. 33, no. 1, pp. 54-67, 2019.
- [127] T. Linjordet, K. Balog, Impact of training dataset size on neural answer selection models, in *Advances in Information Retrieval. ECIR 2019. Lecture Notes in Computer Science*, vol. 11437, Springer, pp. 828-835, 2019.
- [128] A. Alwosheel, S. Cranenburgh, C. G. Chorus, Is your dataset big enough? Sample size requirements when using artificial neural networks for discrete choice analysis, *Journal of Choice Modelling*, vol. 28, pp. 167-182, 2018.
- [129] T. R. Neelakantan, S. Lingireddy, G. M. Brion, Effectiveness of different artificial neural network training algorithms in predicting protozoa risks in surface waters, *Journal of Environmental Engineering*, vol. 128, no. 6, pp. 533-543, 2002.
- [130] A. K. Ilkhchi, M. R. Rezaee, H. R. Bonab, A committee neural network for prediction of normalized oil content from well log data: An example from South Pars Gas Field, Persian Gulf, *Journal of Petroleum Science and Engineering*, vol. 65, no. 1-2, pp. 23-32, 2009.
- [131] R. Koker, N. Altinkok, A. Demir, Neural network based prediction of mechanical properties of particulate reinforced metal matrix composites using various training algorithms, *Materials & Design*, vol. 28, no. 2, pp. 616-627, 2007.
- [132] M. O. Shabani, A. Mazahery, Application of finite element model and artificial neural network in characterization of Al matrix nanocomposites using various training algorithms, *Metallurgical and Materials Transactions A*, vol. 43, no. 6, pp. 2158-2165, 2012.
- [133] S. Haykin, *Neural Networks and Learning Machines (Third Edition)*, Ontario, Canada:

Pearson Education, 2009.

- [134] A. Radi, S. K. Hindawi, Applying artificial neural network hadron – hadron collisions at LHC, in *Artificial Neural Networks – Architectures and Applications*, Croatia, InTech, 2013.
- [135] M. Moreira, E. Fiesler, Neural networks with adaptive learning rate and momentum terms, *IDIAP Technical report*, 1995.
- [136] Z. Cömert, A. F. Kocamaz, A study of artificial neural network training algorithms for classification of cardiocography signals, *Journal of Science and Technology*, vol. 7, no. 2, pp. 93-103, 2017.
- [137] L. Zhou, X. Yang, Training algorithm performance for image classification by neural networks, *Photogrammetric Engineering & Remote Sensing*, vol. 76, no. 8, pp. 945-951, 2010.
- [138] H. Yabe, H. Ogasawara, M. Yoshino, Local and superlinear convergence of quasi-Newton methods based on modified secant conditions, *Journal of Computational and Applied Mathematics*, vol. 205, no. 1, pp. 617-632, 2007.
- [139] A. H. Nandhu Kishore, V. E. Jayanthi, Neuro-fuzzy based medical decision support system for coronary artery disease diagnosis and risk level prediction, *Journal of Computational and Theoretical Nanoscience*, vol. 15, pp. 1027-1037, 2018.
- [140] M. J. D. Powell, Restart procedures for the conjugate gradient method, *Mathematical Programming*, vol. 12, pp. 241-254, 1977.
- [141] J. Shi, Y. Zhu, F. Khan, G. Chen, Application of bayesian regularization artificial neural network in explosion risk analysis of fixed offshore platform, *Journal of Loss Prevention in the Process Industries*, vol. 57, pp. 131-141, 2019.
- [142] J. L. Ticknor, A Bayesian regularized artificial neural network for stock market forecasting, *Expert Systems with Applications*, vol. 40, no. 14, pp. 5501-5506, 2013.
- [143] S. Sholahudin, K. Ohno, N. Giannetti, S. Yamaguchi, K. Saito, Dynamic modeling of room temperature and thermodynamic efficiency for direct expansion air conditioning systems

- using Bayesian neural network, *Applied Thermal Engineering*, vol. 158, pp. 113809, 2019.
- [144] K. Hirschen, M. Schafer, Bayesian regularization neural networks for optimizing fluid flow processes, *Computer Methods in Applied Mechanics and Engineering*, vol. 195, pp. 481 – 500, 2006.
- [145] F. D. Foressee, M. T. Hagan, Gauss-Newton approximation to Bayesian learning, in *Proceedings of International Conference on Neural Networks (ICNN'97)*, vol. 3, pp. 1930-1935, 1997.
- [146] A. Hou , S. Jin , D. Gruber, H. Harmuth, Influence of variation/response space complexity and variable completeness on BP-ANN model establishment: case study of steel ladle lining, *Applied Sciences*, vol. 9, no. 14, pp. 2835, 2019.
- [147] I. López, L. Aragonés, Y. Villacampa , P. Compañ, Artificial neural network modeling of cross-shore profile on sand beaches: The coast of the province of Valencia (Spain), *Marine Georesources & Geotechnology*, vol. 36, no. 6, pp. 698-708, 2018.
- [148] D. B. Huertas, J. Moyano, C. E. R. Jiménez, D. Marín, Applying an artificial neural network to assess thermal transmittance in walls by means of the thermometric method, *Applied Energy*, vol. 233–234, pp. 1-14, 2019.
- [149] D. Chen, S. Singh, L. Gao, A. Garg, Z. Fan, C. T. Wang, A coupled and interactive influence of operational parameters for optimizing power output of cleaner energy production systems under uncertain conditions, *International Journal of Energy Research*, vol. 43, pp. 1294-1302, 2019.
- [150] N. Darajeh, A. Idris, H. R. F. Masoumi, A. Nourani, P. Truong, S. Rezania, Phytoremediation of palm oil mill secondary effluent (POMSE) by *Chrysopogon zizanioides* (L.) using artificial neural networks, *International Journal of Phytoremediation*, vol. 19, no. 5, pp. 413-424, 2017.
- [151] N. Darajeh, H. R. F. Masoumi, K. Kalantari, M. B. Ahmad, K. Shameli, M. Basri, R. Khandanlou, Optimization of process parameters for rapid adsorption of Pb(II), Ni(II), and Cu(II) by magnetic/talc nanocomposite using wavelet neural network, *Research on Chemical*

Intermediates, vol. 42, no. 3, pp. 1977-1987, 2016.

- [152] Z. Cao, N. Guo, M. Li, K. Yu, K. Gao, Back propagation neural network based signal acquisition for Brillouin distributed optical fiber sensors, *Optics Express*, vol. 27, no. 4, pp. 4549-4561, 2019.
- [153] H. Luo, F. Lai, Z. Dong, W. Xia, A lithology identification method for continental shale oil reservoir based on BP neural network, *Journal of Geophysics and Engineering*, vol. 15, no. 3, pp. 895-908, 2018.
- [154] S. Chokphoemphun, S. Chokphoemphun, Moisture content prediction of paddy drying in a fluidized-bed drier with a vortex flow generator using an artificial neural network, *Applied Thermal Engineering*, vol. 145, pp. 630-636, 2018.
- [155] X. Chen, Y. Xun, W. Li, J. Zhang, Combining discriminant analysis and neural networks for corn variety identification, *Computers and Electronics in Agriculture*, vol. 71, no. 1, pp. 48-53, 2010.
- [156] E. K. Onyari, B. D. Ikotun, Prediction of compressive and flexural strengths of a modified zeolite additive mortar using artificial neural network, *Construction and Building Materials*, vol. 187, pp. 1232-1241, 2018.
- [157] A. Amalia, S. Suryono, J. E. Suseno, R. Kurniawati, Ultrasound-assisted extraction optimization of phenolic compounds from *Psidium guajava* L. using artificial neural network-genetic algorithm, in *Journal of Physics: Conference Series*, 2018.
- [158] H. F. Lam, C. T. Ng, The selection of pattern features for structural damage detection using an extended Bayesian ANN algorithm, *Engineering Structures*, vol. 30, no. 10, pp. 2762-2770, 2008.
- [159] S. Karsoliya, Approximating number of hidden layer neurons in multiple hidden layer BPNN architecture, *International Journal of Engineering Trends and Technology*, vol. 3, no. 6, pp. 714 -717, 2012.

7. List of appended publications

Paper I

A. Hou, S. Jin, H. Harmuth, D. Gruber

A method for steel ladle lining optimization applying thermomechanical modeling and Taguchi approaches

JOM, vol. 70, no. 11, pp. 2449-2456, 2018.

Paper II

A. Hou, S. Jin, H. Harmuth, D. Gruber

Thermal and thermomechanical responses prediction of a steel ladle using a back-propagation artificial neural network combing multiple orthogonal arrays

Steel Research International, vol. 90, 2019, DOI: 10.1002/srin.201900116.

Paper III

A. Hou, S. Jin, D. Gruber, H. Harmuth

Influence of variation/response space complexity and variable completeness on BP-ANN model establishment: case study of steel ladle lining

Applied Sciences, vol. 9, no. 14, 2019, DOI: 10.3390/app9142835.

Paper IV

A. Hou, S. Jin, D. Gruber, H. Harmuth

Modelling of a steel ladle and prediction of its thermomechanical behavior by finite element simulation together with artificial neural network approaches

Congress on Numerical Methods in Engineering – CMN 2019, pp. 1109-1117, 2019.

Paper V

S. Jin, A. Hou, D. Gruber, H. Harmuth

Approaches towards a digital tool for optimising lining design – case studies of channel induction furnace and steel ladle

Unified International Technical Conference of Refractories (UNITECR) 2019, accepted in 07.2019.

Remarks

In **paper I to IV**, myself, Aidong Hou, performed all investigations and wrote the manuscripts; Dr. Shengli Jin is acknowledged for his expert guidance and contribution to all these four papers by providing basic ideas for publications along with helpful discussion and support the edition of manuscripts; Dr. Dietmar Gruber and Prof. Harald Harmuth provided helpful discussions during investigations and preparation of the papers.

In **paper V**, myself, Aidong Hou, contributed to the results of steel ladle case and wrote two parts of the manuscript (approaches and the results of steel ladle case).

8. Collection of publications

A Method for Steel Ladle Lining Optimization Applying Thermomechanical Modeling and Taguchi Approaches

AIDONG HOU,¹ SHENGLI JIN ^{1,2} HARALD HARMUTH,¹ and DIETMAR GRUBER¹

1.—Montanuniversitaet, Leoben 8700, Austria. 2.—e-mail: shengli.jin@unileoben.ac.at

Successful lining concept design can avoid the premature wear of refractory linings, allow for more economically efficient configuration of refractories, and improve the efficiency of high-temperature processes and save energy. The present paper introduces the Taguchi method combining finite element (FE) modeling for the lining optimization of a steel ladle from thermal and thermomechanical viewpoints. An orthogonal array was applied to design lining configurations for FE simulations. Analysis of variance and signal-to-noise ratio were used to quantitatively assess the impact of factors on thermal and thermomechanical responses. As a result, two optimal lining concepts using commercially available materials were proposed, which showed a substantial decrease in heat loss through the steel shell and thermomechanical load at the hot face of the working lining. The combined application of FE thermomechanical modeling and Taguchi approaches facilitates the selection of proper commercial materials and thicknesses of linings for the given process conditions.

List of symbols

m	Total number of factors
l	Total number of levels
N	Total number of runs
k	Index referring to factor
i	Index referring to level
j	Index referring to observation
n_i	Number of runs at the i th level of a factor
t	Strength of an orthogonal table
y_{ij}	Value of j th observation at the i th level of a factor
\bar{y}_i	Mean of observations at i th level of a factor
\bar{y}_t	Mean of all observations
SS_T	Total sum of squares
SS_f	Sum of squares for each factor
SS_D	Sum of squares of deviation
MS_f	Mean square for each factor
MS_D	Mean square of deviation
DoF_f	Degrees of freedom of each factor
DoF_D	Degrees of freedom of deviation
F -statistic	Ratio of mean square for each factor to that of the deviation

α	Significance level, the probability of rejecting the null hypothesis when it is true
C	Contribution in percentage

INTRODUCTION

Steel ladles, composed of refractories and steel construction components, act as transportation vessels and refining units for the steel melt. Refractory linings insulate the steel shell from the steel melt, and thus reduce the heat loss from the steel shell. A well-lined steel ladle offers efficient temperature control of the steel melt and is beneficial to the steel quality and productivity.¹⁻⁴

The thermomechanical behavior of steel ladle linings has been extensively studied with regard to relevant process conditions, material properties, and lining configurations by means of finite

element (FE) methods.^{5–12} These studies show that ladles without preheating experience higher compressive stresses at the hot face of the working lining, which may lead to a compressive failure;^{5–7} by preheating for preferably 15–20 h, these stresses can be reduced.⁸ In addition, an increased ladle preheating temperature can reduce the temperature drop of the steel melt and the temperature gradient of ladle linings, mitigate the thermal shock damage of lining materials, and thus extend the service life of the steel ladle.⁹ The effects of insulation in a steel ladle were evaluated from the thermal and thermomechanical points of view. A compliant insulation layer led to a decrease in heat loss and thermomechanical loads at the hot face of the working lining.⁶ The possible application of an insulating material with rather low thermal conductivity was evaluated using FE simulations of a steel ladle.¹²

In contrast to the post-mortem study of an existing vessel lining concept, an a priori method was proposed for the design of lining concepts before putting them into practice with a case study of a channel induction furnace lined with monoliths.^{13–15} An orthogonal array was utilized to systematically design the lining concepts, and the FE method was applied to calculate the temperatures and stresses of the furnace linings. Afterwards, an analysis of the main effects was performed to rank the impact of individual factors and determine the optimal value of each factor. The optimized lining concept was compared with the reference case from the thermal and thermomechanical points of view, taking into account irreversible behavior of the working lining material. The studies established a feasible and efficient methodology for optimization of lining concepts using a considerable number of variables of vessels made of monolithic linings.

The present paper extends the above-mentioned method for the lining concept optimization of vessels with brick working linings. A case study of a steel ladle considers the variations of material properties and lining geometry. Moreover, advanced analysis methods, i.e., analysis of variance (ANOVA) and signal-to-noise (S/N) ratio according to the Taguchi method, were applied to assess the contribution and optimal level of significant factors.

TAGUCHI METHOD

As an improved method of design of experiments, the Taguchi method, developed by G. Taguchi in the late 1940s, is widely used in manufacturing processes,^{16,17} material design and development,¹⁸ and geometry design.¹⁹ A routine set of tools in the Taguchi method includes orthogonal arrays, ANOVA, and the S/N ratio. Their performances are briefly introduced in the following subsections.

Orthogonal Arrays

Orthogonal arrays are highly fractional factorial designs and yield a minimum number of experimental runs. An orthogonal array with the same number of levels l for all m factors is designated with the sign of $L_N(l^m)$, where N is the total number of experiment runs, and L represents Latin squares. When the level size of certain factors is different, for instance, m_1 factors have l_1 levels and m_2 factors have l_2 levels, then it is denoted $L_N(l_1^{m_1} \times l_2^{m_2})$. The former is called a pure orthogonal array and the latter one a mixed-level orthogonal array. In one orthogonal array with a strength of t , the occurrence of each level of one factor in each column is equal and the combination of levels in t factors occurs equally. Additional details are described in other works.^{20,21}

Analysis of Variance (ANOVA)²²

ANOVA is a statistical method used to quantitatively assess the significance of factors to responses and their confidence. Five values are used to assess a factor's significance: the sum of squares, the degrees of freedom, the mean square, the F value, and the percent contribution of the factor.

The total sum of squares (subscript T) measures the overall variability of data and is calculated using all of the observed values for different factors

$$SS_T = \sum_{i=1}^l \sum_{j=1}^{n_i} (y_{ij} - \bar{y}_t)^2, \quad (1)$$

where l is the number of levels, n_i is the number of runs at the i th level, y_{ij} is the value of j th observation at i th level, and \bar{y}_t is the mean of all observations.

The sum of squares for each factor (subscript f) is given by

$$SS_f = n_i \sum_{i=1}^l (\bar{y}_i - \bar{y}_t)^2, \quad (2)$$

where \bar{y}_i is the mean of observations at the i th level.

Subtracting the sum of SS_f of all factors from SS_T leads to

$$SS_D = SS_T - \sum_{k=1}^m SS_f(k), \quad (3)$$

where m is the total number of factors and k is the index referring to a factor. SS_D is the sum of squares of the deviation (subscript D).

The degrees of freedom of each factor, DoF_f , is equal to $(l - 1)$ when the number of its level is l .

The mean square for each factor (subscript f) is

$$MS_f = SS_f / DoF_f, \quad (4)$$

and the mean square of deviation is

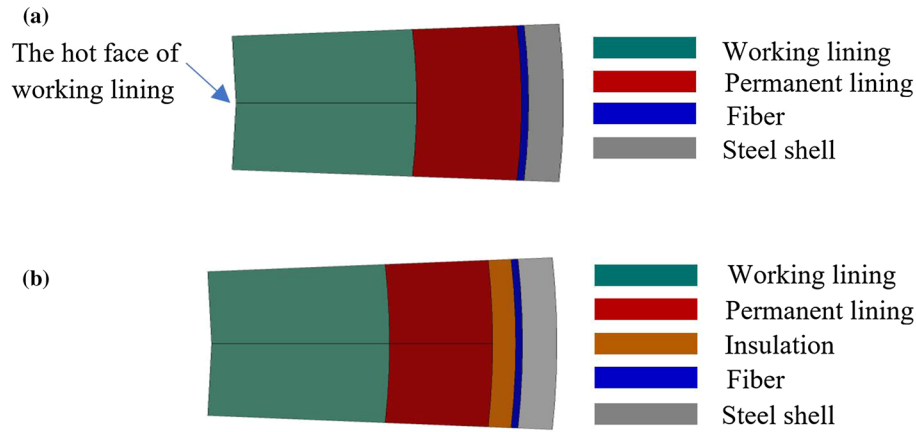


Fig. 1. (a) Two-dimensional model of the reference steel ladle case; (b) two-dimensional model of the steel ladle for the lining concept optimization study.

Table I. Ladle component thickness and material properties of the reference case

Linings	Thickness (mm)	Thermal conductivity (W m ⁻¹ K ⁻¹)	Young's modulus (GPa)	Thermal expansion coefficient (10 ⁻⁶ K ⁻¹)
Working lining	155	8.5	60	11.5
Permanent lining	90	2.2	45	6.0
Fiber	6	0.17	0.3	9.0
Steel shell	30	50	210	12.0

$$MS_D = SS_D / DoF_D, \quad (5)$$

where DoF_D is the degrees of freedom of deviation (subscript D) given by

$$DoF_D = N - 1 - \sum_{k=1}^m (l_k - 1), \quad (6)$$

where N is the total number of runs.

The F -statistic value of each factor is calculated using the equation below,

$$F = MS_f / MS_D. \quad (7)$$

Afterwards, the obtained F value can be compared with the corresponding critical value, F_α (DoF_f , DoF_D) at the $(1 - \alpha)$ confidence level in the F distribution table.²² If the calculated F value is larger than the critical value, the probability of correctly accepting the null hypothesis is $(1 - \alpha)$. The percent contribution of each factor is defined as

$$C = SS_f / (SS_T - SS_D) \times 100\%. \quad (8)$$

Signal-to-Noise (S/N) Ratio²⁰

The S/N ratio is extensively used as a quality index, rather than being merely associated with the signal and noise. Three S/N ratio representations are shown in Eqs. 9–11: smaller-the-better, nominal-the-best, and larger-the-better. For all representations, a higher S/N ratio is desirable. In the

present work, the smaller-the-better equation is used to evaluate the thermal and thermomechanical responses because the equation treats the smallest value of responses as the best quality.

$$\text{Smaller - the - better: } S/N = -10 \log \left(\frac{1}{n_i} \sum_{j=1}^{n_i} y_{ij}^2 \right), \quad (9)$$

$$\text{Nominal - the - best: } S/N = -10 \log \left(\frac{1}{n_i} \sum_{j=1}^{n_i} (y_{ij} - \bar{y}_i)^2 \right), \quad (10)$$

$$\text{Larger - the - better: } S/N = -10 \log \left(\frac{1}{n_i} \sum_{j=1}^{n_i} \frac{1}{y_{ij}^2} \right). \quad (11)$$

Here n_i is the number of runs at the i th level, y_{ij} is the value of the j th observation at the i th level, and \bar{y}_i is the mean number of observations at the i th level of a factor.

FINITE ELEMENT MODEL AND PARAMETER DESIGN

A steel ladle of voestalpine was the object used for lining concept optimization. Figure 1a depicts the simplified two-dimensional model representing a

Table II. Variations in ladle component thicknesses and material properties

Impact factors	Levels				Label of factors
	1	2	3	4	
Thickness (mm)					
Working lining	250	200	155	50	<i>A</i>
Permanent lining	130	110	90	65	<i>B</i>
Insulation lining	37.5	25	15	6	<i>C</i>
Steel shell	30	20			<i>J</i>
Thermal conductivity (W m ⁻¹ K ⁻¹)					
Working lining	9	8.5	7	3	<i>D</i>
Permanent lining	9	5	3	2.2	<i>E</i>
Insulation lining	1.35	0.5	0.35	0.15	<i>F</i>
Young's modulus (GPa)					
Working lining	100	80	60	40	<i>G</i>
Permanent lining	90	45	30	10	<i>H</i>
Insulation lining	35	4	3	0.17	<i>I</i>

horizontal cut through the slag-line position in the upper part of the steel ladle. The model consists of a two half-brick working lining, a monolithic permanent lining, a fiber board, and a steel shell. The radial expansion allowance between two bricks of the working lining was 0.4 mm. The thicknesses and material properties of different linings are listed in Table I. The thermal conductivity and Young's modulus of materials were defined as being temperature-independent.

Another two-dimensional model including an additional insulating lining was established for the lining concept optimization study, as shown in Fig. 1b. In this model, the permanent lining was made of bricks. The radial expansion allowance between two bricks was 0.4 mm. The variations of lining thickness, thermal conductivity, and Young's modulus of materials for the respective linings are shown in Table II. It is worth noting that the material property variations in Table II are those of commercial products and ranked in a descending order. The thermal conductivity and Young's modulus of the materials were also defined as being temperature-independent. The candidate refractory materials for each lining were assumed to possess the same coefficient of thermal expansion ($1.2 \times 10^{-6} \text{ K}^{-1}$) in the present linear elastic modeling and optimization procedure. A consideration of different coefficients of thermal expansion is necessary if the materials for one lining show a significant deviation in the coefficients of thermal expansion or if the irreversible behavior of refractories is taken into account. Finally, in total, ten factors were of interest in this research, nine of which had four levels, together with the thickness of the steel shell, which had two levels. A mixed-level orthogonal array $L_{32}(4^9 \times 2^1)$ according to the Taguchi method was applied.

The finite element modeling of the steel ladle with an elastic material behavior was performed using the commercial software, ABAQUS. The process included preheating of the hot face of the working lining for 20 h to 1100°C and a subsequent thermal shock caused by tapping the steel melt with a temperature of 1600°C into the ladle. After the refining period of 95 min, a 50-min idle period followed. Displacement of linings was allowed in the radial direction and constrained in the circumferential direction. The heat transfer between the interfaces of linings, the liquid melt and hot face of the working lining, and the cold end of the steel shell and atmosphere was considered.

RESULTS

Contribution of Impact Factors to the Thermal and Thermomechanical Responses

The present study aims to decrease the heat loss from the steel shell and the thermomechanical loads on the working lining and steel shell. Thus, the chosen responses were the temperature at the cold end of the steel shell, the maximum tensile stress at the steel shell, and the maximum compressive stress at the hot face of the working lining. ANOVA was applied to quantitatively investigate the significance of impact factors, according to the equations in "Analysis of Variance (ANOVA)[22]" section.

The results for the thermal response are exemplarily shown in Table III. The top four significant impact factors to the temperature at the cold end of the steel shell were the thickness of the working lining (*A*), the thermal conductivity of the insulation material (*F*), the thickness of insulation material (*C*), and the thermal conductivity of the working lining material (*D*), in descending order. Their individual confidence levels were all higher than 90% and, when combined, they contributed 89% of

Table III. ANOVA results of the temperature at the cold end of the steel shell

Factor	DoF _f	SS _f (°C ²)	MS _f (°C ²)	F-V value	Confidence (%)	Contribution (%)
A	3	59,596	19,865.4	14.39	95	31.27
B	3	8473	2824.4	2.05		4.45
C	3	37,878	12,625.9	9.15	90	19.88
D	3	32,659	10,886.4	7.89	90	17.14
E	3	10,464	3488	2.53		5.49
F	3	38,746	12,915.3	9.36	95	20.33
G	3	1958	652.7	0.47		1.03
H	3	261	87	0.06		0.14
I	3	407	135.8	0.1		0.21
J	1	121	121.1	0.09		0.06

SS_T = 194,705, SS_D = 4142, MS_D = 1380.6, DoF_D = 3.

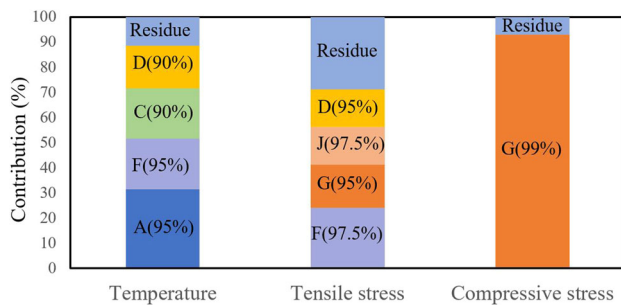


Fig. 2. Contribution and confidence levels (in parentheses) of factors for thermal and thermomechanical responses.

the thermal response. Therefore, further lining concept design will focus primarily on these four impact factors.

The same analysis procedure was carried out for thermomechanical responses. The summarized results with respect to the thermal and thermomechanical responses are shown in Fig. 2. In the case of tensile stress at the steel shell, the thermal conductivity of the insulation material (*F*) contributed the largest portion among the impact factors and is followed by the Young’s modulus of the working lining material (*G*), the thickness of the steel shell (*J*), and the thermal conductivity of the working lining material (*D*). The first four significant impact factors each had confidence levels greater than 95% and contributed 71% of the tensile stress at the steel shell. The Young’s modulus of the working lining (*G*) had an overwhelming influence on the compressive stress at the hot face of the working lining, with a 93% contribution.

Optimization Study of Factor Level

The *S/N* ratios of the thermal and thermomechanical responses were calculated with respect to the factor level and are shown in Fig. 3 and the supplementary figures. For each factor, the level showing the largest *S/N* ratio will be considered the optimal one. Figure 3 shows that the optimal *S/N*

ratios for the temperature at the cold end of the steel shell were A1B2C1D4E4F4G1H1I3J1. The optimal *S/N* ratios for the maximum tensile stress at the steel shell and for the maximum compressive stress at the hot face of the working lining were A4B4C4D4E2F1G4H4I4J1 and A4B2C2D3E1F3-G4H1I1J2, respectively (see “supplementary figures S1 and S2”).

Table IV summarizes the optimal levels for each response with the contribution of each factor according to the ANOVA and *S/N* ratio studies. In the case of the compressive stress at the hot face of the working lining, the Young’s modulus of the working lining (*G*) dominated the contribution, whereas the smallest Young’s modulus of the working lining is preferable. For the tensile stress and temperature responses at the cold end of the steel shell, the factors can be classified into two groups: one with the same optimal level for both responses, and the other with a contradictory trend. The decision can be easily made for the first group of factors (*D*, *I*, *J*). For the second group (*A*, *B*, *C*, *E*, *F*, *H*), the quantitative ANOVA results facilitate the further choice of levels. That is to say, the optimal level of one factor showing a higher contribution to one response (temperature or tensile stress) is preferable. For instance, the working lining and insulation lining thickness (*A* and *C*) occupied 31% and 20% contribution to the steel shell temperature, respectively, whilst only 5% and 7% to the tensile stress of the steel shell. Therefore, the application of a thicker lining is considered to take priority. The thickness of the permanent lining (*B*), the thermal conductivity (*E*), and the Young’s modulus (*H*) of the permanent lining did not play a significant role in either responses. Factor *F* had a rather equal contribution to the two responses and thus a compromise will be made, for example, a moderate insulation effect.

The analysis results according to the Taguchi method were further compared with those from the standard analysis of the mean value method. The mean value method indicates the optimal level and

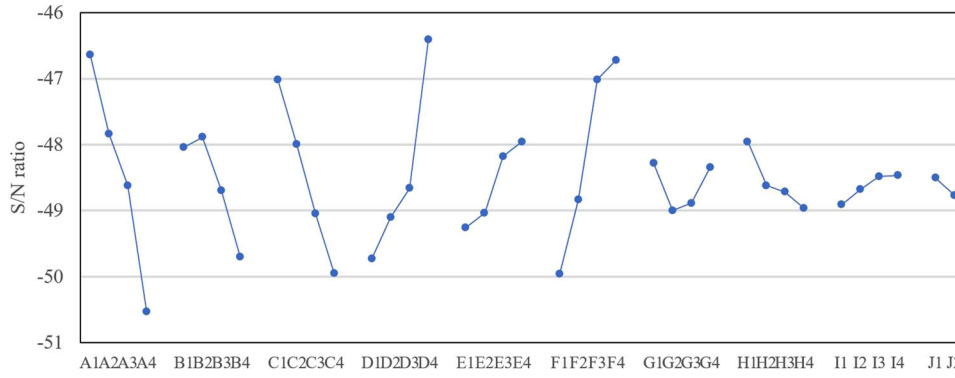


Fig. 3. S/N ratios for the temperature at the cold end of the steel shell, with highest S/N results for the case A1B2C1D4E4F4G1H1I3J1.

Table IV. Results based on analysis with the Taguchi method and standard main effect analysis

Factors	Thickness				Thermal conductivity				Young's modulus											
	Working lining (A)		Perma- nent lining (B)		Insula- tion (C)		Steel shell (J)		Work- ing lin- ing (D)		Perma- nent lining (E)		Work- ing lin- ing (G)		Perma- nent lining (H)		Insula- tion (I)			
	OL	CO (%)	OL	CO (%)	OL	CO (%)	OL	CO (%)	OL	CO (%)	OL	CO (%)	OL	CO (%)	OL	CO (%)	OL	CO (%)		
Taguchi method																				
$T \downarrow$	1	31	2	4	1	20	1	0.06	4	17	4	5	4	20	1	1	1	0.14	4	0.21
$\sigma_{Ten} \downarrow$	4	5	4	3	4	7	1	15	4	15	2	1.09	1	24	4	17	4	6	4	7
$\sigma_c \downarrow$														4	93					
Targets	OL	RK	OL	RK	OL	RK	OL	RK	OL	RK	OL	RK	OL	RK	OL	RK	OL	RK	OL	RK
Standard main effect analysis																				
$T \downarrow$	1	1	2	6	1	4	1	10	4	3	4	5	4	2	1	7	1	9	4	8
$\sigma_{Ten} \downarrow$	4	8	4	9	4	7	1	4	4	3	2	10	1	1	4	2	4	6	4	5
$\sigma_c \downarrow$															4	1				

OL optimal level, CO contribution, RK ranking.

provides the significance ranks of impact factors by comparing the maximum difference of the mean values of response among levels of each factor. By comparing the results in Table IV, one can observe the different outcomes of the two methods. The main effect method with mean calculation provides qualitative results, whilst the Taguchi method offers quantitative values. Certain differences in optimal results between these two methods can also be identified. For instance, when one looks at the contributions to the temperature at the cold end of the steel shell, the Taguchi method indicated that the insulation thickness ranked second in importance, equal to the thermal conductivity of insulation, and the thermal conductivity of the working lining ranked fourth, while the main effect analysis indicated that the insulation thickness and the

thermal conductivity of the working lining ranked fourth and third, respectively. Generally speaking, the Taguchi method is friendlier for decision-making.

Proposal and validation of the optimal lining concept

The final choice examined with the optimal lining concept takes into account the practical materials and the volume capacity of the steel ladle. The thermal conductivity and Young's modulus of material candidates for respective linings can be seen in "supplementary table SII". A compromise between the numerical results and practice has to be made. For instance, the insulation material candidate I4 is actually a fiber material and is unlikely to be widely

Table V. Two proposed optimal lining concepts with different insulation materials

	Thickness (mm)	Thermal conductivity (W m⁻¹K⁻¹)	Young's modulus (GPa)	Thermal expansion coefficient (10⁻⁶ K⁻¹)
Working lining (W1)	155	9	40	12.0
Permanent lining (P4)	52.5	2.2	45	5.0
Insulation (I2) (Case1)	37.5	0.5	3	6.0
Insulation (I3) (Case2)	37.5	0.38	4	5.6
Steel shell (S1)	30	50	210	12.0

used in the insulating lining, given its performance at high temperatures. A volume capacity decrease of the steel ladle is not desirable from an economical point of view. In the present study, the optimization of the lining concept was focused on the partial substitution of the permanent lining with the insulation lining. Thus, the thickness of the working lining and the total thickness of the permanent and insulation lining are the same as those of the reference case. The material with the highest thermal conductivity and lowest Young's modulus was proposed for the working lining. Since a moderate insulation effect is favorable for decreasing the steel shell temperature, while only slightly increasing the tensile stress in the steel shell, two insulation material candidates with lower thermal conductivities were proposed for the insulating lining. The details of lining structure and material properties are shown in Table V.

The thermal and thermomechanical behavior of the proposed lining concepts was studied with finite element modeling. The dimensionless temperature, tensile stress and compressive stress of the first proposed lining concept were 0.81, 1.16, and 0.74, respectively. For the second proposed lining concept, the dimensionless values were 0.75, 1.19, and 0.75 (see "supplementary table SII"). The dimensionless values were calculated by dividing the actual values by those of the reference case. The comparison shows that the temperature at the cold end of the steel shell and the maximum compressive stress at the hot face of the working lining were decreased by 19% and 26% for case 1 and 25% and 25% for case 2, respectively. For both cases, the maximum tensile stress at the steel shell slightly increased. In addition, case 2 showed a 6% lower steel shell temperature than case 1, and a 0.3% higher tensile stress at the cold end of the steel shell.

CONCLUSION

The lining concept parameter study of a steel ladle using the FE method revealed the complicated effects of the lining structure and material properties on the thermal and thermomechanical responses. Using the Taguchi method, the optimal levels and significance of factors can be efficiently

investigated. The statistical study using the Taguchi method facilitates decision making regarding the optimal lining concept. The proposed lining concepts show a significant decrease in temperature at the cold end of the steel shell and compressive stress at the hot face of the working lining, given the elastic material behavior of the refractories. The application of this methodology, while taking into account irreversible refractory material behavior, e.g., tensile failure, shear failure and creep, is of interest for future research.

ACKNOWLEDGEMENTS

Open access funding provided by Montanuniversitaet Leoben. The Competence Center for Excellent Technologies research programme in "Advanced Metallurgical and Environmental Process Development" (K1-MET) is supported by the Austrian Competence Centre Programme COMET (Competence Center for Excellent Technologies) with funds from the Federal Ministry for Transport, Innovation and Technology, the Federal Ministry of Economy, the provinces of Upper Austria and Styria, the Styrian Business Promotion Agency, and the Tyrolian Future Foundation.

OPEN ACCESS

This article is distributed under the terms of the Creative Commons Attribution 4.0 International License (<http://creativecommons.org/licenses/by/4.0/>), which permits unrestricted use, distribution, and reproduction in any medium, provided you give appropriate credit to the original author(s) and the source, provide a link to the Creative Commons license, and indicate if changes were made.

ELECTRONIC SUPPLEMENTARY MATERIAL

The online version of this article (<https://doi.org/10.1007/s11837-018-3063-1>) contains supplementary material, which is available to authorized users.

REFERENCES

1. A. Ghosh, *Secondary Steelmaking: Principles and Applications* (Boca Raton: CRC Press, 2000), pp. 275–285.
2. A. Zimmer, A.N.C. Lima, R.M. Trommer, S.R. Braganca, and C.P. Bergmann, *J. Iron. Steel Res. Int.* 15, 11 (2008).
3. O. Volkova and D. Janke, *ISIJ Int.* 43, 1185 (2003).
4. C.E. Baukal Jr, *Industrial Combustion Pollution and Control* (New York: CRC Press, 2003), p. 567.
5. D. Gruber, T. Auer, H. Harmuth and J. Rotsch, in *2nd International Conference on Simulation and Modeling of Metal: Processes in Steelmaking*, (Graz, Austria, 2007), pp. 291–296.
6. D. Gruber and H. Harmuth, *Steel Res. Int.* 79, 913 (2008).
7. D. Gruber and H. Harmuth, *Steel Res. Int.* 85, 512 (2014).
8. S. Jin, T. Auer, D. Gruber, H. Harmuth, M.H. Frechette, and Y. Li, *Interceram* 61, 37 (2012).
9. B. Cheng, P. Li, S. Tan, and Q. Zhao, *J. Iron. Steel Res. Int.* 27, 39 (2015).
10. L. Rebouillat, Y. Lee, G. Hodren and S. Kumar, in *14th Biennial Worldwide Congress: Unified International Technical Conference on Refractories*, (Vienna, Austria, 2015), p. 466.
11. K. Andreev and H. Harmuth, in *3rd DIANA World Conference*, (Tokyo, Japan, 2002), pp. 61–67.
12. G. Li, J. Liu, G. Jiang, and H. Liu, *Adv. Mech. Eng.* 7, 1 (2015).
13. S. Jin, D. Gruber, H. Harmuth, J. Soudier, P. Meunier, and H. Lemaistre, *Int. J. Cast Metals Res.* 27, 336 (2014).
14. S. Jin, H. Harmuth, and D. Gruber, *Ironmak. Steelmak.* (2017). <https://doi.org/10.1080/03019233.2017.1291153>.
15. S. Jin, H. Harmuth, and D. Gruber, in *60th International Colloquium on Refractories*, (Aachen, Germany, 2017), pp. 66–69.
16. R. Padmanabhan, M.C. Oliveria, J.L. Alves, and L.F. Mezezes, *Finite Elem. Anal. Des.* 43, 1062 (2007).
17. S.K. Karna, R.V. Singh, and R. Sahai, in *Proceedings of the National Conference on Trends and Advances in Mechanical Engineering*, (Faridabad, Haryana, 2012).
18. A. Joshaghani, A.A. Ramezani-pour, O. Ataei, and A. Golroo, *Constr. Build. Mater.* 101, 317 (2015).
19. N.M. Ghazaly, M.M. Makrahy, K.R. Mahmoud, K.A. Abd, A. El-Gwwad, and A.M. Abd-El-Tawwab, *Int. J Mech. Eng.* 3, 1 (2013).
20. R.K. Roy, *A Primer on the Taguchi Method*, 2nd ed. (Dearborn: Society of Manufacturing Engineers, 2010), p. 261.
21. R.N. Kacher, E.S. Lagergren, and J.J. Filliben, *J. Res. Natl. Inst. Stand. Technol.* 96, 577 (1991).
22. D.C. Montgomery, *Design and Analysis of Experiments*, 8th ed. (Singapore: Wiley, 2013), p. 60.

Thermal and Thermomechanical Responses Prediction of a Steel Ladle Using a Back-Propagation Artificial Neural Network Combining Multiple Orthogonal Arrays

Aidong Hou, Shengli Jin,* Harald Harmuth, and Dietmar Gruber

To facilitate industrial vessel lining design for various material properties and lining configurations, a method, being composed of the back-propagation artificial neural network (BP-ANN) with multiple orthogonal arrays, is developed, and a steel ladle from secondary steel metallurgy is chosen for a case study. Ten geometrical and material property variations of this steel ladle lining are selected as inputs for the BP-ANN model. A total of 160 lining configurations nearly evenly distributed within the ten variations space are designed for finite element (FE) simulations in terms of five orthogonal arrays. Leave-One-Out cross validation within various combinations of orthogonal arrays determines 7 nodes in the hidden layer, a minimum ratio of 16 between dataset size and number of input nodes, and a Bayesian regularization training algorithm as the optimal definitions for the BP-ANN model. The thermal and thermomechanical responses of two optimal lining concepts from a previous study using the Taguchi method are predicted with acceptable accuracy.

1. Introduction

Steel ladles, which consist of refractories and steel construction components, act as transportation vessels and refining units in the steelmaking industry. Refractory linings protect steel shells from steel melt, and reduce heat loss from the steel shells. A well-lined steel ladle offers efficient temperature control of the steel melt, and is beneficial to the steel quality and productivity.^[1–4]

The performance of a steel ladle is influenced by many factors; for instance, material properties, lining thicknesses, and process conditions. Efforts have been made to evaluate the performance of steel ladle linings from thermal and thermomechanical viewpoints using finite element (FE) methods, especially taking


into account the application of insulation and preheating time.^[5–10] Integrated consideration of lining concepts for a steel ladle is also of importance to support steel industry 4.0 in refractory application.^[11,12] Recently, the authors applied the Taguchi method to optimize lining design configurations with FE simulations within a defined variable span of lining thickness and material properties.^[5] The impact of factors on the thermal and thermomechanical responses was quantitatively assessed using the analysis of variance and signal-to-noise ratio. Finally, two optimal lining concepts were proposed, which showed a substantial decrease in heat loss through the cylindrical steel shell and the thermomechanical load at the hot face of the working lining. This approach offers a primary tool to assess the significance of

variables and select the optimal lining concept among the defined values of variables. Nevertheless, the instantaneous prediction of thermal and thermomechanical results of several proposed lining concepts after assessment is also desirable for efficient design of lining concepts, which are included in the defined span, but were fully or partly excluded from the defined values in the dataset used for training.

The artificial neural network (ANN) provides a promising technique to fulfil this target, and is one of the most extensively used methods in prediction based artificial intelligence and machine learning.^[13] It can be categorized as feed forward or recurrent. In contrast to recurrent neural networks, a feed forward neural network processes information from the input nodes, through the hidden nodes to the output nodes, without the information transfer process among the hidden nodes.^[14] Multilayer perception is usually preferable in feed forward neural networks trained with different error-back propagation (BP) algorithms.^[15] This type of ANNs has advantageous characteristics; for instance, generalization, adaptation, and robustness.^[16] It is successfully applied in materials engineering to predict the mechanical properties of materials,^[17–19] lifetime limited by fatigue crack propagation, and chemical compositions of alloys.^[15,20]

The predictive quality of an ANN model depends on the quality of the dataset, and on the architectural parameters, including the number of hidden layers and nodes per layer, and the training algorithms.^[21] It is important to collect data in a way that ensures they are representative in the entire variable space

A. Hou, Dr. S. Jin, Prof. H. Harmuth, Dr. D. Gruber
Chair of Ceramics
Montanuniversitaet Leoben
A-8700 Leoben, Austria
E-mail: shengli.jin@unileoben.ac.at

 The ORCID identification number(s) for the author(s) of this article can be found under <https://doi.org/10.1002/srin.201900116>.

© 2019 The Authors. Published by WILEY-VCH Verlag GmbH & Co. KGaA, Weinheim. This is an open access article under the terms of the Creative Commons Attribution-NonCommercial-NoDerivatives License, which permits use and distribution in any medium, provided the original work is properly cited, the use is non-commercial and no modifications or adaptations are made.

DOI: 10.1002/srin.201900116

with low influence from noise; the minimum size of a training dataset largely depends on the complexity of the problem and applied ANN architectures.^[21] The minimum dataset size is approximately proportional to the total number of free parameters divided by the fraction of errors permitted.^[22] For instance, with an error allowance of 10%, the training dataset size shall be about 10 times the number of weights and biases in the network. For complex models, the minimum size of a training dataset may deviate from this rule.^[23]

The numbers of hidden layers and nodes in each layer are significant parameters affecting the performance of an ANN model. With a larger number of hidden layers or nodes, an ANN model can yield more accurate training results and is able to model more complicated relationships, while it also increases the risk of over-fitting. In contrast, with a smaller number of hidden layers or nodes, an ANN model may be insufficient to depict the underlying relationships.^[24] Several empirical equations are proposed to define the node number in a hidden layer.^[25]

$$N_{out} < N_{hid} < N_{inp} \quad (1)$$

$$N_{hid} \approx 2/3 N_{inp} + N_{out} \quad (2)$$

$$N_{hid} \leq 2 N_{inp} \quad (3)$$

where N_{inp} , N_{hid} , and N_{out} are the node number of an input layer, hidden layer, and output layer, respectively.

The training algorithm for the back-propagation procedure also affects the performance of an ANN model. It is used to tune the weights in the network so that the network performs a suitable mapping process from inputs to outputs.^[24] The error function (E) represents a measure of network performance; E is defined as the mean square error between the outputs from network and the target values:

$$E = \frac{1}{N_t} \sum_{i=1}^{N_t} (d_i - y_i)^2 \quad (4)$$

where N_t is the total number of training samples, i is the sample index, d_i is the actual value of the i^{th} training sample, and y_i the predicted value of the i^{th} training sample.

Many training algorithms have been developed to minimize the error function with different strategies.^[26–28] For instance, gradient descent algorithms offer the possibility to define learning rate and momentum for the steepest descent during back-propagation. In contrast with gradient descent algorithms, conjugate gradient algorithms utilize the previous gradient search direction to define the present one; quasi-Newton algorithms use a Hessian matrix to define the descent direction; the Bayesian regularization algorithm minimizes the linear combination of squared errors and weights by applying the Levenberg-Marquardt algorithm. To identify which training algorithm is better is non-trivial; nevertheless, a good training algorithm should show acceptable robustness, computational efficiency, and generalization ability.

The present work aimed to develop a methodology for applying a reliable back-propagation (BP) ANN model to predict the thermal and thermomechanical responses of a steel ladle

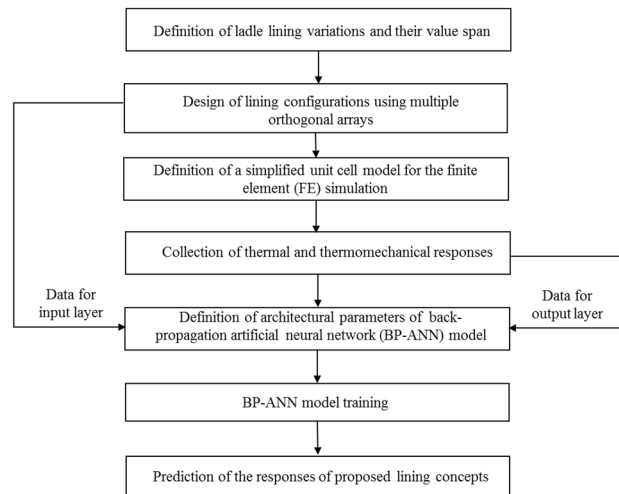


Figure 1. Flowchart of a methodology to predict thermal and thermomechanical responses of a steel ladle.

within a defined variable space. Multiple orthogonal arrays were employed to generate lining configurations for FE simulations and BP-ANN model training. The sufficiency of the dataset, feasible node number in the hidden layer for a case study with 10 variables, and the training algorithms were investigated. Later, a BP-ANN model with optimized settings was applied to predict the results of two lining concepts proposed in the Hou et al.^[5]

2. Methodology

A flowchart of this methodology for predicting the thermal and thermomechanical responses of a steel ladle is illustrated in **Figure 1**, and includes lining configuration design, FE modeling, and BP-ANN model training and prediction.

2.1. Finite Element Model and Boundary Conditions

Figure 2 depicts a simplified two-dimensional model representing a horizontal cut through the slag-line position in the upper part of the steel ladle. The outer diameter of the steel ladle was 1.828 m for all of the established models. The model consists of a two-half brick working and permanent lining, an insulation lining, a fiberboard, and a steel shell. The circumferential expansion allowance between bricks was 0.4 mm. Variations were lining and steel shell thicknesses, thermal conductivity, and Young's modulus of lining materials.

FE-modeling of the steel ladle, taking into account elastic material behavior, was performed using the commercial code

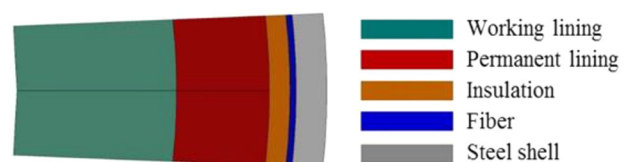


Figure 2. Finite element (FE) model geometry.

Abaqus. The simulation included the preheating of the working lining hot face to 1100 °C over 20 h, and a subsequent thermal shock caused by tapping the steel melt of 1600 °C into the ladle. After a refining period of 95 min proceeded a 50 min idle period. Displacement of linings was allowed in the radial direction and constrained in the circumferential direction with a symmetry condition. The heat transfer between the liquid melt and hot face of the working lining, the cold end of the steel shell, and the atmosphere was defined as being temperature-dependent using the surface film condition function (Table 1) in Abaqus. The interfaces between linings were crossed by heat flux, and a heat transfer coefficient allowing for radiation and convection was applied.

2.2. Sample Screening Approach

Orthogonal arrays are highly fractional factorial designs that yield a minimum number of experimental runs. With orthogonal array design, the combination of each level of two or more variables occurs with equal frequency.^[29]

Multiple orthogonal arrays were applied to arrange the level combination of the ten factors within various defined variable spaces. The definition of values in the respective span of a variable in each orthogonal array was arbitrary, and an even distribution of the values in the maximum span was designed. Detailed variations and the associated intervals are listed in Table 2. Nine of the studied factors had four levels, and the thickness of the steel shell had two levels. A total of 5 variable spaces were defined; thus, 5 mixed-level orthogonal arrays L32 ($4^9 \times 2^1$) with 32 runs were implemented accordingly, which yielded the total dataset size of lining configurations equal to 160. The lining configurations according to the orthogonal array containing the maximum or minimum level value constituted the boundary space, termed space A, and were used only for BP-ANN model training. The lining configurations from the other four orthogonal arrays were named as spaces B, C, D, and E. The maximum level values of all 10 factors in spaces B, C, D, and E were defined in a descending order, and their minimum level

values were in an ascending order accordingly. Spaces B-E were used for BP-ANN model training and testing.

2.3. BP-ANN Model Establishment and Parameter Study Design

The BP-ANN model was made of three layers with various nodes: one input layer, one hidden layer, and one output layer. Nodes in the former layer were connected to each node in the latter layer, as shown in Figure 3. Input variables (X) were introduced to the network as a vector corresponding to the nodes in the input layer. These input variables were multiplied by their respective weights (W) and plused a bias (b) constant, yielding a summation (S) for each node of the hidden layer, as shown in Equation (5). An activation function was used to limit the amplitude of the summation of each hidden layer node, which is the input for the output layer nodes, as depicted by Equation (6). A hyperbolic tangent sigmoid activation function (tansig) was applied as shown in Equation (7).

$$S_k = \sum_{j=1}^{N_{inp}} W_{jk} X_j + b \quad (5)$$

$$O_k = f(S_k) \quad (6)$$

$$f_{\text{tansig}} = \frac{1 - e^{-2S_k}}{1 + e^{-2S_k}} \quad (7)$$

where j is the input factor index, k is the node index in the hidden layer, S_k is the summation at the k^{th} node in the hidden layer, f is the activation function, W_{jk} is the weight of the j^{th} input at the k^{th} node, X_j is the j^{th} input, b is the bias, and O_k is the output of the k^{th} node in the hidden layer. The information transfer

Table 1. Film coefficient ($W \text{ m}^{-2} \text{ K}^{-1}$) defined in the finite element (FE) model.

Temperature (°C)	Hot face of working lining	Temperature (°C)	Cold end of steel shell
10	10	10	10
150	60.1	50	10
250	99	150	15
350	149.9	250	21
400	181.1	350	27
650	409.5	400	32
700	472.3	650	50
800	617.8	700	70
1000	998.5	1000	140
1200	1517	1600	400
1600	3052.3	2000	400

Table 2. Geometrical and material property variations for the selected ladle.

	Ladle linings	Range of variable values	Label of factors
Thickness (m)	Working lining	0.03–0.27	X_1
	Permanent lining	0.05–0.14	X_2
	Insulation	0.003–0.042	X_3
	Steel shell	0.015–0.035	X_4
Thermal conductivity ($W \text{ m}^{-1} \text{ K}^{-1}$)	Working lining	1.5–10.5	X_5
	Permanent lining	1.0–10.0	X_6
	Insulation	0.05–1.55	X_7
Young's modulus (GPa)	Working lining	25–115	X_8
	Permanent lining	5–110	X_9
	Insulation	0.1–39.1	X_{10}

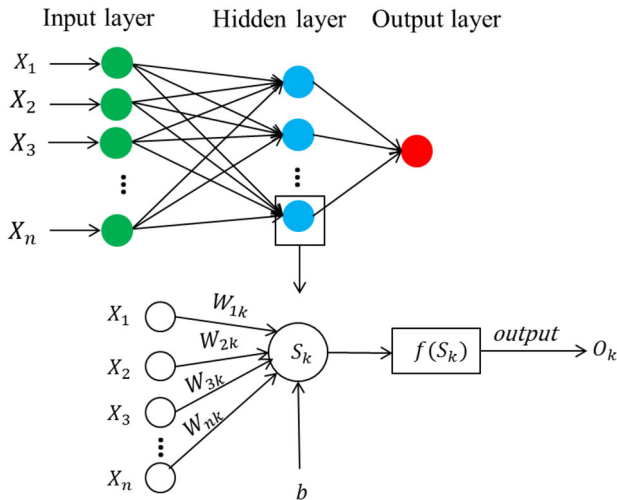


Figure 3. Topology of a three-layer artificial neural network.

between the hidden layer and output layer followed the same mathematical process, and in the present paper a linear activation function (purelin) was applied:

$$f_{\text{purelin}} = S_m \quad (8)$$

where m is the node index in the output layer, and S_m is the summation at the m^{th} node in the output layer.

Before ANN training starts, the input variables of the network must be defined. When the ranges and units of input variables are different from each other, it is wise to normalize input data to mitigate the influence of magnitudes. In the present study, input variables were normalized (X_i) to a scale of 0.1–0.9 using the following equation for a variable x :

$$X_i = \frac{0.1x_{\max} - 0.9x_{\min} + 0.8x_i}{x_{\max} - x_{\min}} \quad (9)$$

where x_{\max} and x_{\min} represent the maximum and minimum of the variable x .

To determine the optimal BP-ANN architectural parameters for thermal and thermomechanical responses, three tests were carried out with temperature response and parameters optimized sequentially. Afterwards, thermomechanical responses were used to test the generality of the established BP-ANN model. Training was terminated by reaching any defined criterion; for instance, the minimum performance gradient (10^{-5}), the minimum target error (0), or a maximum number of epochs (one epoch includes one forward pass and one backward pass of all the training samples, 10 000 as default value if there is no explicit definition).

First, a test was performed to explore the optimal node number in the hidden layer. All 160 samples were used for BP-ANN training, and the training algorithm was a gradient descent with momentum and adaptive learning rate back-propagation (GDx; Table 3). The number of nodes in the hidden layer varied from 1 to 12. The objective of the second test was to identify the minimum sample size for the lining concept study. The dataset was divided into three groups, which

Table 3. Training algorithms employed in this study. [30]

Training algorithm	Brief description
GDx	Gradient descent with momentum and adaptive learning rate back-propagation
CGB	Conjugate gradient back-propagation with Powell-Beale restarts
CGF	Conjugate gradient back-propagation with Fletcher-Reeves updates
CGP	Conjugate gradient back-propagation with Polak-Ribière updates
SCG	Scaled conjugate gradient back-propagation
BFG	BFGS quasi-Newton back-propagation
OSS	One-step secant back-propagation
BR	Bayesian regularization back-propagation

contained 96, 128, and 160 samples. All three groups included 32 samples in boundary space A. The residual samples in each group were the combination of any two, three, and four variable spaces except boundary space A. Eight training algorithms (Table 3) in the Deep Learning Toolbox of Matlab^[30] were employed individually in the third test to detect the training algorithm most favorable for the steel ladle. A summary of these three tests is listed in Table 4.

Leave-one-out (LOO) cross validation and figures of merit were employed in these three tests to quantitatively assess the performance of the established BP-ANN model. LOO applies one sample for prediction and the residual samples of the entire dataset for training. Four quantities were used: maximum relative error (RE_MAX), mean relative error (MRE), relative root mean squared error (RRMSE), and coefficient of determination (B), as shown in Equations (10)–(13):

Maximum relative error of all testing samples:

$$\text{REMAX} = \text{Max} \left(\frac{|d_i - y_i|}{d_i} \right) \quad (10)$$

$$\text{Mean relative error : MRE} = \frac{1}{n} \sum_{i=1}^n \frac{|d_i - y_i|}{d_i} \quad (11)$$

Relative root mean squared error:

$$\text{RRMSE} = \frac{\sqrt{\frac{1}{n} \sum_{i=1}^n (d_i - y_i)^2}}{\bar{d}} \quad (12)$$

Table 4. Tests for the design of BP-ANN model architectural parameters.

Test	Architectural factors of BP-ANN model	Testing parameters
1	The number of nodes in hidden layer	12 (from 1 to 12)
2	Dataset size	3 groups (96, 128, and 160 samples)
3	Training algorithms	8 (GDx, CGB, CGF, CGP, SCG, BFG, OSS, BR; available in Matlab)

$$\text{Coefficient of determination : } B = 1 - \frac{\sum_{i=1}^n (d_i - y_i)^2}{\sum_{i=1}^n (d_i - \bar{d})^2} \quad (13)$$

where n is the number of testing samples, y_i is the predicted value of the i^{th} testing sample by the BP-ANN model with LOO, d_i is the response value of the i^{th} testing sample from FE modeling, and \bar{d} is the mean response value of all testing samples received from the FE modeling.

3. Results and Discussion

3.1. Node Number in the Hidden Layer

The BP-ANN model predicts the temperatures at the steel shell at the end of the idle period with various numbers of nodes in the hidden layer with epochs of 1000. Low values of RE_MAX, MRE, and RRMSE, and a larger value of B are desirable. Dimensionless calculation was performed for each quantity relative to its largest value. As shown in **Figure 4**, the node number in the hidden layer affects BP-ANN performance in a complex manner. Generally speaking, cases with node numbers of 4-7 and 9 showed satisfying results. Although the case with the node number 7 showed slightly higher RE_MAX, its MRE and RRMSE were the minima among the 12 cases.

Therefore, for an input layer with 10 nodes, node number 7 of the hidden layer was proposed for the further study. This result was consistent with a previously stated rule,^[25] which defines that the node number of the hidden layer shall be approximately equal to two thirds of the node number in the input layer plus the node number in the output layer, as stated in Equation (2). In the present study, this rule yielded 7.67.

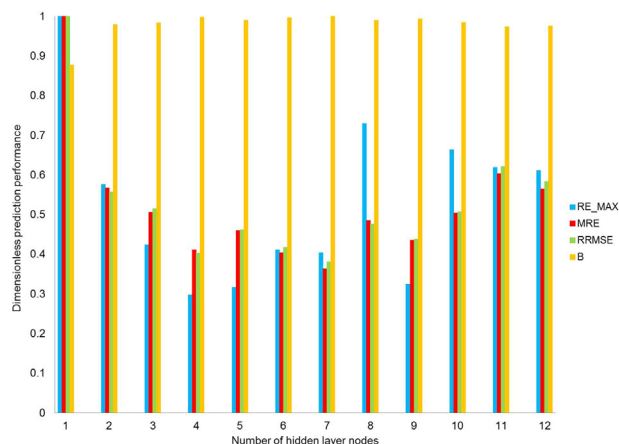


Figure 4. Performance assessment of the back-propagation artificial neural network (BP-ANN) model for temperature prediction with different node numbers in the hidden layer and by applying the GDx (gradient descent with momentum and adaptive learning rate back-propagation) training algorithm.

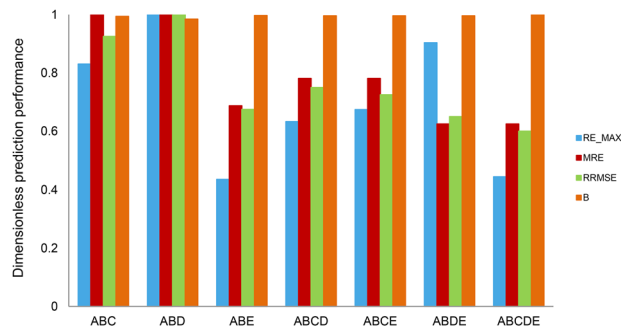
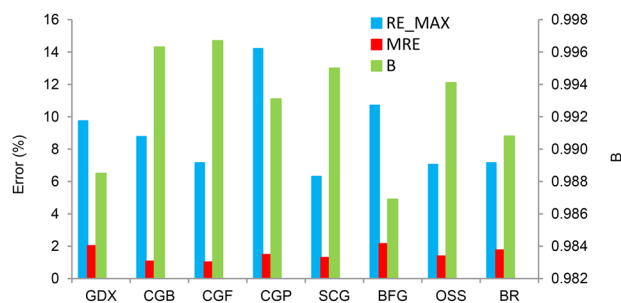


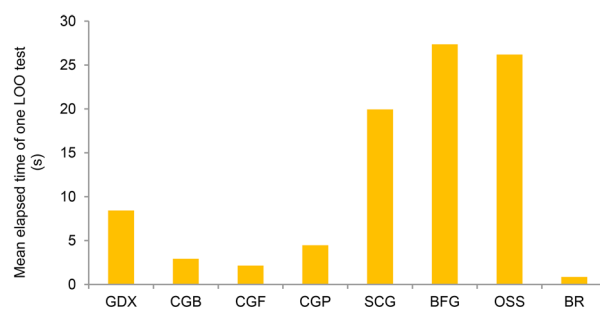
Figure 5. Performance assessment of the back-propagation artificial neural network (BP-ANN) model for temperature prediction with different dataset sizes and by applying the GDx (gradient descent with momentum and adaptive learning rate back-propagation) training algorithm.

3.2. Dataset Size

Seven cases with different combinations of orthogonal arrays were defined to test the appropriate dataset size for reliable BP-ANN models to predict the temperature response. The dataset size of ABC, ABD, and ABE is 96; that of ABCD, ABCE, and ABDE is 128, and that of ABCDE is 160. The dimensionless performance of BP-ANN models for the seven cases is represented in **Figure 5**. In general, better performance was achieved by increasing the dataset size. The BP-ANN model with



(a)



(b)

Figure 6. Performance assessment of the back-propagation artificial neural network (BP-ANN) model for (a) temperature prediction based errors, and (b) computation time with different training algorithms.

Table 5. Thermomechanical responses prediction performance of BP-ANN models with CGF and BR.

Criteria	End temperature		Maximum tensile stress		Maximum compressive stress	
	CGF	BR	CGF	BR	CGF	BR
RE_MAX (%)	7.15	7.15	16.62	12.43	3.12	4.09
MRE (%)	1.02	1.76	2.43	2.37	0.93	0.78
B	0.9967	0.9908	0.9279	0.9348	0.9963	0.9966
Mean elapsed time of one LOO test (s)	2.15	0.86	3.16	1.12	1.38	0.68

96 samples from spaces of A, B, and E showed good prediction performance; Given the worse performance was of ABC and ABD, a conservative minimum sample size for the present study was 160, which is 16 times the number of inputs.

3.3. Training Algorithms

Eight training algorithms to predict end temperature at the cold end of the steel shell were employed individually in order to train the BP-ANN model with the above determined architectural parameters. Besides RE_MAX, MRE, and B, the mean elapsed time for training 159 samples and prediction of one sample in LOO tests was additionally applied to evaluate the efficiency of the model. The performance results are presented in **Figure 6**. Lower error values, larger B, and shorter computation time are favorable. As shown in Figure 6a, the RE_MAX and MRE from the cases with algorithms CGF, SCG, OSS, and BR were less than those from GDX, CGB, CGP, and BFG, and showed acceptable coefficients of determination. However, calculations with algorithms SCG and OSS were time consuming (Figure 6b). Therefore, the algorithms CGF and BR were proposed for further study.

3.4. Extension to Thermomechanical Response Study

To finalize the model infrastructure, the above-determined BP-ANN model with 7 nodes in the hidden layer and 160 samples in the dataset was trained, using both CGF and BR, to predict thermomechanical responses. **Table 5** summaries the prediction performance comparison of algorithms CGF and BR in thermal and thermomechanical responses. The BP-ANN model trained using BR performed better than the model with CGF for the maximum tensile stress and compressive stress. Therefore, a BP-ANN model with BR was proposed for the steel ladle study.

It is noteworthy that the prediction performance of this BP-ANN model with BR for maximum tensile stress is inferior to that for end temperature and maximum compressive stress. A previous study^[5] showed that 7 of the 10 defined factors contribute 91% to the maximum tensile stress, followed by 5 factors contributing 94% to the end temperature, and 1 factor contributing 93% to the maximum compressive stress. The high dimensionality occurring in the factor-response space increases the complexity of the problem and results in under-fitting. Conversely, if the maximum tensile stress prediction was used for parameter study, one could expect over-fitting of the end temperature and maximum compressive stress. An alternative could be establishing the BP-ANN models with regard to the individual response, instead of the three responses. Nevertheless, the RE_MAX for the maximum tensile stress was 12.43%, which is less than the 15% empirical error tolerance of prediction.^[19,31,32] Moreover, the MSE was as low as 2.37%; therefore, the BP-ANN model was sufficient for the research requirements.

3.5. Prediction with the Optimized BP-ANN Model

The optimal configuration of the BP-ANN model contains 7 nodes in the hidden layer, and applies the Bayesian regularization method, with 160 samples for training. The configurations and the results of the comparison of predicted values for two proposed lining concepts are given in **Table 6** and **Table 7**, respectively. The temperature difference between the BP-ANN model and the FE results was 4 K for lining concept 1, and the BP-ANN model predicted the same temperature as the FE modeling of lining concept 2. The maximum tensile stress differences between BP-ANN prediction and FE modeling for the two lining concepts were 62 and 37 MPa, representing 4.1% and 2.4%, respectively. The differences in maximum compressive stress between BP-ANN prediction and FE modeling for the two lining concepts were 5 and 2 MPa, representing 0.97% and 0.39%, respectively.

Table 6. Two proposed optimal lining concepts with different insulation materials. ^[5]

	Thickness (mm)	Thermal conductivity ($W m^{-1}K^{-1}$)	Young's modulus (GPa)	Thermal expansion coefficient ($10^{-6}K^{-1}$)
Working lining	155	9	40	12.0
Permanent lining	52.5	2.2	45	5.0
Insulation (Lining concept 1)	37.5	0.5	3	6.0
Insulation (Lining concept 2)	37.5	0.38	4	5.6
Steel shell	30	50	210	12.0

Table 7. Comparison of simulated and predicted values of two proposed optimal lining concepts from FE modeling and BP-ANN.

	Steel shell temperature (°C)		Maximum tensile stress (MPa)		Maximum compressive stress (MPa)	
	FE modeling	Prediction	FE modeling	Prediction	FE modeling	Prediction
Lining concept 1	280	276	1495	1433	512	517
Lining concept 2	259	259	1539	1576	517	515

4. Conclusion and Outlook

A BP-ANN model was developed to predict the thermal and thermomechanical responses of a steel ladle considering 10 geometrical and material property variations of ladle linings. The optimized architectural parameters of the proposed BP-ANN model were 7 nodes in the hidden layer, a dataset size not less than 16 times the number of input nodes, and a Bayesian regularization training algorithm. The LOO tests for 128 samples showed that the coefficient of determination of the end temperature, the maximum tensile stress at the steel shell, and the maximum compressive stress at the hot face of the working lining were high. The proposed BP-ANN model was further utilized to predict the responses of two lining configurations proposed by previous work, and the high prediction accuracy confirmed the reliable performance of the BP-ANN model.

As an alternative to the conventional trial-and-error method, the numerical investigation of lining concepts for a given industrial vessel can be beneficial in saving time, materials, and labor by avoiding unnecessary industrial trials. On the other hand, the BP-ANN method allows an efficient search for optimized lining concepts for vessels from both energy savings and better thermomechanical performance points of view.

The proposed multiple orthogonal arrays and BP-ANN methods developed in the present paper are also promising for the optimization of ironmaking and steelmaking processes and material recipe development. Especially, the application of multiple orthogonal arrays is an advanced tool to achieve a representative variations-response space, which defines the establishment of BP-ANN model and affects the prediction performance.

Acknowledgements

The Competence Center for Excellent Technologies research programme in “Advanced Metallurgical and Environmental Process Development” (K1-MET) is supported by the Austrian Competence Centre Programme COMET (Competence Center for Excellent Technologies) with funds from the Federal Ministry for Transport, Innovation and Technology, the Federal Ministry of Economy, the provinces of Upper Austria and Styria, the Styrian Business Promotion Agency, and the Tyrolian Future Foundation.

Conflict of Interest

The authors declare no conflict of interest.

Keywords

artificial neural network, back-propagation, orthogonal array, lining concept, steel ladle, thermomechanical responses

Received: March 4, 2019
Revised: April 2, 2019
Published online: April 29, 2019

- [1] A. Ghosh, *Secondary Steelmaking: Principles and Applications*, CRC Press, Florida, USA, **2000**.
- [2] A. Zimmer, A. N. C. Lima, R. M. Trommer, S. R. Braganca, C. P. Bergmann, *J. Iron. Steel. Res. Int.* **2008**, *15*, 11.
- [3] O. Volkova, D. Janke, *ISIJ Int.* **2003**, *43*, 1185.
- [4] C. E. Baukal Jr, *Industrial Combustion Pollution and Control*, CRC Press, New York, USA **2003**.
- [5] A. Hou, S. Jin, H. Harmuth, D. Gruber, *JOM.* **2018**, *70*, 2449.
- [6] D. Gruber, H. Harmuth, *Steel. Res. Int.* **2008**, *79*, 913.
- [7] G. Li, J. Liu, G. Jiang, H. Liu, *Adv. Mech. Eng.* **2015**, *7*, 1.
- [8] D. Gruber, T. Auer, H. Harmuth, *Rotsch J, in Steelsim 2007*, TIB, Graz, Austria **2007**, p. 291.
- [9] D. Gruber, H. Harmuth, *Steel. Res. Int.* **2014**, *85*, 512.
- [10] S. Jin, T. Auer, D. Gruber, H. Harmuth, M. H. Frechette, Y. Li, *Intereram/Refractories Manual.* **2012**, 37.
- [11] S. Jin, D. Gruber, H. Harmuth, J. Soudier, P. Meunier, H. Lemaistre, *Int. J. Cast. Met. Res.* **2014**, *27*, 336.
- [12] S. Jin, H. Harmuth, D. Gruber, Proc. 60th Int Colloq Refract, TIB, Aachen, Germany, **2017**, p. 66.
- [13] A. Alibakshi, *Anal. Chim. Acta.* **2018**, *1026*, 69.
- [14] L. Fausett, *Fundamentals of Neural Networks: Architecture, Algorithms, and Applications*, Prentice Hall, NJ, USA **1994**.
- [15] J. R. Mohanty, B. B. Verma, D. R. K. Parhi, P. K. Ray, *Arch. Comput. Mat. Sci. Surface Eng.* **2009**, *01*, 133.
- [16] J. M. O. Rodriguez, M. R. M. Blanco, J. M. C. Viramontes, H. R. V. Carrillo, in *Artificial Neural Networks – Architectures and Applications*, (Ed: K. Suzuki), InTech, Croatia **2013**, Ch. 4.
- [17] S. H. Sadati, J. A. Kaklar, R. Ghajar, in *Artificial Neural networks – Industrial and Control Engineering Applications*, (Ed: K. Suzuki), InTech, Croatia **2010**, Ch. 5.
- [18] J. Ghaisari, H. Jannesari, M. Vatani, *Adv. Eng. Softw.* **2012**, *45*, 91.
- [19] C. Bilim, C. D. Atis, H. Tanyildizi, O. Karahan, *Adv. Eng. Softw.* **2009**, *40*, 334.
- [20] Y. Sun, W. D. Zeng, Y. F. Han, X. Ma, Y. Q. Zhao, *Comput. Mater. Sci.* **2011**, *50*, 1064.
- [21] L. A. Dobrzański, J. Trzaska and A. D. Dobrzańska-Danikiewicz, in *Comprehensive Materials Processing*, Vol. 2, (Eds: S. Hashmi, G. F. Batalha, C. J. Van Tyne, B. Yilbas), Elsevier, CO, USA **2014**, Ch. 9.
- [22] S. Haykin, *Neural Networks and Learning Machines*, Pearson Education, Ontario, Canada **2009**.
- [23] A. Alwosheel, S. Cranenburgh, C. G. Chorus, *J. Choice Model.* **2018**, *28*, 167.
- [24] A. Radi, S. K. Hindawi, in *Artificial Neural Networks – Architectures and Applications*, (Ed: K. Suzuki), InTech, Croatia **2013**, Ch. 9.
- [25] S. Karsoliya, *IJETT.* **2012**, *31*, 714.
- [26] M. Moreira, E. Fiesler, IDIAP Technical Report, Martigny, Switzerland **1995**.

- [27] Z. Cömert, A. F. Kocamaz, Bitlis. Eren. Univ. J. Sci. & Technol. **2017**, 7, 93.
- [28] M. Fernandez, J. Caballero, in Artificial Neural Network for Drug Design, Delivery and Disposition, (Eds: M. Puri, Y. Pathak, V. K. Sutariya, S. Tipparaju, W. Moreno), Academic Press, **2016**, Ch. 4.
- [29] R. K. Roy, A Primer on the Taguchi Method, Society of Manufacturing Engineers, USA **2010**.
- [30] MathWorks. Deep Learning Toolbox: User's Guide (R2018b).
- [31] Z. Yuan, L. N. Wang, X. Ji, *Adv. Eng. Softw.* **2014**, 67, 156.
- [32] J. L. G. Rosa, in Artificial Neural Networks – Architectures and Applications, (Ed: K. Suzuki), InTech, Croatia **2013**, Ch. 2.

Article

Influence of Variation/Response Space Complexity and Variable Completeness on BP-ANN Model Establishment: Case Study of Steel Ladle Lining

Aidong Hou *, Shengli Jin , Dietmar Gruber and Harald Harmuth

Chair of Ceramics, Montanuniversitaet Leoben, 8700 Leoben, Austria

* Correspondence: aidong.hou@unileoben.ac.at

Received: 28 May 2019; Accepted: 13 July 2019; Published: 16 July 2019



Abstract: Artificial neural network (ANN) is widely applied as a predictive tool to solve complex problems. The performance of an ANN model is significantly affected by the applied architectural parameters such as the node number in a hidden layer, which is largely determined by the complexity of cases, the quality of the dataset, and the sufficiency of variables. In the present study, the impact of variation/response space complexity and variable completeness on backpropagation (BP) ANN model establishment was investigated, with a steel ladle lining from secondary steel metallurgy as the case study. The variation dataset for analysis comprised 160 lining configurations of ten variables. Thermal and thermomechanical responses were obtained via finite element (FE) modeling with elastic material behavior. Guidelines were proposed to define node numbers in the hidden layer for each response as a function of the node number in the input layer weighted with the percent value of the significant variables contributing above 90% to the response, as well as the node number in the output layer. The minimum numbers of input variables required to achieve acceptable prediction performance were three, five, and six for the maximum compressive stress, the end temperature, and the maximum tensile stress.

Keywords: backpropagation artificial neural network; space complexity; variable completeness; lining concept; steel ladle; thermomechanical responses

1. Introduction

Artificial neural network (ANN), a technique for artificial intelligence and machine learning, is often applied as a tool to deal with nonlinear problems and offer predictions in civil engineering [1–4], material science [5,6], etc. The extension of its applications into the iron and steel industry is also reported [7–11].

Architecture establishment of a suitable ANN model is still challenging in the definition of the layer number and node number in the respective layer. Generally, a three-layer ANN model is sufficient to build the relations among variables and responses [12]. Therefore, the determination of the proper node number in the single hidden layer is the key issue. Table 1 lists the publications on the optimization of the single hidden layer node number. To seek an optimal one, many applied the trial and error method in a diverse range of the node numbers [13–17]; whilst others merely followed the rules of thumb proposed in the literature [18–24], and the application of rules can significantly reduce the number of trials. Six selected rules of thumb [18–25] used in the respective publication are given below and indicated in Table 1 with an asterisk. The node number or number range for each study was calculated according to the six rules of thumb and compared to the optimal hidden layer node number determined in the respective study. It is evidently shown that the extended applications of six

empirical equations into other fields are far less satisfying. Equations (1) and (2) show more robust applications, yet they yield a rather larger number for trials.

$$N_h = (N_i + N_o)^{1/2} + a, a \in [1, 10] \quad (1)$$

$$N_h = (N_i + N_o)^{1/2} + a, a \in [0, 10] \quad (2)$$

$$N_h = (N_i \times N_o)^{1/2} \quad (3)$$

$$N_h = N_{train}/(N_i + 1) \quad (4)$$

$$N_h = 1/2 (N_i + N_o) + N_{train}^{1/2} \quad (5)$$

$$N_h = 2/3 (N_i) + N_o \quad (6)$$

where, N_i , N_h , and N_o are the node numbers in the input, hidden, and output layer, N_{train} is the dataset size for training, and a is an empirical integer not larger than 10.

Several reasons contribute to the diverse results of the hidden layer node number optimization with the six rules of thumb. One is the problem nature or complexity. As shown in Table 1, the optimal values of erosion of beaches and energy conservations in old buildings are out of the range defined by the empirical equations. One empirical equation may show consistent performance for the problems within similar complexity. For instance, the prediction of Equation (3) for beach erosion [13] is rather close to the optimal value that was used as the rule of thumb in the study of the mechanical behavior of mortar [22]. The second reason is the quality of the dataset for training. The optimal training dataset size was suggested to be ten times larger than the total number of weights and biases [12]. A steel ladle lining study showed that the dataset size could be 16 times larger than the variable number in the input layer, in the case of a well-distributed dataset in variation/response spaces [26]. Table 1 also shows the size of the dataset for training and the ratio of the training dataset size to the number of variables quoted in literature. Mostly, the information of dataset quality is missing and insufficient dataset size relative to the variable number could be expected. Finally, the sufficiency of important variables or factors, i.e., the variable completeness, in the problem definition shall also be taken into account.

The present paper investigates the influence of variation/response space complexity and variable completeness on the required node numbers for a three-layer backpropagation (BP)-ANN model using steel ladle lining as a case study. A representative dataset was obtained by a sample screening approach applying multiple orthogonal arrays [26]. The dataset contains 160 samples constituted by ten variables and three responses. The first part of the paper examines the prediction performance of three-layer BP-ANN models with various node numbers in the hidden layer, to reveal the correlation among the node numbers of input and output layers, the ratio of the number of variables contributing above 90% to the response to the total number of variables, and the node number of the hidden layer for each response. In the second part, several combinations of variables were tested as inputs for given three-layer BP-ANN models to assess the influence of the ratio of input variables to the total number of variables on the prediction performance.

Table 1. Literature study of rules to define the node number in the hidden layer.

Research Field	N_{train}	N_i	N_{train}/N_i	N_o	N_h Range	Number of Trials	Optimal N_h	Equation (1)	Equation (2)	Equation (3)	Equation (4)	Equation (5)	Equation (6)
Erosion of beaches [13]	105	3	35	15	1–20	20	3	[5, 15]	[4, 15]	4, 5	26, 27	19, 20	17
Energy conservation in old buildings [14]	66	7	9.4	1	4–15	12	15	[3, 13]	[2, 13]	2, 3	8, 9	12, 13	5, 6
Power output [15]	–	5	–	1	1–11	11	7	[3, 13] ^Δ	[2, 13] ^Δ	2, 3	–	–	4, 5
Phytoremediation of palm oil secondary effluent [16]	30	3	10	2	1–15	15	13	[3, 13] ^Δ	[2, 13] ^Δ	2, 3	7, 8	7, 8	4
Adsorption of metal ions [17]	13	3	4.3	3	1–15	15	14	[4, 14] ^Δ	[3, 14] ^Δ	2, 3	3, 4	6, 7	5
Extraction of sensing information [18]	500	100	5	1	11–20	10	19	[11, 20] [*]	[10, 20] ^Δ	10, 11	4, 5	72, 73	67, 68
Lithology identification for shale oil reservoir [19]	220	11	20	4	7–11	5	10	[4, 14] [*]	[3, 14] ^Δ	3, 4	18, 19	22, 23	11, 12
Moisture content prediction in paddy drying process [20]	–	3	–	1	2–12	11	2	[3, 12]	[2, 12] [*]	2 ^Δ	–	–	3
Corn variety identification [21]	–	10	–	3	3–14	12	8	[4, 14] ^Δ	[3, 14] [*]	3, 4	–	–	9, 10
Mechanical behavior of mortar [22]	30	6	5	1	1–9	9	2	[3, 13]	[2, 13] ^Δ	2, 3 [*]	4, 5	8, 9	5
Extraction of phenolic compounds [23]	12	3	4	1	1–3	3	2	[3, 12]	[2, 12] ^Δ	2 ^Δ	3 [*]	5, 6	3
Damage pattern of structural systems [24]	113	10	11.3	4	17, 18	2	17	[4, 14]	[3, 14]	3, 4	10, 11	17, 18 [*]	10, 11

N_{train} is the dataset size for training.

N_i, N_h, N_o are the nodes numbers in the input, hidden, and output layer, respectively.

– Data are not available in the literature.

* The rule was used to define nodes number in the hidden layer by the authors in their publication.

^Δ Rules that optimal N_h are coincident with.

2. Methodology

2.1. Numerical Experiments

2.1.1. Lining Concept Design

Ten main variables prescribing steel ladle linings were selected for numerical experiments design. These variables (Table 2) were the thicknesses of refractory linings and the steel shell, thermal conductivity and Young's modulus of lining materials. The dataset of lining configurations was designed by a sample screening approach developed in the previous work [26], applying five mixed-level orthogonal arrays $L_{32} (4^9 \times 2^1)$ with nine four-level variables, and a two-level variable for the thickness of the steel shell. This gives a total amount of 160 experiments (See Supplementary Material).

Table 2. Geometrical and material property variables of steel ladle [26].

	Variables	Range of Variable Values	Label of Variables
Thickness (m)	Working lining	0.03–0.27	A
	Permanent lining	0.05–0.14	B
	Insulation	0.003–0.042	C
	Steel shell	0.015–0.035	J
Thermal conductivity ($\text{Wm}^{-1}\text{K}^{-1}$)	Working lining	1.5–10.5	D
	Permanent lining	1.0–10.0	E
	Insulation	0.05–1.55	F
Young's modulus (GPa)	Working lining	25–115	G
	Permanent lining	5–110	H
	Insulation	0.1–39.1	I

2.1.2. Finite Element Models

Finite element (FE) modeling was carried out with a commercial software ABAQUS to obtain the thermal and thermomechanical responses of the steel ladle considering elastic material behavior. The simplified two-dimensional numerical model representing a horizontal cut through the slag-line position in the upper part of the steel ladle is depicted in Figure 1. The model was composed of five layers, namely, a two-half brick working and permanent lining, an insulation lining, a fiberboard, and a steel shell. There was 0.4 mm circumferential expansion allowance between bricks. The modeling considered the first process cycle of the steel ladle, which included preheating the hot face of the working lining to 1100 °C over 20 h, tapping the steel melt of 1600 °C into the ladle, transport and refining for 95 min, and a 50 min idle period. The radial displacement of linings was free and the circumferential one was constrained by a symmetry condition. The temperature-dependent surface film condition function in ABAQUS was applied to define the heat transfer between both the melt and the hot face of the working lining and the steel shell and the ambient atmosphere. A heat flux crossed the interfaces between linings, and radiation and convection were allowed by applying a heat transfer coefficient. From 160 numerical experiments, the end temperature and the maximum tensile stress at the cold end of the steel shell and the maximum compressive stress at the hot face of the working lining were obtained from FE modeling.

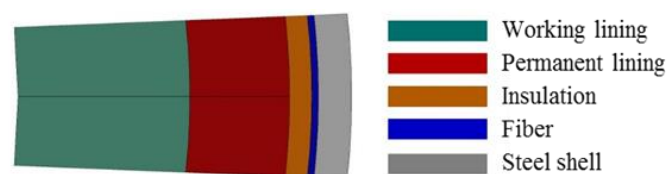


Figure 1. Two-dimensional model representing steel ladle slag zone linings [26].

2.2. BP-ANN Modeling

2.2.1. BP-ANN Architecture

A three-layer BP-ANN model, which includes one input, one hidden, and one output layer, is one of the most popular ANN models. The input variables are introduced to the input layer by a vector (X). A summation for each node in the hidden layer is conducted by multiplying input values with their respective weights (W) plus a bias (b) constant. The summation is processed by an activation function and transferred to the hidden layer. The same procedure is carried out between the hidden and output layers. The predicted values at the output layer are compared with the target values and errors are calculated. Weights and biases among layers are updated iteratively until a user-defined performance goal is achieved. The schematic of a three-layer ANN model is demonstrated in Figure 2.

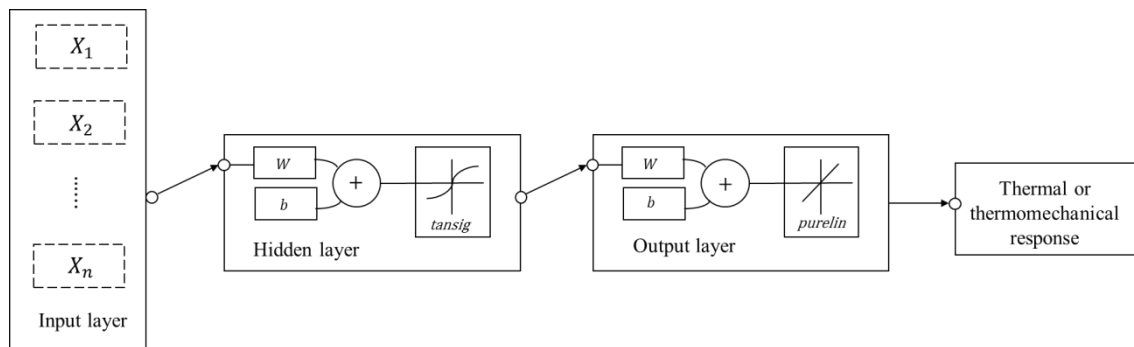


Figure 2. A schematic of a three-layer artificial neural network (ANN) model.

In the present study, two groups of three-layer BP-ANN models were employed to investigate the optimal range of the node numbers in the hidden layer for individual response and the influence of the ratio of input variables to the ten variables (indicating the variable completeness) on the prediction performance. In the first group, there were ten nodes in the input layer, one node in the output layer, and the node number in the hidden layer varied from 1 to 20. The preferable node number range in the hidden layer for each response was proposed afterward. In the second group, different combinations of significant input variables for the individual response were selected according to the ANOVA results of the previous work [27] and listed in Table 3 with their contribution summations to the response. For each combination, several BP-ANN models were employed with the node number of the hidden layer in the range proposed from the first group tests. For both groups, the activation function between the input and hidden layers was a hyperbolic tangent sigmoid function [28], and a linear function was applied between the hidden and output layers. The training algorithm was the gradient descent with momentum and adaptive learning rate [28]. Training was terminated by reaching any defined criterion, for instance, a maximum number of epochs (10,000), the minimum performance gradient (10^{-5}), or a minimum target error (0).

Before starting the network modeling, input variables were normalized to a scale of 0.1–0.9 to mitigate the influence of magnitudes. The normalization of a variable (X_i) can be carried out according to Equation (7).

$$X_i = \frac{0.1x_{max} - 0.9x_{min} + 0.8x_i}{x_{max} - x_{min}} \quad (7)$$

where x_{max} and x_{min} are the maximum and minimum values of the variable x .

Table 3. Variable combinations of each response for backpropagation (BP)-ANN models.

Response	Number of Input Variables	Variable Labels	Contribution to Response (%)
Compressive stress	1	G	93
	2	G, J	96
	3	G, J, D	98
	10	A–J	100
End temperature	3	A, D, F	71
	4	A, D, F, C	89
	5	A, D, F, C, E	94
	10	A–J	100
Tensile stress	4	F, G, D, J	71
	5	F, G, D, J, C	78
	6	F, G, D, J, C, H	85
	7	F, G, D, J, C, H, I	91
	10	A–J	100

2.2.2. Performance Assessment of BP-ANN Models

The responses were predicted by the leave-one-out (LOO) cross-validation method, i.e., one simulation result was left for testing and the remaining results were used for training. Three quantities were used to quantitatively assess the performance of the BP-ANN models. They were the maximum relative error of all testing results (*RE_MAX*), mean relative error (*MRE*), and coefficient of determination (*B*) calculated by the following equations:

$$RE_MAX = \text{Max} \left(\frac{|d_i - y_i|}{d_i} \right) \tag{8}$$

$$MRE = \frac{1}{n} \sum_{i=1}^n \frac{|d_i - y_i|}{d_i} \tag{9}$$

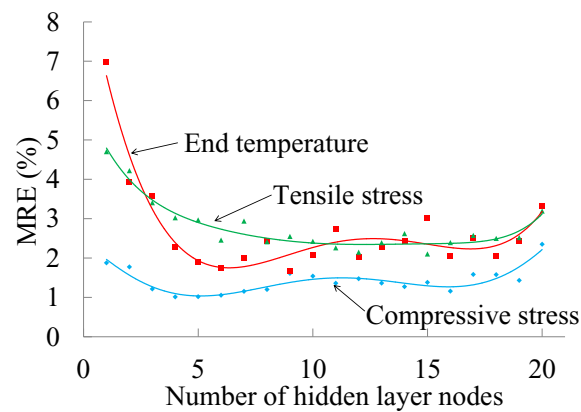
$$B = 1 - \frac{\sum_{i=1}^n (d_i - y_i)^2}{\sum_{i=1}^n (d_i - \bar{d})^2} \tag{10}$$

where *n* is the total number of testing experiments, *d_i* is the FE-simulated value of the *i*th testing experiment, \bar{d} is the mean FE-simulated value of all the testing experiments, *y_i* is the BP-ANN predicted value of the *i*th testing experiment with the LOO method.

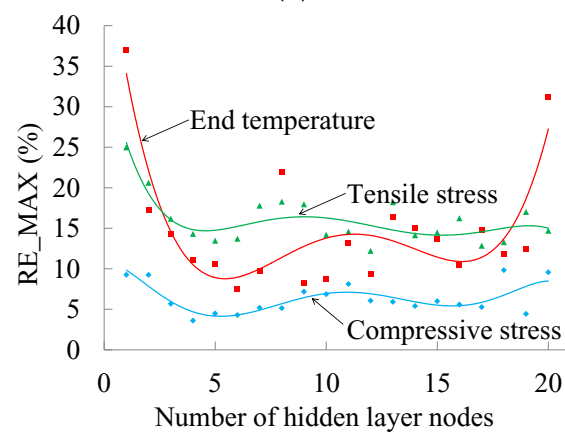
3. Results and Discussion

3.1. Influence of Variation/Response Space Complexity on BP-ANN Model Establishment

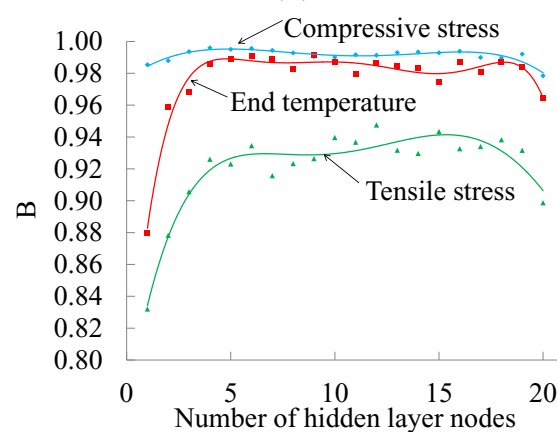
The relation between the complexity of variation/response space and the node number in the hidden layer for each response was revealed. Except the 32 experiments acting as boundaries, the remaining 128 experiments were tested by leave-one-out cross-validation. The node number in the hidden layer was varied from 1 to 20 for each response. The assessment of the prediction performance is shown in Figure 3. Lower *RE_MAX* and *MRE* and larger *B* are preferable.



(a)



(b)



(c)

Figure 3. Performance assessment (a) *RE_MAX*—maximum relative error of all testing results, (b) *MRE*—mean relative error, and (c) *B*—coefficient of determination of the BP-ANN models with different node numbers in the hidden layer.

Figure 3 shows that the performance is significantly improved by increasing the node number in the hidden layer to seven. However, the performance is oscillatory with further increasing node number; the larger number of nodes may lead to over-fitting and affect the generalization capability. For instance, when the node number is 20, the mean relative errors increase for all three responses; the coefficients of determination decrease; the maximum relative error for end temperature is quite high. Furthermore, it shows that each response has different optimal ranges.

Considering the particular behavior of each response, error criteria were specifically defined for each response and a preferable range of the node number in the hidden layer was proposed for each response (Table 4). The range was 4–6 for the maximum compressive stress at the hot face of the working lining, 5–7 for the end temperature of the steel shell, and 10–12 for the maximum tensile stress at the cold end of the steel shell. These ranges can be correlated with the node numbers in the input and output layers, as shown in Table 5. The number of variables that contribute more than 90% to the response was used to calculate the *PF* value, which represents the variation/response complexity. This number was divided by ten (the total number of variables) and multiplied by 100, which gave a *PF* value in percent. Table 5 shows that the *PF* equaled 10, 50, and 70 for the maximum compressive stress, end temperature, and maximum tensile stress, respectively. Therefore, the relation between the complexity of the variation/response space and the node number in the hidden layer can be associated with the *PF* and the node numbers in the input and output layers explicitly. Two equations were deduced from Table 5.

$$\text{Lower boundary: } N_h = AN_i + N_o \tag{11}$$

$$\text{Upper boundary: } N_h = (A + 0.2) N_i + N_o \tag{12}$$

where *A* is a function of the *PF*, *N_i*, *N_h*, and *N_o* are the node numbers in the input, hidden, and output layers, respectively.

Table 4. Optimal node number range in the hidden layer for each response according to predefined error criteria.

Response	RE_MAX (%)	MRE (%)	N _h Range
Compressive stress	5	1.5	[4, 6]
End temperature	11	2	[5, 7]
Tensile stress	15	2.5	[10, 12]

Table 5. Correlation between *PF* and node numbers in the input and output layers.

Response	PF	N _h	
		Lower Boundary	Upper Boundary
Maximum compressive stress	10	$\frac{3}{10}N_i + N_o$	$\frac{5}{10}N_i + N_o$
End temperature	50	$\frac{4}{10}N_i + N_o$	$\frac{6}{10}N_i + N_o$
Maximum tensile stress	70	$\frac{9}{10}N_i + N_o$	$\frac{11}{10}N_i + N_o$

The relation between *A* and *PF* was fitted by an exponential equation (Equation (13)) as shown in Figure 4. Equations (11)–(13) provide guidelines to define node number in the hidden layer for a steel ladle system based on *PF* and node numbers in the input and output layers.

$$A = f(PF) = 0.2982 - 0.001242 (1 - e^{0.08836 * PF}) \tag{13}$$

The above established guidelines were applied to validate the optimal node numbers in several publications [15,19,20,22–24], which fall under the topics of temperature, mechanical behavior, and material development. The calculations of the node number range of the hidden layer for these publications were performed with *PF* values of 10 and 70, respectively. A wide range was created by the lower boundary value with *PF* values of 10 and the upper boundary value with *PF* values of 70. The optimal node numbers in the hidden layer obtained from literature and the calculated ranges from proposed guidelines are given in Table 6. It shows that the optimal values in five publications are in the range defined by Equations (11)–(13), except that the optimal node number in literature [24] is slightly different to the calculated range. Four [19,20,22,23] of them are in the range with an assumption *PF* equal to 10 and one [15] in the range with *PF* equal to 70. The possible total numbers of trials are also

given in Table 4, and fewer trials are needed, compared with the trial and error method [15] and some empirical equations [20,22].

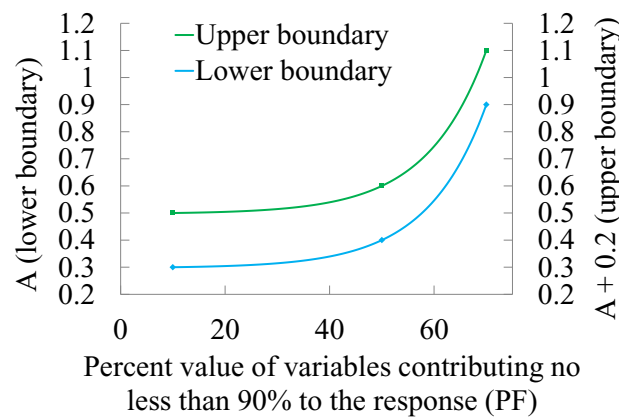


Figure 4. The relation between *PF* and *A* (a function of *PF*).

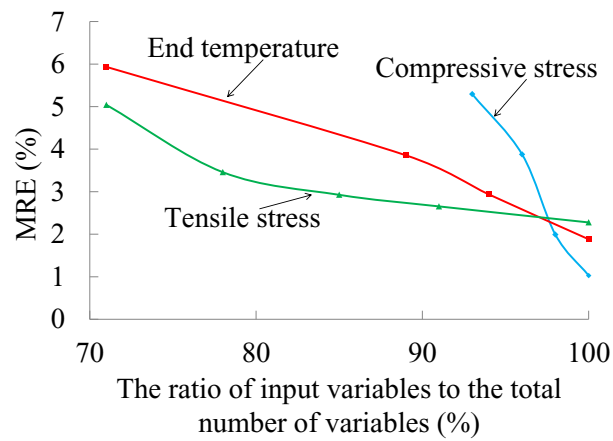
Table 6. Comparison of optimal node numbers in literature and the predicted ranges from the proposed guidelines.

Research Topics	Literature Information		Proposed Guidelines		
	Optimal N_h	N_h Range ($PF = 10$)	N_h Range ($PF = 70$)	N_h Range ($PF = 10-70$)	Total Number of Trials
Power output [15]	7	[2, 4]	[5, 7] *	[2, 7]	6
Lithology identification for shale oil reservoir [19]	10	[7, 10] *	[13, 17]	[7, 17]	11
Moisture content prediction in paddy drying process [20]	2	[1, 3] *	[3, 5]	[1, 5]	5
Mechanical behavior of mortar [22]	2	[2, 4] *	[6, 8]	[2, 8]	7
Extraction of phenolic compounds [23]	2	[1, 3] *	[3, 5]	[1, 5]	5
Damage pattern of structural systems [24]	17	[7, 9]	[13, 15]	[7, 15]	9

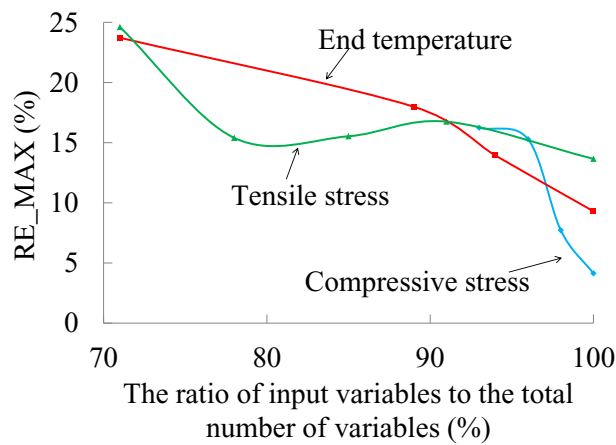
* The range includes the optimal node number in the literature.

3.2. Influence of the Variable Completeness on the BP-ANN Prediction Performance

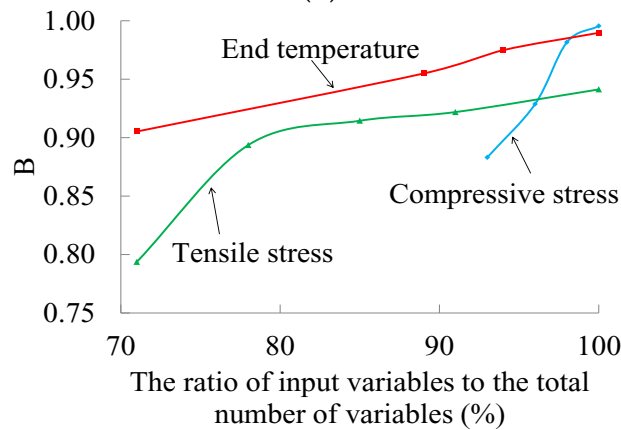
The combinations of input variables for each response are listed in Table 3. Each combination was fed as input to BP-ANN models with the node numbers in the hidden layer proposed in Table 4. For instance, the optimal node number in the hidden layer was 4, 5, and 6 for the maximum compressive stress. That is to say, three BP-ANN modeling were conducted for each input combination. The prediction performance was evaluated by the mean values of *RE_MAX*, *MRE*, and *B* of three BP-ANN models, shown in Figure 5. In general, for all three responses, lower *RE_MAX* and *MRE* and larger *B* can be achieved with increasing variable completeness. The minimum number of variables for each response was determined by an arbitrary chosen error tolerance, i.e., 15% of *RE_MAX*, 3% of *MRE*, and 0.90 of *B* and listed in Table 7 with contribution summations of these variables to the response. The combinations consisted of the minimum number of variables that are capable of predicting the relation between input variables and corresponding outputs. It also indicates that the minimum number of variables changes with respect to the complexity of the problem. A larger number of variables shall be considered if the problem shows significant complexity, which shall contribute a certain value to the response. For instance, this value could be 90% for the tensile stress. This information further confirms the top priority of the significant factors of lining concepts analyzed with the Taguchi method.



(a)



(b)



(c)

Figure 5. Performance assessment (a) RE_{MAX} , (b) MRE , and (c) B of BP-ANN models with different variable completeness (the ratio of input variables to the total number of variables).

Table 7. Selection of the minimum number of input variables satisfying the predefined criteria.

Response	Minimum Number of Input Variables	Contribution to Response (%)
Compressive stress	3	98
End temperature	5	94
Tensile stress	6	85

4. Conclusions

The influence of variation/response space complexity and variable completeness on BP-ANN model establishment was investigated. The guidelines to define node numbers in the hidden layer were proposed for a steel ladle lining system according to the variation/response space complexity. The preferable node number ranges for maximum compressive stress at the hot face of the working lining, the end temperature, and the maximum tensile stress at the cold end of the steel shell were 4–6, 5–7, and 10–12, respectively. The minimum numbers of input variables of significance determined by the Taguchi method for the BP-ANN model were three, five, and six for the maximum compressive stress, the end temperature, and the maximum tensile stress.

The results evidently and exemplarily show that the variation/response complexity plays a determinant role in the architecture establishment of a BP-ANN model, which is often neglected in the applications of ANN models. The comparison study also demonstrates that the proposed guidelines in the present paper are efficient and can be extended into other fields in defining an optimal node number of the hidden layer in a three-layer BP-ANN model.

Supplementary Materials: The following are available online at <http://www.mdpi.com/2076-3417/9/14/2835/s1>, Table S1: Database.

Author Contributions: Investigation, A.H.; supervision, S.J., D.G., and H.H.; writing—original draft preparation, A.H.; writing—review and editing, S.J. and D.G.

Funding: This research received no external funding.

Acknowledgments: The Competence Center for Excellent Technologies research program in “Advanced Metallurgical and Environmental Process Development” (K1-MET) is supported by the Austrian Competence Centre Program COMET (Competence Center for Excellent Technologies) with funds from the Federal Ministry for Transport, Innovation, and Technology; the Federal Ministry of Economy; the provinces of Upper Austria and Styria; the Styrian Business Promotion Agency; and the Tyrolian Future Foundation.

Conflicts of Interest: The authors declare no conflict of interest.

References

1. Flood, I. Towards the next generations of artificial neural networks for civil engineering. *Adv. Eng. Inform.* **2008**, *22*, 4–14. [[CrossRef](#)]
2. Mohandes, S.R.; Zhang, X.Q.; Mahdiyar, A. A comprehensive review on the application of artificial neural networks in building energy analysis. *Neurocomputing* **2019**, *340*, 55–75. [[CrossRef](#)]
3. Rodrigues, E.; Gomes, A.; Gaspar, A.R.; Antunes, G.H. Estimation of renewable energy and built environment-related variables using neural networks—A review. *Renew. Sustain. Energy Rev.* **2018**, *94*, 959–988. [[CrossRef](#)]
4. Ongpeng, J.M.C.; Oreta, A.W.C.; Hirose, S. Investigation on the sensitivity of ultrasonic test applied to reinforced concrete beams using neural network. *Appl. Sci.* **2018**, *8*, 405. [[CrossRef](#)]
5. Zhou, J.; Li, E.; Wei, H.; Li, C.; Qiao, Q.; Armaghani, D.J. Random forests and cubist algorithms for predicting shear strengths of rockfill materials. *Appl. Sci.* **2019**, *9*, 1621. [[CrossRef](#)]
6. Dobrzański, L.A.; Trzaska, J.; Dobrzańska-Danikiewicz, A.D. Use of neural network and artificial intelligence tools for modeling, characterization, and forecasting in material engineering. In *Comprehensive Materials Processing*; Hashmi, S., Batalha, G.F., Van Tyne, C.J., Yilbas, B., Eds.; Elsevier: Amsterdam, The Netherlands, 2014; Volume 2, pp. 161–198.
7. Park, T.C.; Kim, B.S.; Kim, T.Y.; Jin, I.B.; Yeo, Y.K. Comparative study of estimation methods of the endpoint temperature in basic oxygen furnace steelmaking process with selection of input parameters. *Korean J. Met. Mater.* **2018**, *56*, 813–821. [[CrossRef](#)]
8. Cox, I.J.; Lewis, R.W.; Ransing, R.S.; Laszczewski, H.; Berni, G. Application of neural network computing in basic oxygen steelmaking. *J. Mater. Process. Technol.* **2002**, *120*, 310–315. [[CrossRef](#)]
9. He, F.; Zhang, L. Prediction model of end-point phosphorus content in BOF steelmaking process based on PCA and BP neural network. *J. Process Control* **2018**, *66*, 51–58. [[CrossRef](#)]

10. Tunckaya, Y.; Koklukaya, E. Comparative performance evaluation of blast furnace flame temperature prediction using artificial intelligence and statistical methods. *Turk. J. Electr. Eng. Comput. Sci.* **2016**, *24*, 1163–1175. [[CrossRef](#)]
11. Strakowski, R.; Pacholski, K.; Wiecek, B.; Olbrycht, R.; Wittchen, W.; Borechi, M. Estimation of FeO content in the steel slag using infrared imaging and artificial neural network. *Measurement* **2018**, *117*, 380–389. [[CrossRef](#)]
12. Haykin, S. *Neural Networks and Learning Machines*; Pearson Education: Toronto, ON, Canada, 2009; p. 166.
13. Lopez, I.; Aragones, L.; Villacampa, Y.; Compan, P. Artificial neural network modeling of cross-shore profile on sand beaches: The coast of the province of Valencia (Spain). *Mar. Georesour. Geotechnol.* **2018**, *36*, 698–708. [[CrossRef](#)]
14. Bienvenido-Huertas, D.; Moyano, J.; Rodriguez-Jimenez, C.E.; Marin, D. Applying an artificial neural network to assess thermal transmittance in walls by means of the thermometric method. *Appl. Energy* **2019**, *233*, 1–14. [[CrossRef](#)]
15. Chen, D.; Singh, S.; Gao, L.; Garg, A.; Fan, Z. A coupled and interactive influence of operational parameters for optimizing power output of cleaner energy production systems under uncertain conditions. *Int. J. Energy Res.* **2019**, *43*, 1294–1302. [[CrossRef](#)]
16. Darajeh, N.; Idris, A.; Masoumi, H.R.F.; Nourani, A.; Truong, P.; Rezanian, S. Phytoremediation of palm oil mill secondary effluent (POMSE) by *Chrysopogon zizanioides* (L.) using artificial neural networks. *Int. J. Phytoremediat.* **2017**, *19*, 413–424. [[CrossRef](#)] [[PubMed](#)]
17. Darajeh, N.; Masoumi, H.R.F.; Kalantari, K.; Ahmad, M.B.; Shameli, K.; Basri, M.; Khandanlou, R. Optimization of process parameters for rapid absorption of Pb(II), Ni(II), Cu(II) by magnetic/talc nanocomposite using wavelet neural network. *Res. Chem. Intermediat.* **2016**, *42*, 1977–1987. [[CrossRef](#)]
18. Cao, Z.; Guo, N.; Li, M.H.; Yu, K.; Gao, K. Back propagation neural network based signal acquisition for Brillouin distributed optical fiber sensors. *Opt. Express* **2019**, *27*, 4549–4561. [[CrossRef](#)] [[PubMed](#)]
19. Luo, H.; Lai, F.; Dong, Z.; Xia, W. A lithology identification method for continental shale oil reservoir based on BP neural network. *J. Geophys. Eng.* **2018**, *15*, 895–908. [[CrossRef](#)]
20. Chokphoemphum, S.; Chokphoemphum, S. Moisture content prediction of paddy drying in a fluidized-bed drier with a vortex flow generator using an artificial neural network. *Appl. Therm. Eng.* **2018**, *145*, 630–636. [[CrossRef](#)]
21. Chen, X.; Xun, Y.; Li, W.; Zhang, J. Combining discriminant analysis and neural networks for corn variety identification. *Comput. Electron. Agr.* **2010**, *71*, 48–53. [[CrossRef](#)]
22. Onyari, E.K.; Ikotun, B.D. Prediction of compressive and flexural strengths of a modified zeolite additive mortar using artificial neural network. *Constr. Build. Mater.* **2018**, *187*, 1232–1241. [[CrossRef](#)]
23. Amalia, A.; Suryono, S.; Suseno, J.E.; Kurniawati, R. Ultrasound-assisted extraction optimization of phenolic compounds from *Psidium guajava* L. using artificial neural network-genetic algorithm. In Proceedings of the 7th International Seminar on New Paradigm and Innovation on Natural Science and Its Application, Semarang, Indonesia, 17 October 2017. [[CrossRef](#)]
24. Heung, F.; Ching, T. The selection of pattern features for structural damage detection using an extended Bayesian ANN algorithm. *Eng. Struct.* **2008**, *30*, 2762–2770. [[CrossRef](#)]
25. Karsoliya, S. Approximating number of hidden layer neurons in multiple hidden layer BPNN architecture. *IJETT* **2012**, *31*, 714–717.
26. Hou, A.; Jin, S.; Harmuth, H.; Gruber, D. Thermal and thermomechanical responses prediction of a steel ladle using a back-propagation artificial neural network combining multiple orthogonal arrays. *Steel Res. Int.* **2019**, *90*. [[CrossRef](#)]
27. Hou, A.; Jin, S.; Harmuth, H.; Gruber, D. A method for steel ladle lining optimization applying thermomechanical modeling and Taguchi approaches. *JOM* **2018**, *70*, 2449–2456. [[CrossRef](#)]
28. MathWorks. *Deep Learning Toolbox: User's Guide*; MathWorks: Natick, MA, USA, 2018.



MODELLING OF A STEEL LADLE AND PREDICTION OF ITS THERMOMECHANICAL BEHAVIOUR BY FINITE ELEMENT SIMULATION TOGETHER WITH ARTIFICIAL NEURAL NETWORK APPROACHES

Aidong Hou¹, Shengli Jin¹, Dietmar Gruber¹ and Harald Harmuth¹

1: Chair of Ceramics, Department Mineral Resources Engineering
Montanuniversitaet Leoben, A-8700 Leoben, Austria
e-mail: aidong.hou@unileoben.ac.at

Keywords: Steel ladle, Finite element simulation, Thermomechanical behaviour, Artificial neural network

Abstract *Refractory linings of industrial vessels are of decisive importance for high temperature industries. To facilitate the lining design for various material properties and lining configurations, quantitative prediction of thermomechanical responses is of importance prior to industrial application. 192 lining configurations including 10 geometrical and material property variations of a steel ladle lining were defined by six orthogonal arrays for finite element (FE) simulations. The maximum compressive stress at the hot face of the working lining and the maximum tensile stress at the cold end of the steel shell were the selected responses of interest. The impact of geometrical and material property variations on thermomechanical performance of the selected ladle was assessed by analysis of variance (ANOVA) and signal-to-noise (S/N) ratio using 32 lining concept results from one out of six orthogonal arrays. Two optimized lining concepts were proposed accordingly. Their responses were well predicted by a three-layer back-propagation artificial neural network (BP-ANN) model.*

1. INTRODUCTION

Many factors could affect the performance of a steel ladle, for instance, lining configurations, slag compositions, and operation processes [1]. An optimal lining configuration under defined service conditions is crucial for steel ladle campaign life. With the development of computer techniques and algorithms, many advanced techniques, e.g. the finite element method and Taguchi method, can be easily utilized or integrated to facilitate the refractory lining design [2-4]. Especially, the artificial neural network (ANN) is promising in the instantaneous prediction of thermomechanical responses after sufficient training [5].

In the present paper the Taguchi method is applied to design 192 lining configurations for FE

modelling of a steel ladle. Afterwards, the significant factors and their contributions to the thermomechanical responses were identified for 32 lining concepts from one orthogonal array. Taking into account available material data, optimal lining concepts were proposed. Later, an ANN model was trained by different algorithms with 160 lining concepts from the remaining orthogonal arrays and employed to predict the maximum tensile and compressive stresses of two proposed lining concepts.

2. METHODOLOGY

2.1. Taguchi method

Ten geometrical and material property variations of a steel ladle were defined. They were the thicknesses of refractory linings and the steel shell, thermal conductivity and Young's modulus of lining materials. Lining configurations were designed according to orthogonal arrays. Nine variations have four levels, and one variation, the thickness of the steel shell, has two levels; the mixed-level orthogonal array with 32 runs was used to arrange the level combination of these ten variations. 32 lining concepts from one orthogonal array were used to assess the significance of variations and select the optimal levels. The detailed variations and levels information for this orthogonal array is shown in Table 1. The other five orthogonal arrays (corresponding to 160 lining concepts) were employed to evenly distribute the levels of variations in the variation-response space and the results were used to train the ANN model.

Impact factors		Levels				Label of factors
		1	2	3	4	
Thickness (mm)	Working lining	250	200	155	50	A
	Permanent lining	130	110	90	65	B
	Insulation lining	37.5	25	15	6	C
	Steel shell	30	20			J
Thermal conductivity (Wm ⁻¹ K ⁻¹)	Working lining	9	8.5	7	3	D
	Permanent lining	9	5	3	2.2	E
	Insulation lining	1.35	0.5	0.35	0.15	F
Young's modulus (GPa)	Working lining	100	80	60	40	G
	Permanent lining	90	45	30	10	H
	Insulation lining	35	4	3	0.17	I

Table 1. Geometrical and material property variations for the orthogonal array [3].

Analysis of variance (ANOVA) was applied to quantitatively assess the contribution of factors to the overall sum of variances. The necessary quantities used to calculate a factor's percentage contribution (C) were the total sum of squares (SS_T), the sum of squares of each factor (SS_f), and the sum of squares of the deviation (SS_D). The percentage contribution of one factor was calculated in terms of equations 1-4:

$$SS_T = \sum_{i=1}^l \sum_{j=1}^{n_i} (y_{ij} - \bar{y}_t)^2 \quad (1)$$

$$SS_f = n_i \sum_{i=1}^l (\bar{y}_i - \bar{y}_t)^2 \quad (2)$$

$$SS_D = SS_T - \sum_{k=1}^m SS_f(k) \quad (3)$$

$$C = \frac{SS_f}{\sum_{k=1}^m SS_f(k)} \times 100\% \quad (4)$$

where, l is the number of levels, n_i is the number of runs at the i^{th} level, y_{ij} is the value of j^{th} observation at i^{th} level, \bar{y}_t is the mean of all observations, \bar{y}_i is the mean of observations at the i^{th} level, and k is the index referring to a factor.

The S/N ratio represents the effect of the factor levels on the response value. The smaller-the-better equation was used to evaluate the thermomechanical responses as it considers the smallest value as the best quality. The formula of the smaller-the-better S/N ratio is shown as below:

$$\frac{S}{N} = -10 \log \left(\frac{1}{n_i} \sum_{j=1}^{n_i} y_{ij}^2 \right) \quad (5)$$

where, n_i is the number of runs at the i^{th} level, y_{ij} is the value of j^{th} observation at i^{th} level. The equation shows that the higher value of S/N ratio corresponds to a better performance.

2.2 Finite element model and boundary conditions

A simplified two-dimensional model representing a horizontal cut through the slag-line position in the upper part of the steel ladle is depicted in Fig. 1. The model is composed of a two half-brick working lining, a two half-brick permanent lining, an insulation lining, a fibreboard, and a steel shell. The circumferential expansion allowance between bricks was 0.4 mm.

Finite element modelling of the steel ladle was carried out by the commercial software ABAQUS with considering an elastic material behaviour. The simulated processes included the preheating of the hot face of working lining to 1100 °C in 20 h, the tapping of the 1600 °C steel melt into the ladle in a short time, a 95 min refining and 50 min idle time. The ambient temperature is 25 °C. The thermal conductivity and Young's modulus of materials were considered as temperature-independent. The heat transfer between the liquid melt and the hot face of the working lining, the cold end of the steel shell, and the atmosphere was defined as temperature-dependent using the surface film condition function in ABAQUS. The interfaces

between linings were crossed by heat flux, and a heat transfer coefficient allowing for radiation and convection was applied.

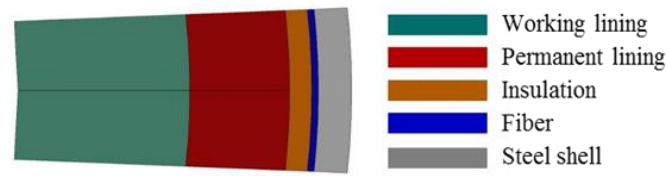


Figure 1. Finite element (FE) geometry [3].

2.3 Back-propagation artificial neural network (BP-ANN)

A three-layer BP-ANN model with one input layer, one hidden layer, and one output layer was applied with a hyperbolic tangent sigmoid transfer function (tansig) between input and hidden layers, and a linear (purelin) function between hidden and output layers [6]. There were seven nodes in the hidden layer. The BP-ANN model was trained by eight training algorithms [6]. The brief description of these algorithms is given in Table 2. The input variables are introduced to the network as a vector and processed by the nodes of the input layer. The summation of all input variables multiplied by their respective weights and plus a bias constant yields the input for each node in the hidden layer. These inputs are transferred by a transfer function as the output of each node in the hidden layer. The outputs from the hidden layer are processed in the same way to the output layer. The predicted outputs from the output layer are compared with the desired values, and the error (difference between the predicted and the desired values) is sent back to the hidden layer for updating weights.

Training algorithm	Brief description
GDX	Gradient descent with momentum and adaptive learning rate back-propagation
CGB	Conjugate gradient back-propagation with Powell-Beale restarts
CGF	Conjugate gradient back-propagation with Fletcher-Reeves updates
CGP	Conjugate gradient back-propagation with Polak-Ribière updates
SCG	Scaled conjugate gradient back-propagation
BFG	BFGS quasi-Newton back-propagation
OSS	One-step secant back-propagation
BR	Bayesian regularization back-propagation

Table 2. Training algorithms employed in the present study [6].

3. RESULTS

3.1 Contribution of variations to thermomechanical responses

The ANOVA was applied to quantitatively investigate the contribution of defined variations to the thermomechanical responses according to the Eqs. (1,2,3,4). The results for maximum tensile and compressive stresses are show in Table 3. The top five significant impact variations for the maximum tensile stress at the cold end of the steel shell were the thermal conductivity of the insulation material (F), the Young's modulus of the working lining material (G), the thickness of the steel shell (J), the thermal conductivity of the working lining material (D), and the Young's modulus of the insulation material (I). These five variations contributed 79% to the variance of results for the tensile stress at the steel shell. The variations of the Young's modulus of the working lining (G) had an overwhelming impact on the results for the compressive stress at the working lining, with a 93% contribution to its variance.

<i>Factor</i>	<i>SS_f (MPa²)</i>		<i>Contribution (%)</i>		<i>Ranking</i>	
	<i>Tensile</i>	<i>Compressive</i>	<i>Tensile</i>	<i>Compressive</i>	<i>Tensile</i>	<i>Compressive</i>
A	134270	5559	4.83	0.51	8	5
B	80720	209	2.90	0.02	9	10
C	188547	3192	6.78	0.29	6	6
D	415173	19406	14.93	1.78	4	3
E	30313	1336	1.09	0.12	10	8
F	667526	334	24.01	0.03	1	9
G	474788	1013329	17.07	93.00	2	1
H	161662	2374	5.81	0.22	7	7
I	208307	10153	7.49	0.93	5	4
J	419299	33670	15.08	3.09	3	2

$SS_T = 2\,821\,827, SS_D = 41\,222$ for maximum tensile stress
 $SS_T = 1\,089\,684, SS_D = 122$ for maximum compressive stress

Table 3. ANOVA results of the maximum tensile and compressive stresses.

3.2 Optimization study of variation levels

The S/N ratios of the thermomechanical responses were calculated with respect to the variation levels according to Eq. (5) and the results are show in Fig. 2. For each variation, the level showing the largest S/N ratio will be considered as the optimal one, this means that lower stresses for both selected responses are preferred. The optimal S/N ratios for the maximum tensile stress at the cold end of steel shell were A4B4C4D4E2F1G4H4I4J1. The optimal levels for the maximum compressive stress at the hot face of the working lining were A4B2C2D3E1F3G4H1I4J2.

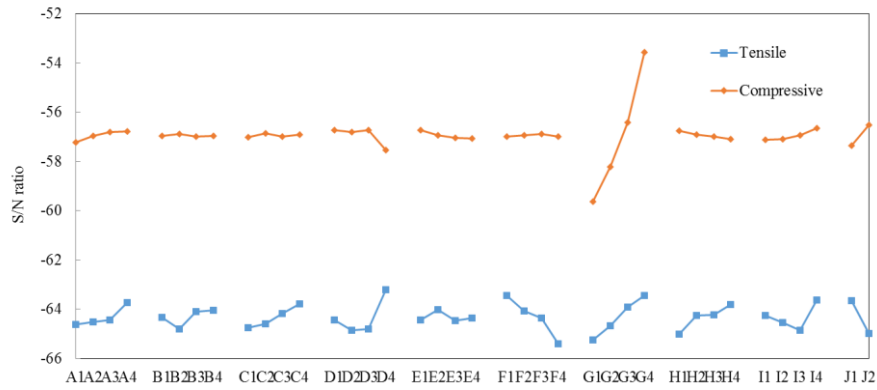


Figure 2. S/N ratio graph for the maximum tensile and compressive stresses and highest S/N results are A4B4C4D4E2F1G4H4I4J1 and A4B2C2D3E1F3G4H1I4J2, respectively [3].

The lining concept of the steel ladle can be optimized with the guidance of ANOVA and S/N ratio analyses. Two optimized lining concepts were proposed taking into account the practical materials and the volume capacity of the steel ladle. The configurations of the two proposed lining concepts are given in Table 4.

	Thickness (mm)	Thermal conductivity ($\text{W m}^{-1} \text{K}^{-1}$)	Young's modulus (GPa)	Thermal expansion coefficient (10^{-6}K^{-1})
Working lining	155	9	40	12.0
Permanent lining	52.5	2.2	45	5.0
Insulation (Case1)	37.5	0.5	3	6.0
Insulation (Case2)	37.5	0.38	4	5.6
Steel shell	30	50	210	12.0

Table 4. Two proposed optimized lining concepts with different insulation materials [3].

3.3 Prediction of the thermomechanical responses of the optimized lining concepts with BP-ANN model

The BP-ANN model with seven nodes in the hidden layer was applied to predict thermomechanical responses. The BP-ANN model was trained with 160 lining configurations and the performance of eight algorithms were evaluated in terms of the relative error, which was the difference between the predicted and the simulated values divided by the simulated value. The prediction performance of the BP-ANN model with different training algorithms for maximum tensile and compressive stresses was given in Fig. 3 (a) and (b), respectively.

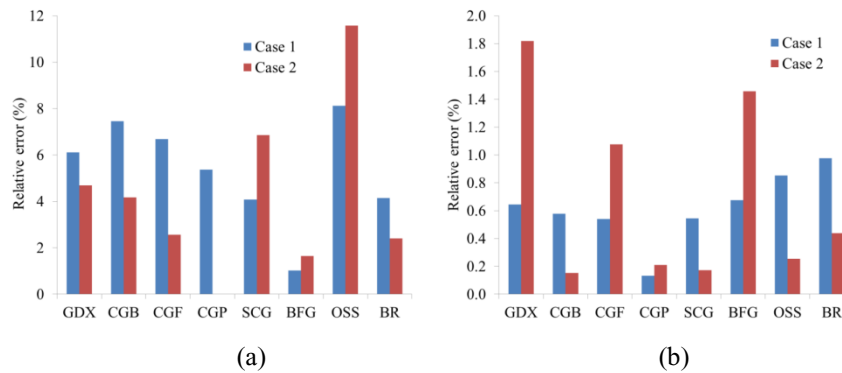


Figure 3. Relative errors of (a) maximum tensile stress and (b) maximum compressive stress predicted with the BP-ANN model applying different training algorithms for the two optimized cases.

4. CONCLUSION

The Taguchi method facilitates decision making for optimizing lining concept by calculating the percentage contribution of each factor variations to the overall sum of variances and assessing the optimal level of each variation. Stresses were calculated using transient finite element simulations. Two lining concepts were proposed based on the information received from ANOVA and S/N ratio and available material data.

Furthermore, the BP-ANN model was successfully applied to predict the thermomechanical responses and an acceptable prediction accuracy was achieved. The combined application of the Taguchi method, finite element method and BP-ANN is promising in the prediction and optimization of lining concept performance prior to industrial application.

ACKNOWLEDGEMENTS

The Competence Center for Excellent Technologies research programme in “Advanced Metallurgical and Environmental Process Development” (K1-MET) is supported by the Austrian Competence Centre Programme COMET (Competence Center for Excellent Technologies) with funds from the Federal Ministry for Transport, Innovation and Technology, the Federal Ministry of Economy, the provinces of Upper Austria and Styria, the Styrian Business Promotion Agency, and the Tyrolian Future Foundation.

REFERENCES

- [1] A. Ghosh. CRC Press. *Secondary steelmaking: principles and applications*, (2000).
- [2] R.K. Roy. Society of Manufacturing Engineers. *A Primer on the Taguchi Method: 2nd edition*, (2010).
- [3] A. Hou, S. Jin, H. Harmuth, D. Gruber, A method for steel ladle lining optimization applying thermomechanical modeling and Taguchi approaches. *JOM*, Vol. **70**, pp. 2449–2456, (2018)

- [4] S. Jin, D. Gruber, H. Harmuth, J. Soudier, P. Meunier, H. Lemaistre, Optimisation of monolithic lining concepts of channel induction furnace. *International Journal of Cast Metals Research*, Vol. **27**, pp. 336-340, (2014).
- [5] L.A. Dobrzański, J. Trzaska, A.D. Dobrzańska-Danikiewicz. *Use of neural network and artificial intelligence tools for modeling, characterization, and forecasting in material engineering*. Hashmi S, Batalha GF, Van Tyne CJ and Yilbas B (eds.). *Comprehensive materials processing*, Vol. **2**, Elsevier; (2014), pp. 161-198.
- [6] MathWorks. Deep learning toolbox: user's guide (R2018b).

Approaches towards a digital tool for optimising lining design – case studies of channel induction furnace and steel ladle

Shengli Jin, Aidong Hou, Harald Harmuth, Dietmar Gruber*
Montanuniversitaet Leoben, Austria

Abstract

Digitalization of high temperature industries, especially in iron and steel making industry, is a worldwide trend being supported by different initiatives, e.g. Industrial Internet of Things in USA, Industry 4.0 in Germany. As the foundation of high temperature industries, refractory linings of industrial vessels are one of importance integrated chains of digitalization. This necessitates the computerized design system of refractory linings offering the functions of experimental design, decision making, and prediction. A methodology is proposed for the refractory lining design utilizing analytical and numerical methods, which are the Taguchi method, thermomechanical finite element modelling and artificial neural network. The case studies of a channel induction furnace and steel ladle demonstrate the success of semi-quantitative analysis of lining concept variations and determination of the principal factors, with respect to the thermal and thermomechanical responses. Multiple orthogonal arrays were applied to achieve a representative factor-response dataset for training with a back propagation artificial neural network. With the optimized infrastructure of back propagation artificial neural network, the thermal and thermomechanical responses of two proposed lining concepts of a steel ladle in terms of existing commercial refractories were well predicted.

1. Introduction

The digitalization of iron and steel industries mainly consists of production management system (PMS), through-process optimization (TPO) and computerized maintenance management system (CMMS)¹. Presently, focus is given to the process optimization and digital transformation of knowledge in the iron and steel plants². As transportation units or/and refining sites, the continuous and controllable operation of industrial metallurgical vessels lined with refractories is preferable, which contributes to the cost-efficiency of metallurgical processes. In this sense, the industrial metallurgical vessel lining concept design could also be integrated into the digitalizing process of iron and steel industries and will play an active role in the computerized maintenance management system. To this end, advanced methods such as the Taguchi method, finite element method and artificial neural network can be applied. The present paper introduces the methods and their applications for a channel induction furnace and a steel ladle³⁻⁶.

The former one applies monolithic materials and the latter shaped materials as working linings.

2. Approaches

The methodology including the Taguchi method, finite element (FE) method and artificial neural network (ANN) were defined to study and optimize the industrial vessel lining design. Fig. 1 shows the flowchart of this methodology.

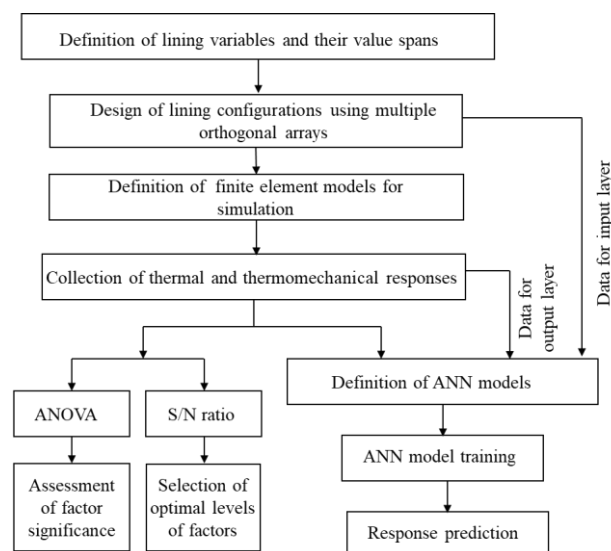


Fig. 1 Flowchart of a methodology for the lining optimization.

For the Taguchi method mainly orthogonal arrays, analysis of variance (ANOVA), and the signal-to-noise (S/N) ratio are applied. It was used to design refractory lining configurations and quantitatively assess the significance of factors to responses. An orthogonal array is a highly fractional factorial design and thus yields a minimum number of experimental runs. With applying the orthogonal array, variations are evenly distributed in a variable space. Considering the possible complexity of variation/response spaces, multiple orthogonal arrays are feasible to achieve a representative dataset with even distribution of variations, as schematically shown in Fig. 2. It is also important to define largest spans of variables as the boundaries, because the extrapolation out of these boundaries is rather risky. Those lining concepts from the boundary space will only be used for training artificial neural network models.

The finite element (FE) simulations act as “virtual trials” of various lining concepts. From those one can obtain the interested responses of lining concepts and perform further analysis. For the present study, the responses of interest are the

temperature and thermomechanical stress.

An artificial neural network (ANN) is a mathematical model extensively used for prediction without explicitly knowing the relations among inputs and outputs. The topology of a three-layer ANN (input, hidden and output layers) is depicted in Fig. 3. The connections among a hidden layer node and input layer nodes are given by a summation function composed of individual weight of each input layer and a bias. The summation result in a hidden layer node is transformed with a transfer function. The same procedure is applied for the hidden and output layers.

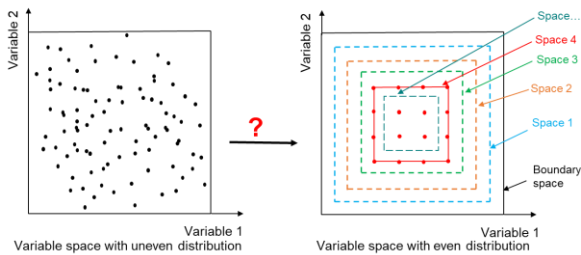


Fig. 2 The distribution of variations in a two-dimensional space.

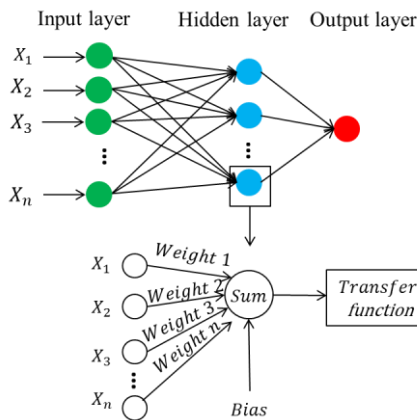


Fig. 3 The topology of a three-layer artificial neural network⁶⁾.

3. Case studies

3.1 Channel induction furnace^{3,4)}

The main objective of this study was to reduce the heat loss from the steel shell and extend the volume capacity of a channel induction furnace by applying materials with strong insulation effect, meanwhile being without significant adverse effects to the residual linings of this furnace. To this end, a simplified two dimensional representation of a channel induction furnace lining concept, made of monolithic refractories, the fiber and steel shell, was established (Fig. 4). More details are given in refs.3 and 4.

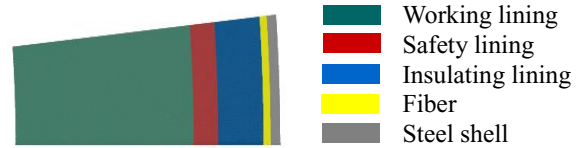


Fig. 4 Two-dimensional representation of a channel induction furnace lining³⁾.

Table 1 lists the variations of lining concepts for optimization study. Four monolithic materials mainly composed of light weight components were the candidates for the insulating lining and sorted by the descending sequence of thermal conductivities named as A1, A2, A3 and A4. In the case of the working lining and safety lining, E2 and D2 showed relative lower thermal conductivity than E1 and D1, respectively. A particular mixed level orthogonal array $L_{16} (4^3 \times 2^2)$ suited the present study. Finite element modelling taking into account elastic behavior of materials was performed. The simulated processes were 9-day preheating of the new working lining to 1200°C and 3-day casting at 1500°C and 2-day holding.

Table 1 Materials and thicknesses for the monolithic lining of a channel induction furnace³⁾.

Factor Level	A	B	C	D	E
1	A1*	1.00	0.96	D1*	E1*
2	A2	1.05	0.85	D2	E2
3	A3	1.11	0.70		
4	A4	1.16	0.65		

(A-insulating lining material; B-dimensionless insulating lining thickness; C-dimensionless working lining thickness; D-safety lining material; E-working lining material. Asterisk* indicates the reference material.)

The maximum tensile stresses at the working lining hot face caused by the shrinkage of monoliths and at the steel shell cold face, and the interface temperature between safety and insulating linings (S-I) and the steel shell temperature were the selected responses for the main effect analysis. To save the space, Fig. 5 only demonstrates the S-I interface temperature with respect to variations. The mean value was obtained by dividing the sum of the responses at each level of one factor to the occurrence number of this level in the orthogonal array; the contribution of the other factors was ignored intentionally. The differences between the maximum and minimum mean responses at each factor were used to assess the main effect. It showed that the working lining thickness and the insulating lining play a major role in the interface temperature. The analysis yielded an optimal lining concept

A1B1C1D2E2 to achieve a low S-I interface temperature.

Combined with the analysis of other three responses, A4B1C1D1E1 was proposed to be an alternative one. The thermomechanical modeling allowing creep of E1 showed that the application of the insulating material A4 with strong insulation effect is beneficial in energy savings without posing severe thermomechanical loads on the residual linings. For instance, the relative difference between ultimate equivalent creep strains of two lining concepts at a critical area was just 7.3% and can be technically neglected, as shown in Fig. 6.

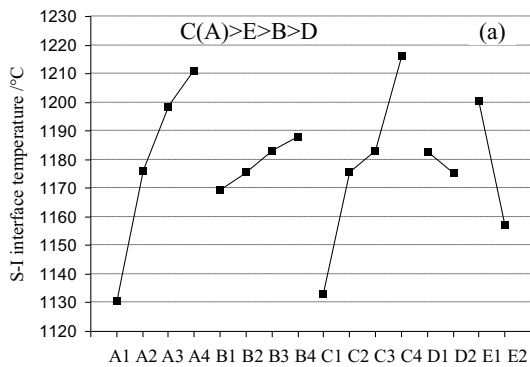


Fig. 5 Main effect analysis of various factors on the temperature³⁾.

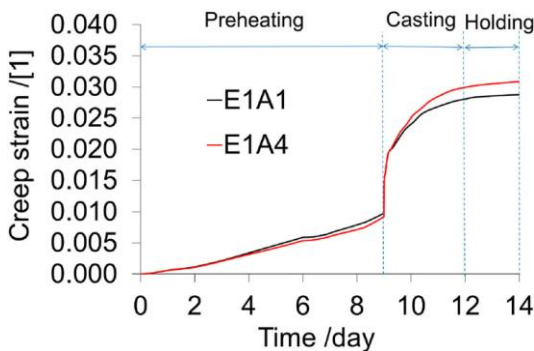


Fig. 6 Equivalent creep strain evolution of the working lining with respect to the process time⁴⁾.

3.2 Steel ladle^{5,6)}

Fig. 7 depicts a simplified two-dimensional model representing a horizontal cut through the slag-line position in the upper part of a steel ladle. The model consisted of a two-half brick working and permanent lining, an insulation lining, a fiberboard, and a steel shell. Ten variables were lining and steel shell thicknesses, thermal conductivity, and Young's modulus of lining materials as listed in Table 2. Two datasets of lining concepts were designed by applying orthogonal arrays considering ten defined variables. The first dataset included 32 cases from one array and the second dataset included 160 cases from other 5 orthogonal arrays.

Finite element modelling of the steel ladle was

performed taking into account elastic material behavior. The simulated process included the preheating of the hot face of working lining to 1100 °C in 20h, the tapping of the 1600 °C steel melt into the ladle in a short time, a 95min refining and 50min idle time. The thermal conductivity and Young's modulus of materials were considered as being temperature independent. The interested responses were the end temperature, the maximum tensile stress at the cold face of the steel shell, and the maximum compressive stress at the hot face of the working lining.

Table 2 Variables of a steel ladle lining⁵⁾.

	Ladle linings	Labels of variables
Thickness	Working lining	A
	Permanent lining	B
	Insulation	C
	Steel shell	J
Thermal conductivity	Working lining	D
	Permanent lining	E
	Insulation	F
Young's modulus	Working lining	G
	Permanent lining	H
	Insulation	I

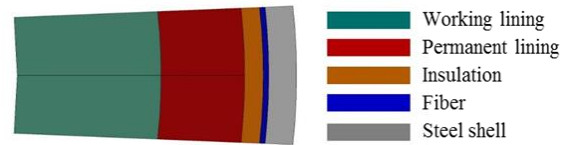


Fig. 7 Two dimensional representation of a steel ladle⁵⁾.

ANOVA and S/N ratio were performed with 32 cases in the first dataset, as shown in Fig. 8. The top four significant impact variables on the temperature at the cold end of the steel shell were A, F, C, and D, in descending order. Their individual confidence levels were all higher than 90%, and when combined, they contributed 89% to the end temperature. In the case of tensile stress at the steel shell, the first four significant impact variables were F, G, J, and D. They contributed 71% to the tensile stress at the steel shell. The variable G had an overwhelming influence on the compressive stress at the hot face of the working lining, with a 93% contribution.

Two optimized lining concepts were proposed with consideration of significant variables, optimal levels of variables according to S/N ratio analysis, and the available practical materials. For both lining concepts, lower temperatures and compressive stresses were achieved comparing with the reference ladle.

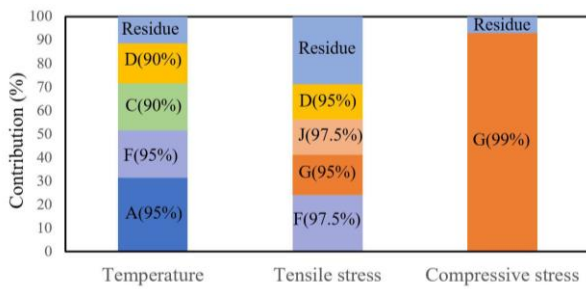


Fig. 8 Contribution and confidence levels (in parentheses) of variables for three responses⁵⁾.

A three-layer back-propagation artificial neural network (BP-ANN) model was applied for training and prediction. The model consisted of 7 nodes in the hidden layer, a hyperbolic tangent sigmoid transfer function between input and hidden layers, a linear function between hidden and output layers, and a Bayesian regularization training algorithm. The dataset were the 160 lining concepts. Leave-one-out (LOO) cross validation was applied to predict three responses of 128 lining concepts. Three quantities were used to assess the prediction performance of the BP-ANN model: maximum relative error of all testing cases (RE_MAX), mean relative error (MRE), and coefficient of determination (B)⁶⁾.

Table 3 summarizes the prediction performance. The three RE_MAXs were less than the 15% empirical error tolerance of prediction. The MSE values were lower than 2.5% and B values were higher than 0.93 for all three responses.

The three responses of two optimal lining concepts proposed by the Taguchi method were predicted with the above ANN model⁶⁾. For these two concepts, the temperature differences between the BP-ANN model and the FE results were less than 4K; the maximum tensile stress differences between BP-ANN prediction and FE modeling were 4.1% and 2.4%; the differences in the maximum compressive stress were 0.97% and 0.39%.

Table 3 BP-ANN model prediction performance for three responses⁶⁾.

Criterion	Steel shell temperature	Maximum tensile stress	Maximum compressive stress
RE_MAX (%)	7.15	12.43	4.09
MRE (%)	1.76	2.37	0.78
B	0.9908	0.9348	0.9966

5 Conclusion

An optimized refractory lining concept is beneficial for both refractory suppliers and users. To achieve it, an optimization process of vessel lining concepts was realized in a digital manner with a holistic consideration of material properties, lining

geometry and operation conditions, as an alternative to the trial-and-error method. The methodology consists of the Taguchi method, finite element method and artificial neural network, covering efficient lining variation design to achieve a representative dataset, numerical experiments and new lining concept prediction. The case studies demonstrate their successful utilizations. The developed methodology is also promising in optimization of other different industrial vessel linings under different operation conditions.

Acknowledgements

The Competence Center for Excellent Technologies research programme in “Advanced Metallurgical and Environmental Process Development” (K1-MET) is supported by the Austrian Competence Centre Programme COMET (Competence Center for Excellent Technologies) with funds from the Federal Ministry for Transport, Innovation and Technology, the Federal Ministry of Economy, the provinces of Upper Austria and Styria, the Styrian Business Promotion Agency, and the Tyrolian Future Foundation.

References

- 1) K.Herzog, G.Winter, G.Kurka, K.Ankermann, R. Binder and M. Ringhofer: *Iron&Steel Technology*, **10** 38-44 (2017).
- 2) D. Bettinger, H. Fritschek, T. Kronberger, J. Mauhart and M. Schaler, *Iron&Steel Technology*, **10** 30-41 (2018).
- 3) S. Jin, D. Gruber, H. Harmuth, J. Soudier, P. Meunier and H. Lemaistre, *Int. J. Cast. Metal. Res.*, **27**[6] 336-340 (2014).
- 4) S. Jin, H. Harmuth and D. Gruber, *Ironmak. Steelmak.*, **45**[6] 514-518 (2018).
- 5) A. Hou, S. Jin, H. Harmuth and D. Gruber, *JOM*, **70**[11] 2449-2456 (2018).
- 6) A. Hou, S. Jin, D. Gruber and H. Harmuth, *Steel. Res. Int.*, **90** [7] 1900116 (2019).